Structure of High-Speed Sprays

Grant DAAG29-85-K-0028
U.S. Army Research Office
December 84 - December 87

Final Technical Report

By

F. V. Bracco

Princeton University
Department of Mechanical and Aerospace Engineering
Princeton, NJ 08544

REPORT DOCUMENTATION PAGE

Form Approved
OMB No. 0704-0188

1. AGENCY USE ONLY (Leave blank)	2. REPORT DATE	3. REPORT TYPE AND DATES COVERED
	Jan 95	Final 15 Dec 84 - 14 Feb 89

4. TITLE AND SUBTITLE
Structure of High-Speed Sprays

5. FUNDING NUMBERS
DAAG29-85-K-0028

6. AUTHOR(S)
Frediano V. Bracco

7. PERFORMING ORGANIZATION NAME(S) AND ADDRESS(ES)
Princeton University
Princeton, NJ 08544

8. PERFORMING ORGANIZATION REPORT NUMBER

9. SPONSORING / MONITORING AGENCY NAME(S) AND ADDRESS(ES)
U.S. Army Research Office
P.O. Box 12211
Research Triangle Park, NC 27709-2211

10. SPONSORING / MONITORING AGENCY REPORT NUMBER
ARO 21781.10-EG

11. SUPPLEMENTARY NOTES
The views, opinions and/or findings contained in this report are those of the author(s) and should not be construed as an official Department of the Army position, policy, or decision, unless so designated by other documentation.

12a. DISTRIBUTION / AVAILABILITY STATEMENT
Approved for public release; distribution unlimited.

12b. DISTRIBUTION CODE

13. This work covered both measurements and computations and its results are documented in eight appendices. Measurements were made of drop velocity in vaporizing, steady, full-cone sprays and of drop velocity and drop size in non-vaporizing steady full-cone sprays. In similar conditions, measurements had previously been made of the intact core and of the size of the drops in the immediate vicinity of the injector, thus generating an extensive set of data which were particularly useful for the assessment and the development of multidimensional models of engine sprays. On the computational side, a line source technique was introduced to simulate the intact-core in engine sprays and two extensive numerical studies were carried out to explain the strong anisotropy of the drop velocity fluctuations that had been found in the measurements. In another interesting and timely study, the accuracy of the stochastic method of computing drop collisions and coalescence (which is the one universally used) was assessed by corresponding deterministic computations (more accurate but much more time consuming). It was concluded that the accuracy of the stochastic method in practical computations can be wanting. Finally, a numerical study of the structure of hollow-cone sprays was initiated that has since been followed by significant experimental and computational work on liquid-only and air-assisted hollow-cone injectors and sprays.

14. SUBJECT TERMS			15. NUMBER OF PAGES
			16. PRICE CODE
17. SECURITY CLASSIFICATION OF REPORT	18. SECURITY CLASSIFICATION OF THIS PAGE	19. SECURITY CLASSIFICATION OF ABSTRACT	20. LIMITATION OF ABSTRACT
UNCLASSIFIED	UNCLASSIFIED	UNCLASSIFIED	UL

CONTENTS

ABSTRACT

This work covered both measurements and computations and its results are documented in eight appendices. Measurements were made of drop velocity in vaporizing, steady, full-cone sprays and of drop velocity and drop size in non-vaporizing steady full-cone sprays. In similar conditions, measurements had previously been made of the intact core and of the size of the drops in the immediate vicinity of the injector, thus generating an extensive set of data which were particularly useful for the assessment and the development of multidimensional models of engine sprays. On the computational side, a line source technique was introduced to simulate the intact-core in engine sprays and two extensive numerical studies were carried out to explain the strong anisotropy of the drop velocity fluctuations that had been found in the measurements. In another interesting and timely study, the accuracy of the stochastic method of computing drop collisions and coalescence (which is the one universally used) was assessed by corresponding deterministic computations (more accurate but much more time consuming). It was concluded that the accuracy of the stochastic method in practical computations can be wanting. Finally, a numerical study of the structure of hollow-cone sprays was initiated that has since been followed by significant experimental and computational work on liquid-only and air-assisted hollow-cone injectors and sprays.

REPORT

This work covered both measurements and computations of full-cone sprays and also an initial computational study of hollow-cone sprays.

The measurements were natural continuations and completions of earlier efforts. Thus the paper of Appendix D reports measurements of the axial component of the drop velocity under vaporizing conditions; all other parameters were kept as close as possible to those in which measurements had been made of drop velocity in non-vaporizing sprays [1], of the intact core [2] and of drop size near the nozzle [3]. In the work of Appendix D, "The axial component of the drop velocity was measured by laser Doppler velocimetry (LDV) within steady hexane-into-nitrogen sprays from a cylindrical nozzle at gas temperatures from 300 to 500 K. Also varied were the injection velocity and the gas-to-liquid density ratio. It was found that the gas temperature had no effect on the mean centerline velocity for distances smaller than 200 and greater than 650 nozzle diameters. At short distances, the core of the spray is not sensitive to the gas temperature; at long distances, the large amount of entrained gas renders inconsequential the degree of vaporization. Beyond 300 nozzle diameters, so much gas has been entrained that the mean axial velocity approaches the fully developed incompressible jet structure. The approach is accelerated by higher gas temperatures and gas-to-liquid density ratios. The axial drop velocity fluctuation amplitude responds to variations in gas temperature similarly to the mean axial drop velocity. Skewness and flatness indicate nearly Gaussian distributions near the axis and rapid increases beyond the half-radius and differ somewhat from those of incompressible jets, possibly because small drops vaporize fast and large ones do not follow the flow as closely as the small ones."

In the paper of Appendix G, simultaneous measurements of drop size and velocity with a phase Doppler analyzer are reported. Again the experimental conditions were kept as close as possible to those of earlier studies [1-3] in an effort to generate a complete set of data. The data were never to my complete satisfaction primarily because the measured quantities were very sensitive to instrument setting and in some cases the change was monotonic (e.g. versus shift velocity) so that it was not possible to say which was the most likely value of the measured quantity. It is for that reason that I declined to publish the work even though it had been completed (including the writing of the paper) at Princeton. But Dr. Chehroudi, who had taken the data at Princeton, decided to publish them under his own name. Dr. Chehroudi was very explicit in noting the instrument problems and in that sense the work contributed to the further development of the phase Doppler analyzer. Moreover, the data are likely to be qualitatively correct and therefore of some use in themselves. In that work, "A single-holed round nozzle with diameter of 127 μm, length-to-nozzle diameter ratio of 4, and fuel differential pressure of 13.6 MPa was used to generate a narrow, fast, steady Diesel type spray of hexane into nitrogen at 1.46 MPa and 65.C. Effects of instrument variables of a phase Doppler particle analyzer (PDPA) on the mean and rms of the drop axial velocity and SMD at a distance-to-diameter ratio of 410 were investigated. It was found that a seemingly good choice of instrument parameters based on SMD may not necessarily be appropriate for velocity measurements. Although all measured quantities tend to level out at sufficiently high values of the photo multiplier voltage, no such tendency was exhibited by changes in the shift velocity. Optical arrangements with smaller measurement volume showed less sensitivity to the instrument parameters and produced mean and rms velocities in agreement with 8% with those obtained with a single-component, dual Bragg-cell LDV system. The SMD decreased radially from 26 μm at the axis and 24 μm and then increased to about 32 μm where the mean velocity was virtually zero. Further drop size (and velocity) measurements are necessary at various axial

locations, particularly closer to the nozzle where the spray becomes denser, possibly using different instruments such as the PDPA, the Malvern particle analyzer, the pulse height and visibility technique (and LDV)."

The rest of the work was computational and was carried out roughly in parallel with the experiment efforts.

The significant contribution of the paper of Appendix A is the introduction of the line source technique in the modeling of Diesel sprays. The intact core, whose length had been assessed experimentally in [2], is modeled as a line within the computational domain. The length of the line changes during injection reflecting expected changes in the length of the intact core. Droplets are introduced along the line into the computational domain in an attempt to locate them where they are actually expected to be generated. This method of drop introduction was incorporated into the Princeton REC (reciprocating and rotary engine combustion) code [4, 5] and has since been used in computations that have led to the improvement of engines [e.g. 6-8]. In particular, "a dense-spray model, that already accounted for drop collisions and coalescence and the influence of liquid volume-fraction on the exchange rates of mass, momentum, and energy between gas and drops, is here extended, using a line source technique, to account also for the intact liquid core in full-cone sprays from jet atomizers. The intact core significantly modifies the computed structure of the near field. The far field is found again not to be sensitive to the near field events and representation and the computed far field drop velocities are shown to compare favorably with measurements."

The paper of Appendix C summarized what had been learned at Princeton after 10 years of work on the structure of full-cone sprays, starting from what had been established prior to the Princeton program (that had been supported primarily by ARO). The review was well received and remains the starting point for serious current work. The abstract of that paper lists only the subjects reviewed and some specific and general conclusions. As such the abstract is not sufficiently comprehensive and informative and the paper must be read in its entirety.

The report of Appendix E (only Table of Contents given) and the paper of Appendix F deal with an insightful peculiarity that we observed in our drop velocity measurements within full-cone sprays: the measured fluctuations of the drop velocity in the radial and axial directions are strongly anisotropic even though the mean drop velocity suggests nearly equilibrium with the mean gas velocity. Since the gas turbulence is nearly isotropic, if equilibrium prevails, the drop fluctuations should be nearly isotropic as well. Several explanations were investigated and the one we selected in Appendices E, F was the wrong one! In our research we have made many mistakes, but we also caught all but a few of them before publishing. This one is one of the few we did not catch. The abstract of Appendix F reads: "Computations have been performed to study the fluctuations of drops in dense spray jets. Previous computations of axial drop velocity fluctuations had not agreed well with the measurements, and no satisfactory explanation had been provided. In this work we have studied the effect of "added mass," drop collisions and coalescences, grid distribution, residence time of drops in eddies, injection velocity, k-ε model constants, and gas phase anisotropy. It is concluded that both gas and drop fluctuations in dense spray jets are strongly anisotropic and therefore cannot be satisfactorily reproduced with a k-ε model. However, such a model has reproduced well all mean quantities and the total turbulence kinetic energy of both gas and drops." The conclusion that the gas velocity in dense sprays is strongly anisotropic, and therefore responsible for the measured anisotropic drop velocity fluctuations, is wrong. Fortunately, we were not totally pleased with it and continued work on the subject until we finally got it right [8] and all pieces of the puzzle

fitted in. Quoting the abstract of [9]: "Drops and particles in steady fully-developed gas jets exhibit anisotropic radial and axial velocity fluctuations and even models of two-phase flows that use isotropic k-ε turbulence sub-models generally reproduce the anisotropy. It is shown that the drop velocity fluctuations can be separated into radial fluctuations that depend mainly on gas turbulence, and axial fluctuations that depend also on the drop radial motion across a mean drop velocity gradient. Drop equilibration time scales are defined and used to evaluate quantitatively the drop fluctuating velocities for different drop sizes, gas turbulence properties and local mean drop velocity gradients." In other words, the gas turbulence is roughly isotropic and the drop fluctuation in the axial direction is significantly greater than that in the radial direction because of the radial motion of drops from regions of higher mean drop velocity to regions of lower mean drop velocity. Actually, the explanation had been provided by Hinze ("Turbulent Fluid and Particle Interactions," *Prog. Heat and Mass Transfer* , Vol. 6, pp. 433-452, 1972) but we were not aware of it at the time of our work.

The work of Appendix H was of considerable value in assessing the numerical error associated with the stochastic treatment of drop collisions and coalescence, which is the current universal way of making such computations. "Comparisons of stochastic and deterministic computations of drop collision and coalescence within selected numerical cells of a self-consistent multiphase spray-flow computation were presented. The numerical resolution was greater than that currently used in practical spray computations. The selected spray is narrow, fast, dense, and of the type found in diesel and stratified-charge engines. However, the spray computed was steady, and drop vaporization and breakup were not considered. The stochastic method was found to underestimate drop collision and coalescence rates by about a factor of 2 with respect to those computed deterministically. A significant fraction of the difference is not due specifically to the stochastic technique of computing drop collision frequencies but originates in the stochastic parcel treatment of the spray. In addition, it is expected that the difference will decrease when drop breakup and vaporization are considered, because both effects tend to narrow the drop size and velocity distribution function, which, in turn, reduces both collision and coalescence frequencies. Indeed, one origin of the difference is that a large fraction of the drops that enter a numerical cell undergo collisions and coalescences within the cell, thus causing significant changes in the drop number density. The stochastic technique assumes a uniform distribution of drops within a cell, whereas the deterministic technique computes the spatial variation of that distribution. The obvious remedy is to increase the numerical resolution, but since the drop distribution function changes significantly within distances of the order of the drop mean free path, impractically small grinds may be necessary for all numerical techniques. Actually, the reported work has progressed only to the point of identifying some inaccuracies of the stochastic method of computing drop collisions and coalescences. Further work is needed to determine the specific sources of the inaccuracies and the conditions necessary to avoid them." This work, that is very important in determining the numerical accuracy of current spray computations and is detailed and time consuming, was not continued, unfortunately.

Finally, Appendix B gives the Table of Content of a report, prepared by Professor T. Tatagi during a one-year visit to Princeton, summarizing his computations of hollow-cone sprays made with our spray code. "Numerical computations of transient hollow-cone sprays are performed to clarify the flow and drop dispersion characteristics in the sprays for various conditions and parameters. The effects are investigated of parameters such as drop size, ambient gas pressure (gas density), injection velocity and injection mass flow rate, and spray cone angle. Computations of full-cone sprays are included for comparison with hollow-cone sprays. Sprays with evaporation and with intermittent injection are also included. Detailed descriptions are given of the drop dispersion, gas and drop velocity,

drop size distribution, drop size-velocity correlation, etc., for each spray condition. A scaling analysis based on the fundamental equations is developed to get the fundamental parameters that govern the spray flow characteristics. The analysis interprets the spray flow characteristics in terms of unified variables and parameters." In particular Takagi's comparisons of the structure of hollow-cone sprays with that of full-cone sprays led to better understanding of both types of spray. Takagi's work was also the beginning of much subsequent experimental and computational effort at Princeton on full-cone sprays, both liquid-only and air-assisted.

REFERENCES

1. Wu, K.-J., Coghe, A., Santavicca, D.A. and Bracco, F.V., "LDV Measurements of Drop Velocity in Diesel-Type Sprays," AIAA Journal, Vol. 22, No. 9, pp. 1263-1270, September 1984.

2. Chehroudi, B. Chen, S.-H., Onuma, Y. and Bracco, F.V., "On the Intact Core of Full-Cone Sprays," Society of Automotive Engineers, 1985 Congress and Exposition, Paper 850126, February 1985. Also in SAE Transactions, Vol. 94, Sec. 1, pp. 764-781, 1985 and 1985 A.T. Colwell Merit Award.

3. Wu, K.-J., Reitz, R.D. and Bracco, F.V., "Measurements of Drop Sizes at the Spray Edge Near the Nozzle in Atomizing Liquid Jets," Physics of Fluids, Vol. 29, No. 4, pp. 941-951, April 1986.

4. Magi, V. and Grasso, F., "A Computer Program for Two-Dimensional Axisymmetric Flows with Sprays and Combustion," MAE Department, Princeton University, Princeton, NJ, Report No. 1766, November 1985.

5. Magi, V., "REC-87 - A New 3-D Code for Flows, Sprays and Combustion in Reciprocating and Rotary Engines," MAE Department, Princeton University, Princeton, NJ, Report No. 1793, October 1987.

6. Grasso, F., Wey, M.-J., Abraham, J. and Bracco, F.V.," Three-Dimensional Computations of Flows in a Stratified-Charge Rotary Engine," Society of Automotive Engineers, 1987 Congress and Exposition, Paper 870409, February 1987.

7. Abraham, J., Wey, M.-J. and Bracco, F.V., "Pressure Non-Uniformity and Mixing Characteristics in Stratified Charge Rotary Engine Combustion," Society of Automotive Engineers, 1988 Congress and Exposition, Paper 880624, February 1988.

8. Abraham, J. and Bracco, F.V., "3-D Computations to Improve Combustion in a Stratified-Charge Rotary Engine - Part II: A Better Spray Pattern for the Pilot Injector," Society of Automotive Engineers, 1989 Fuels and Lubricants Meeting, Paper 892057, September 1989.

9. Tomboulides, A., Andrews, M.J. and Bracco, F.V., "On the Anisotropy of Drop and Particle Velocity Fluctuations in Two Phase Round Gas Jets," Modern Research Topics in Aerospace Propulsion," (G. Angelino, L. DeLuca, W.A. Sirignano, Editors). Springer Verlag, NY, 1991.

APPENDIX A

COMPUTATION OF DENSE SPRAY JETS

Inter. Conf. on Liquid Atomization and Spray Systems (ICLASS 85), Paper 1B/1/1, Proceedings published by the Institute of Energy, 18 Devonshire Str., London W1N 2AU, July 1985.

A U Chatwani and F V Bracco*

A dense-spray model, that already accounted for drop collisions and coalescence and the influence of liquid volume-fraction on the exchange rates of mass, momentum, and energy between gas and drops, is here extended, using a line source technique, to account also for the intact liquid core in full-cone sprays from jet atomisers. The intact core significantly modifies the computed structure of the near field. The far field is found again not to be sensitive to the near field events and representation and the computed far field drop velocities are shown to compare favorably with measurements.

INTRODUCTION

A dense spray is a spray in which the drops can affect each other directly and not just through their influence on the gas. Dense spray effects include drop collisions, that may be followed by coalescence or separation, and the effect of the liquid volume-fraction on the rates of exchange of mass, momentum, and energy between the drops and the gas. Parts of full-cone sprays from single-hole jet atomisers, as used in most Diesel engines and in other mobile power-plants with direct fuel injection, are in the dense spray regime up to hundreds of nozzle diameters from the exit of the atomiser.

For liquids such as water and hydrocarbon fuels injected around room temperature into standard or compressed air, or similar gases, such full-cone sprays are found at injection velocities of $O(10^2 m/s)$. The high velocity requires pressure differences of O(10MPa) and generates large flow rates even with nozzles of diameter of $O(10^2 \mu m)$. Drop diameters are of O(10 μm). The breakup of the liquid jet starts in the immediate vicinity of the nozzle exit and is due mainly to aerodynamic interactions between its surface and the ambient gas (1-3). The outer surface of the liquid column is progressively eroded, and the diameter of the intact core reduced, until the disintegration into drops is completed at a distance approaching 100 nozzle diameters for Diesel-type conditions. Under steady conditions, after breakup, the spray continues its entrainment of the ambient gas and its

*Department of Mechanical and Aerospace Engineering, Princeton University, Princeton, N.J., 08544.

development until, at sufficient distance from the nozzle, it attains the structure of incompressible jets (4). This steady-state structure is outlined in Fig. 1 where x_1 represents the intact core length, or the break up length, x_2 the end of the development region, and x_0 the virtual origin of the fully developed far field. Thus, under steady conditions, a full-cone spray has a structure similar to that of incompressible jets except that all lengths are stretched by a factor the dominant component of which is the liquid-to-gas density ratio (5). Around the intact core, where the gas volume-fraction is zero, there is a thin churning-flow region within which such fraction increases rapidly to 90%. The dense-spray region is next and is followed by the dilute spray region in which the gas volume-fraction is nearly unity.

Multidimensional spray models for dilute sprays have been in use for more than three decades (6,7) but their extension to include the dense spray effects mentioned in the first paragraph is relatively recent (8,9) and practically useful constitutive equations for churning flows do not seem to be available.

In this paper a first effort is made to extend the dense spray model of O'Rourke and Bracco (8) and Martinelli, Reitz and Bracco (10) to account also for the presence of the intact core in full-cone sprays from jet atomisers. At this time the thin layer of churning flow around the intact core is neglected and computations are made only of the dense and dilute spray regions.

THE MODEL

The equations of the two-dimensional unsteady dense spray model are not listed here to save space and since they are available elsewhere (8,10,5). The model (8) employs a stochastic Lagrangian formulation for the drops (11) and an Eulerian one for the gas. Gas turbulence is represented with a k-ε submodel (10). The scattering effect of turbulence on the drops is accounted for but drop effects on turbulence are not, at present, and this could be a limitation in the near field (12,13). The equations are solved numerically in fully coupled form. Because of the stochastic formulation for the drops, many computations should be made to obtain smooth average values. But computer costs limit the averaging and the reported quantities show some scatter. The results of this model generally have compared favorably with several sets of measurements in steady and transient incompressible jets and non vaporizing full-cone sprays (8,14-16,10). But several difficulties remain in simulating full-cone sprays including the introduction of drops into the gas. The original approach of injecting drops into the gas directly from the nozzle exit is inadequate to reproduce the near field because the exchange of momentum between drops and gas is functionally different from that between jets and gas. To lessen this problem, computations were started (8) some 10 nozzle diameters downstream of the actual nozzle exit plane, where the cross-sectional area of the actual spray is about twice that of the nozzle, and by injecting a mixture of small drops and entrained chamber gas moving at the same velocity. Then the average initial gas volume-fraction is about 90%, so that dense spray equations are applicable, and computations start with a jet, thus reproducing

the development region somewhat better. But sufficiently close to the nozzle this approach fails too because it does not account for the intact liquid core.

A line source drop injection technique is now introduced in which advantage is taken of the fact that the length of the intact core is much longer than the nozzle radius and drops are injected into the gas from a line along the axis of the spray. The idea of injecting drops into the gas from the vicinity of their generating surface has already been used with some success in reproducing the measured drop sizes in the immediate vicinity of the nozzle exit(17).

More specifically, the following three equations are used to identify the initial angle of the spray, size of the drops, and length of the intact core

$$\tan \frac{\theta}{2} = \frac{1}{A_\theta} 4\pi \left(\frac{\rho_g}{\rho_\ell}\right)^{1/2} f_m^* \qquad (1)$$

$$\bar{d}_{d,0} = B_d \frac{2\pi\sigma}{\rho_g V_T^2} \lambda_m^* \qquad (2)$$

$$\frac{x_1}{d_j(0)} = C_c \left(\frac{\rho_\ell}{\rho_g}\right)^{1/2} f_m^* - 1 \qquad (3)$$

where f_m^* and λ_m^* are known (1,5) functions of $\rho_\ell\sigma^2/\rho_g\mu_\ell^2 V_T^2$. These equations follow from the supplemented aerodynamic theory of jet break up (1,3) and are applicable to full-cone sprays from single-hole nozzles when the break up of the outer surface of the jet starts in the immediate vicinity of the nozzle exit. The constants A_θ, B_d, and C_c are determined experimentally and A_θ and C_c depend on the nozzle geometry. Strictly, Eqs. 1 and 2 are applicable only in the vicinity of the nozzle exit and Eq. 3 requires many questionable assumptions (1,5). Associated with Eq. 3 is the prediction that the intact core is a straight cone with length x_1 and base $d_j(0)$. A large number of measurements support the validity of Eq. 1 (3,18,19) whereas only a few data are available in support of Eqs. 2(17) and 3(20,21). For lack of better information, Eqs. 1-3 are here assumed to be valid wherever drops are formed. The diameter of the jet at the nozzle exit plane, $d_j(0)$, generally is somewhat smaller (21) than the nozzle diameter, d_n, but in this paper the two are taken to be equal for lack of adequate information.

Computations start at the beginning of injection. The volume of the liquid core in any computational cell is only a small fraction of the cell volume and is neglected. Thus the drop generating surface is treated as a line source of variable intensity and it is not necessary to use a surface-fitted grid. All numerical details, including grid cells, boundary conditions, and time step, are identical to those of (10). With the line source approximation, different shapes of the liquid core result in different intensities of the line source and are equally easy to implement. The line source is along the axis of the jet. The

instantaneous length of the line source is determined by the assumption that its tip moves at 70% of the injection velocity (22). The instantaneous drop generating surface is the surface of the truncated cone of base $d_j(0)$ and height equal to the instantaneous length of the line source. The maximum length of the line source is x_1. The initial diameter of the drops is given by Eq. 2 (but drop coalescence generates a distribution of drop sizes very quickly); the initial drop number flow rate is determined by mass conservation; the initial drop axial velocity is the mass-mean injection velocity; and the initial drop radial velocity is selected so that the computed initial spray angle is that of Eq. 1 (in practice, θ influences the results very weakly because it is small, $5° < \theta/2 < 10°$, and because collisions, coalescence, and turbulence scatter the drops very quickly). In Eqs. 1-3, the velocity V_T is the local relative velocity between the liquid surface and the ambient gas (1,5). In the vicinity of the nozzle exit, V_T is a fraction of the mass-mean injection velocity, V_a, since the gas is nearly stationary and the liquid surface moves at a fraction of V_a due to the persistence of the nozzle wall boundary layer (17). Away from the nozzle exit, V_T is again a fraction of V_a because the liquid core moves at the mass-mean injection velocity (or even at the ideal injection velocity, $V_a = C_D V_j$, as the axis of the jet is approached) but the local entrained gas has been accelerated and its velocity is closer to that of the liquid. As the tip of the intact core is approached, V_T should tend to a small fraction of the liquid velocity. In the absence of any information on the actual value and axial variation of V_T, we have taken $V_T = V_a/B_T$. The value of the constant B_T has negligible influence on Eqs. 1 and 3, because f_m and λ_m are near their asymptotic values for our sprays, but it has a strong effect on the initial drop size through V_T^2 in Eq. 2. Thus computations are made with different values of B_T and its influence on the results is studied.

COMPARISONS AND DISCUSSION

The model results are first compared with the rather extensive and adequately documented far field drop velocity measurements of (4) for the three cases of Table I. In each case, the transient was computed and the calculations were continued past the time when the spray tip reached the farthest location of interest so as to sample the results at appropriate time intervals and to compute averages. The following constants were used $A_\theta = 4(L_n/d_n = 4(19))$, $B_d = (3/\pi A_\theta)^{1/3}$, $(C_c f_m^{*-1}) = 7.5$ (21), and $B_T = 4$. In Fig. 2 the computed radial profiles of the average drop axial velocity are compared with the measured ones at two axial locations for the three cases of Table I. The agreement is satisfactory over the entire range. The computed average drop and gas axial velocities in the numerical cells next to the centerline are shown in Fig. 3. The velocities are normalized by the mass-mean injection velocity and the axial distance by the scale $d_n(\rho_\ell/\rho_g)^{1/2}$. In the immediate vicinity of the nozzle the average axial velocity of the drops is seen to be significantly lower than the injection velocity because a few drops accelerate gas that was initially stationary. Going downstream, more drops get into the gas and both drop and gas velocities at first increase but the average drop velocity soon starts decaying whereas the average gas

velocity continues to increase until x^* is about 7, i.e. up to about the length of the intact core. Eventually both drop and liquid velocities decrease and tend to approach the line corresponding to the limit (for $x^* >> x_0^*$) of the centerline velocity decay of incompressible jets, as also shown by the measurements (4). From the measurements, and after a review of the literature, Wu et al. (4) concludes that the coefficient of the line should be 6.3 ± 0.57. Near the nozzle, the three cases give results that do not overlap in Fig. 3. This is expected because the axial scale $d_n(\rho_\ell/\rho_g)^{1/2}$ is the correct one for the far field but not necessarily for the development region (4,5). On the other hand, Eq. 3 also exhibits the same scale suggesting that a near field scale may exist and may not be very different from the far field one. Also interesting is that, for large values of x^*, drop and gas velocities tend to be more equal for cases B and C than for case A. Less complete equilibration of drop and gas velocities in case A is also suggested by the ratio of the drop velocity relaxation time, $\rho_\ell\, d_d^2/18\, \mu_g$, to the turbulence characteric time, $0.2\, k/\varepsilon$. At $x^* = 80$, the average drop diameter near the centerline is 15 μm in case A and 3 μm in case C (because the initial size of the drops in case C is much smaller due to the higher gas density and injection velocity; see Table 1 and Eq. 2). And the ratio of the two times is O(1) for case A but O(0.1) in case C (case B is in between). In reality there are ranges of drop sizes and turbulent eddies and equilibration is selective. But a large degree of equilibration seems to occur soon within these sprays as indicated by the small differences between corresponding average drop and gas velocities in Fig. 3. Experimentally, Wu et al. (4) concluded that, within the sensitivity and accuracy of their measurements, equilibration along the centerline is virtually complete at $x^* = 50$ for a spray very similar to spray A. On the other hand, even $x^* = 50$ corresponds to some 10 cm in a Diesel engine with $d_n = 200$ μm. Even if equilibration is aided by vaporization, the complex development region remains the one of interest in Diesel applications (5). Other comparisons were made. The computed local standard deviation of the axial component of the drop velocity remains a factor of two smaller than the measured one, whereas corresponding skewness and flatness appear to be in reasonable agreement with the measurements, as for Martinelli et al. (10). The computed gas phase diffusivity is also similar to that reported earlier (10) and agrees with that of incompressible jets in the far field.

Next we consider some transient and near field results. The transient development of the centerline gas velocity of case A is shown in Fig. 4. A very sharp change in the gas phase velocity defines the spray tip location. A progressive penetration of the spray tip with increasing time and a maximum in the gas velocity are evident. Also, whereas previous computations (23) based on a constant gas phase diffusivity, showed that the velocity behind the head vortex reaches its steady state value very quickly, the present results show a longer lag due to the time required for the gas phase turbulence to be produced and to reach its steady state.

Due to the opacity of the spray, velocity measurements near the nozzle are not available and only a parametric study of this region can be undertaken. We varied the length of the intact core, the core tip velocity, the initial angle of the spray, and

the initial size of the drops. The computed centerline gas velocities 1 ms after the beginning of injection are shown in Fig. 5 for case C (the results of computations C4, C5, and C6 are shifted upward to reduce crowding and C6 = C1 for ease of comparison). Computation C1 = C6 is the reference one. In C2 the core length is increased by a factor of 2 ($C_c f_m^{-1} = 15$); the entrainment of the gas is distributed over a longer length, the initial gas velocity is decreased; the spray tip penetration is increased slightly with drops reaching about 10% further; and the position of the maximum gas velocity is shifted downstream and again tends to coincide with the intact core length. Reduction of the initial angle by a factor of 2 has a small effect on the gas velocity and the spray tip penetration is increased only by 10% (C3). Increasing the core tip velocity from 70% to 100% of the injection velocity has no significant influence on the gas velocity. Any difference is restricted to within the time of propagation of the core tip (C4). Slightly more significant changes are obtained when the initial drop diameter is increased (C5) from 1 μm to 6.26 μm ($B_T = 10$). The larger drops have gone further 1ms after the beginning of injection and the tip of the spray is some 15% further downstream. However the increase in the initial size of the drop results in a decrease in drop coalescence. With $\bar{d}_{d,0} = 1$ μm, the average drop diameters increased rapidly to 10 μm inside the spray and to 12 μm at the perifery. With $\bar{d}_{d,0} = 6.26$ μm the corresponding numbers are 10 μm and 20 μm. The drop coalescence tends to reduce the influence of the initial drop size, particularly inside the spray. In non vaporizing sprays, this reduction of the sensitivity of the results to the initial drop size when drop collisions and coalescence are considered had been reported before (8,15).

CONCLUSIONS

A variable-intensity line source has been used to simulate the intact liquid core of full-cone sprays from single-hole jet atomisers of the type used in Diesel engines. The line source injection technique was implemented in a multi-dimensional spray model that already accounted for several dense spray effects. Under steady conditions, those sprays are characterized by a development region, that includes the intact liquid core, and a far field, that has the structure of incompressible jets.

Computed far field mean values, standard deviation, skewness and flatness of the axial drop velocity were compared at various axial and radial locations with corresponding measurements and the agreement was found generally satisfactory as in earlier computations without the line source injection technique. Such agreement confirms the numerical accuracy of the present results and the insensitivity of the far field to actual and simulation details of the development region, including the presence or absence of the intact core. Although there cannot be a precise distance at which the far field starts, measurements and computations of non vaporizing sprays indicate that the far field may start in the range $50 < x/d_n(\rho_\ell/\rho_g)^{1/2} < 100$, as it does in incompressible ($\rho_\ell = \rho_g$) jets (24).

The intact core length is estimated (20,21) to be $7 < x/d_n (\rho_\ell/\rho_g)^{1/2} < 15$, again in parallel with the potential core of incompressible jets, and the development region, that includes the intact core, is found to be the most sensitive to the way the intact core is modeled, not surprisingly. In particular, when the line source technique is used, the production of gas turbulence and gas entrainment are different from what they were when earlier injection techniques were used. The gas velocity inside the spray is found to increase gradually, and to achieve a maximum near the tip of the intact core, before decreasing. The parameters describing the intact core and the drops were varied, simulating our uncertainty about them, and the results were found rather insensitive to them, even in the vicinity of the nozzle (but different from corresponding results obtained with earlier injection techniques). The most influential parameter would have been the initial drop size but drop collisions and coalescence, that are more frequent for numerous small drops than for less-numerous large ones, drastically reduce its effect. Drops at the edge of the spray were found to be the one most influenced by the initial drop size. Unfortunately it was not possible to check the theoretical results that concern the development region because adequate measurements do not seem to be available.

ACKNOWLEDGMENTS

Support for this work was provided by the Department of Energy (Contract DE-AC-04-81AL16338), the Army Research Office (DAAG29-85-K-0028), General Motors, Komatsu, and Cummins Engine.

NOMENCLATURE

A_θ = constant of the initial spray angle equation

B_d = constant of the initial drop size equation

B_T = relative-velocity constant for initial drop size

C_c = constant of the intact core length equation

C_D = nozzle discharge coefficient

d_d = drop diameter

$\bar{d}_{d,0}$ = initial drop diameter

$d_j(0)$ = intact jet diameter at nozzle exit

d_n = nozzle diameter

k = turbulent kinetic energy

L_n = nozzle length

p_ℓ = injector upstream liquid pressure

p_g = injector downstream gas pressure

$V_a = C_D V_i$ mass-mean liquid injection velocity

$V_i = [2 \Delta p_n/\rho_\ell]^{1/2}$ ideal injection velocity

V_T = relative liquid-gas velocity for drop formation

x_0 = location of virtual origin

x_1 = end of potential or intact core

x_2 = end of development region

$x^* = x/d_j(0)(\rho_\ell/\rho_g)^{1/2}$ dimensionless jet axial length

Δp_n = pressure drop across the nozzle

ϵ = rate of dissipation of turbulence kinetic energy

θ = spray full angle

μ_g = gas viscosity

μ_ℓ = liquid viscosity

ρ_g = gas density

ρ_ℓ = liquid density

σ = surface tension

REFERENCES

1. Batchelor, G. K. (Editor), 'Collected Works of G. I. Taylor', Cambridge University Press (Cambridge, MA), 1958.

2. Levich, V. G., 'Physicochemical Hydrodynamics', Prentice-Hall (Englewood Cliffs, NJ), 1962.

3. Reitz, R. D. and Bracco, F. V., Phys. Fluids 25 (1982) 1730.

4. Wu, K.-J., Coghe, A., Santavicca, D. A., and Bracco, F. V., AAIA J. 22 (1984) 1263.

5. Bracco, F. V., 'Modeling of Engine Sprays', SAE Paper 850394 (also in SAE P-156), 1985.

6. Lambiris, S., Combs, L. P., and Levine, R. S., 'Stable Combustion Processes in Liquid Propellant Rocket Engines', Fifth Colloquium of the Combustion and Propulsion Panel, AGARD, 1962.

7. Borman, G. L. and Johnson, J. H., 'Unsteady Vaporization Histories and Trajectories of Fuel Drops Injected into Swirling Air', SAE Paper 598C, 1962.

8. O'Rourke, P. J. and Bracco, F. V., 'Modeling of Drop Interations in Thick Sprays and a Comparison with Experiments', The Institution of Mechanical Engineers, Publication 1980-9, 1980.

9. Faeth, G. M., Progress in Energy and Combustion Science 9 (1983) 1.

10. Martinelli, L., Reitz, R. D., and Bracco, F. V., 'Comparisons of Computed and Measured Dense Spray Jets', 9th Int. Coll. on Dyn. of Expl. and Reactive Systems, Poitiers, France, 1983; AIAA Progress in Astr. and Aero., 95 (1984) 484.

11. Dukowicz, J. K., J. Comp. Phys. 35 (1980) 229.

12. Elghobashi, S. E. and Abou-Arab, T. W., Physics of Fluids 26 (1983) 931.

13. Elghobashi, S. E., Chem. Eng. Commun. 28 (1984) 341.

14. O'Rourke, P. J., 'Collective Drop Effects on Vaporizing Liquid Sprays', Princeton University, Department of Mechanical and Aerospace Engineering, Ph.D. Thesis 1532-T, 1981.

15. Kuo, T.-W. and Bracco, F. V., 'Computations of Drop Sizes in Pulsating Sprays and of Liquid-Core Length in Vaporizing Sprays', SAE Paper 820133, 1982.

16. Kuo, T.-W., and Bracco, F. V., J. Fluids Eng. 104 (1982) 191.

17. Wu, K.-J., Reitz, R. D., and Bracco, F. V., 'Drop Sizes of Atomizing Jets', submitted for publication.

18. Hiroyasu, H., Shimizu, M., and Arai, M., 'The Breakup of High Speed Jet in a High Pressure Gaseous Atmosphere', ICLASS-82, Madison, WI, 1982.

19. Wu, K.-J., Su, C. C., Steinberger, R. L., Santavicca, D.A., and Bracco, F. V., J. Fluids Engineering 105 (1983) 406.

20. Hiroyasu, H. and Kadota, T., 'Fuel Droplet Size Distribution in Diesel Combustion Chamber', SAE Paper 74015, 1974.

21. Chehroudi, B., Onuma, Y., Chen, S.-H., and Bracco, F. V., 'On the Intact Core of Full-Cone Sprays', SAE Paper 850126, 1985.

22. Reitz, R. D. and Bracco, F. V., Phys. Fluids 22 (1979) 1054.

23. Kuo, T.-W., and Bracco, F. V., 'On the Scaling of Transient Laminar, Turbulent, and Spray Jets', SAE Paper 820038, 1982.

24. Wygnanski, I, and Fiedler, H., J. Fluid Mech. 38 (1969) 577.

Table I: Spray conditions of the drop velocity measurements (4) and the computations.

Case	p_g (MPa)	ρ_g/ρ_ℓ	Δp_n (MPa)	V_a (m/s)	Nozzle d_n(μm) - L_n/d_n
A	1.48	0.0256	11.0	127	127-4
B	4.24	0.0732	11.0	127	127-4
C	4.24	0.0732	26.2	194	127-4

Liquid: n-hexane, ρ_ℓ = 665 kg/m^3, μ_ℓ = 3.2 x 10^{-4} N·s/m^2, σ = 1.84 x 10^{-2} N/m. Gas: nitrogen. Room temperature.

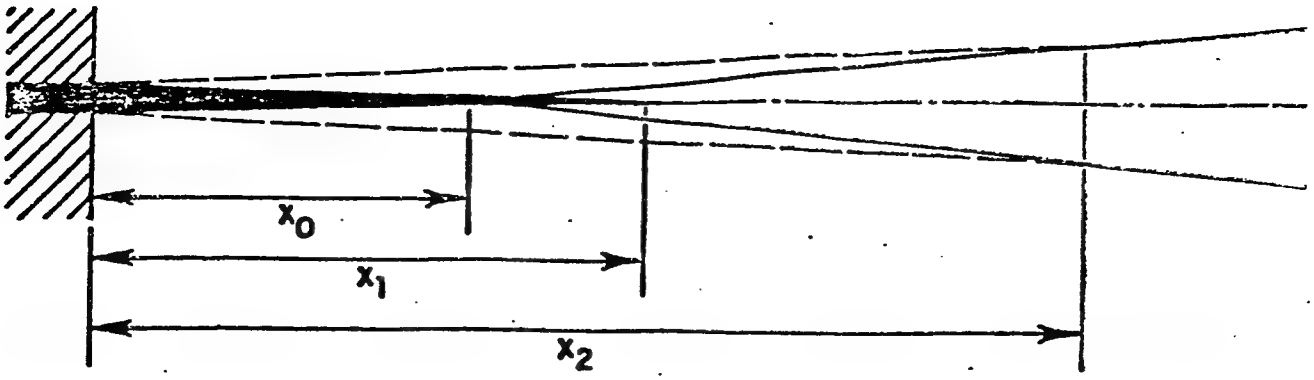

Figure 1 Schematic structure of incompressible jets and full-cone sprays.

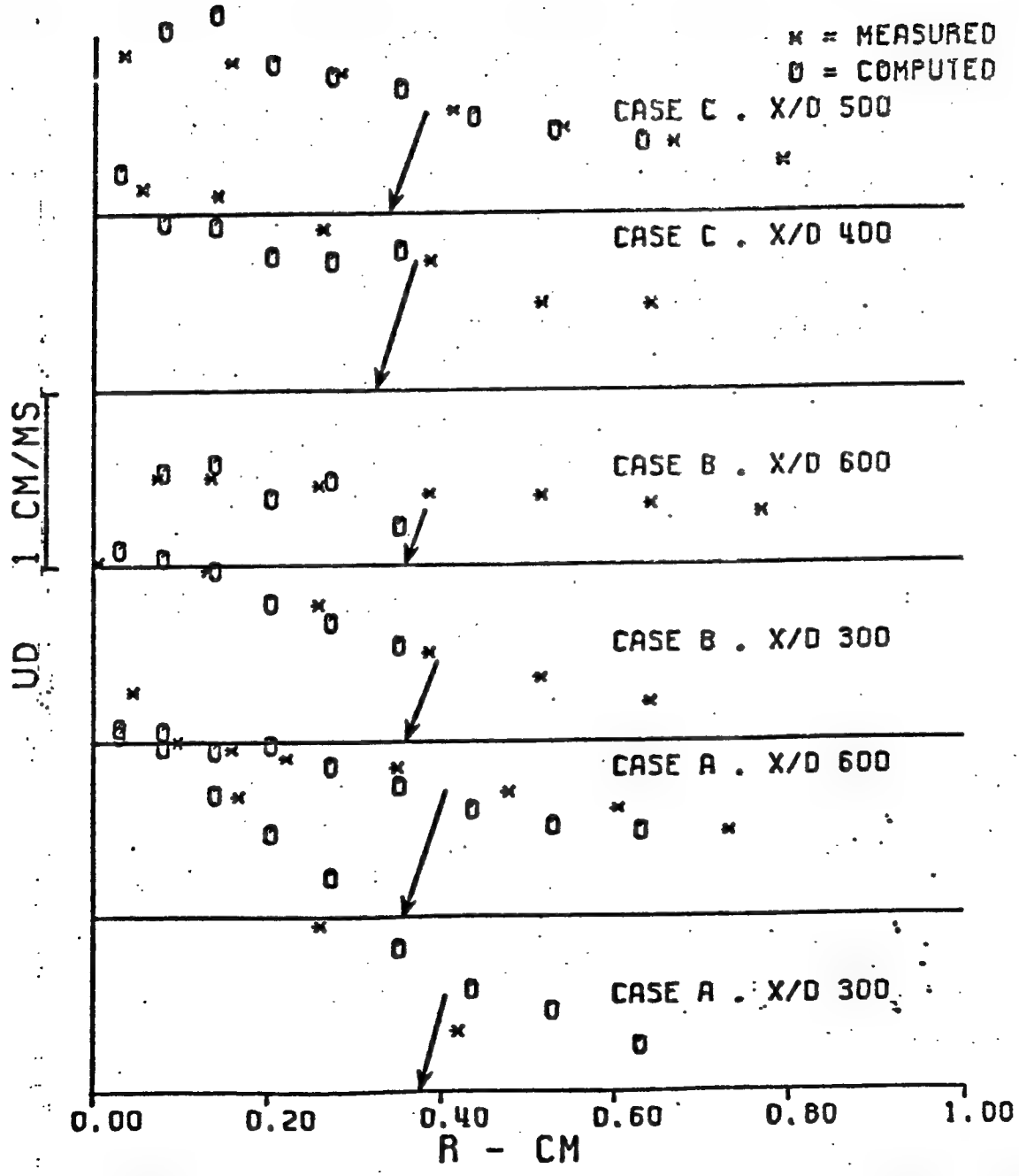

Figure 2 Measured (x) and computed (0) radial profiles of the average drop axial velocity at various axial locations for the three sprays of Table I($D \equiv d_n$).

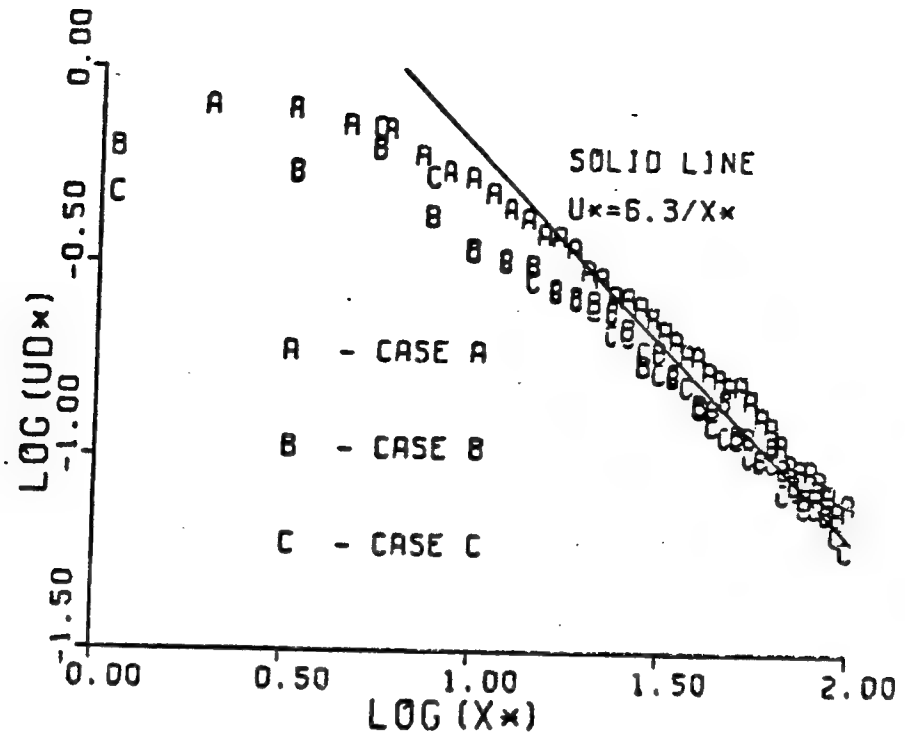

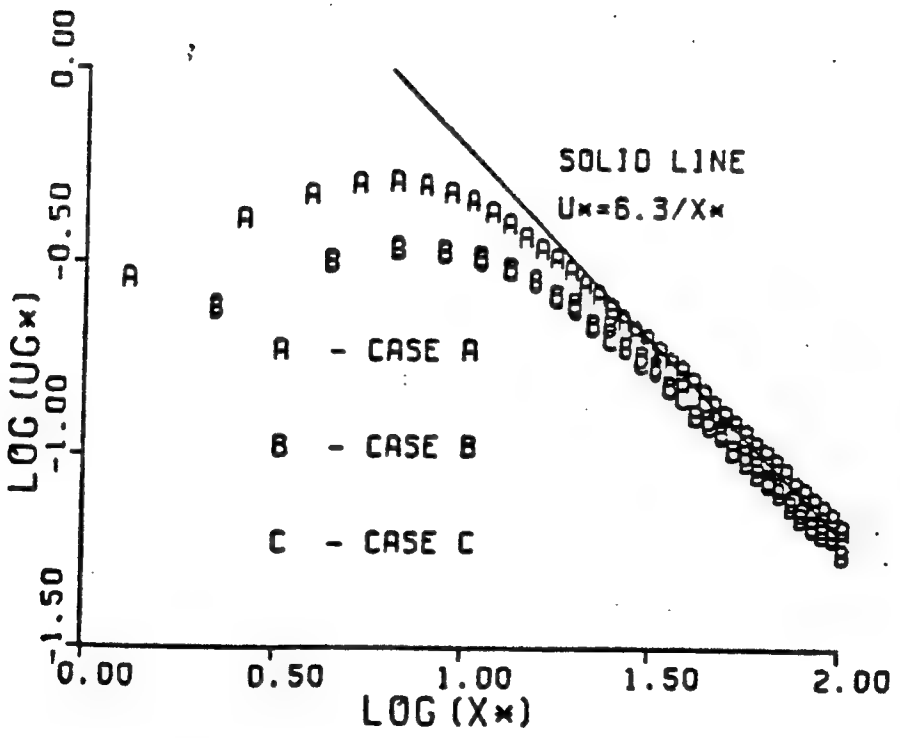

Figure 3 Computed average drop and gas axial velocities for the three sprays of Table I.

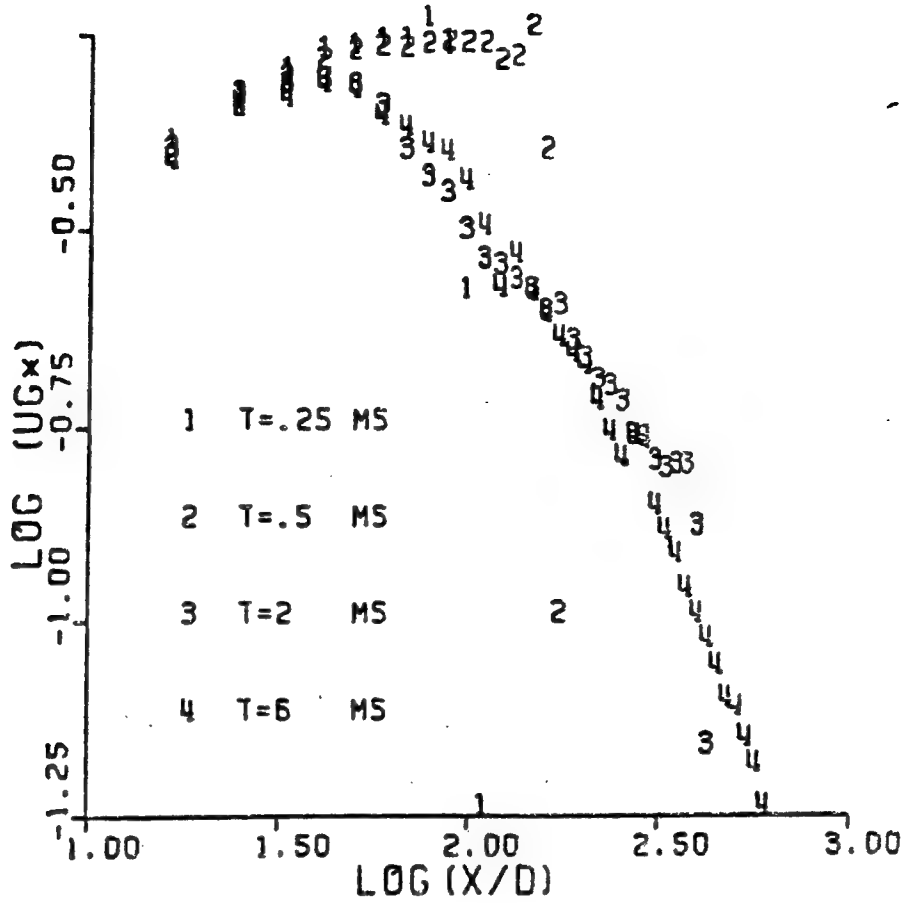

Figure 4 Computed transient centerline gas velocity for case A of Table I. ($D \equiv d_n$).

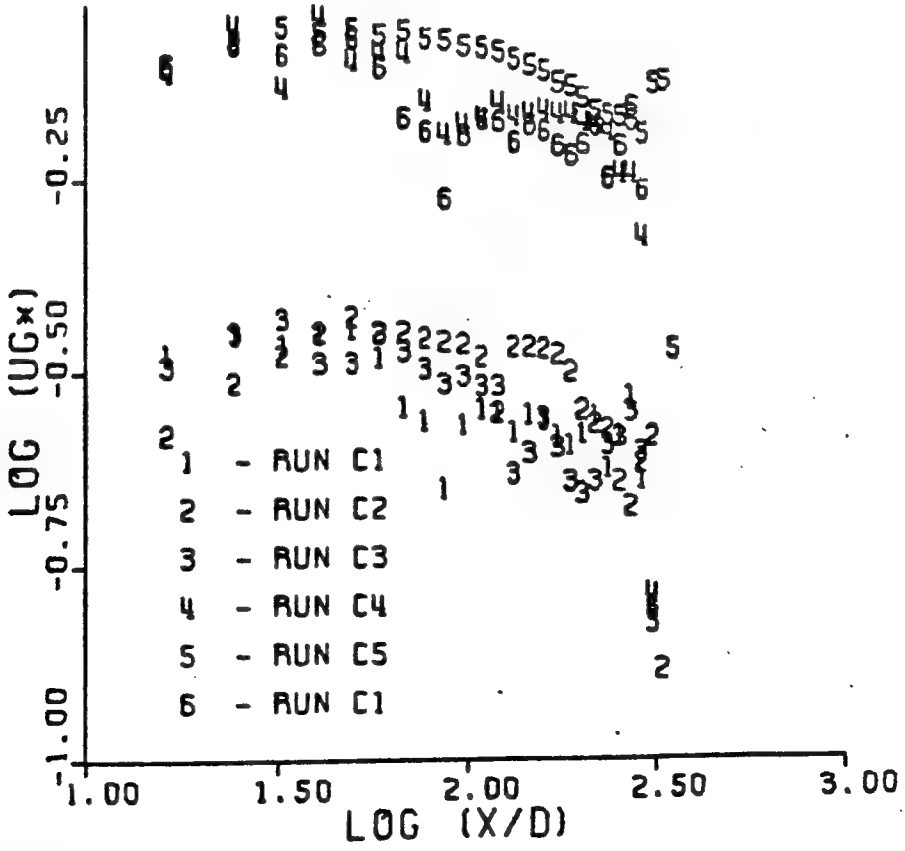

Figure 5 Effect of various parameters on the computed centerline gas velocity 1 ms after beginning of injection. Case C of Table I ($D \equiv d_n$).

$$M^* = M(\rho_\ell/\rho_g) \tag{7}$$

$$Q_0^* = Q_0\rho_\ell \tag{8}$$

$$D_t^* = D_t(\rho_\ell/\rho_g)^{1/2} \tag{9}$$

$$r_{0.5}^* = r_{0.5} \tag{10}$$

$$\bar{u}_{x,CL}^* = \bar{u}_{x,CL}\,(\rho_\ell/\rho_g)^{1/2} \tag{11}$$

$$Q_e^*/Q_0^* = (Q_\ell/Q_0)(\rho_g/\rho_\ell)^{1/2} \tag{12}$$

$$d^* = d(\rho_\ell/\rho_g)^{1/2} \tag{13}$$

$$\frac{\tau^*_{diff}}{\tau_{drop}} = 18\left(\frac{r_{0.5}}{d_\ell}\right)^2\left(\frac{\mu_g}{\rho_\ell D_t^*}\right) \tag{14}$$

$$M = C_m \pi \bar{u}_{0,CL}^2 d^2/4 \tag{1}$$

$$Q_0 = C_q \pi \bar{u}_{0,CL} d^2/4 \tag{2}$$

$$D_t = C_t [C_m \pi \bar{u}_{0,CL}^2 d^2/4]^{1/2} \tag{3}$$

$$r_{0.5} = 8 (\pi(2^{1/2} - 1)/3)^{1/2} C_t (x-x_0) \tag{4}$$

$$\bar{u}_{x,CL} = (3 C_m^{1/2}/16\pi^{1/2} C_t) d \bar{u}_{0,CL}/(x-x_0) \tag{5}$$

$$Q_e/Q_0 = (16\pi^{1/2} C_t C_m^{1/2}/C_q)(x-x_0)/d \tag{6}$$

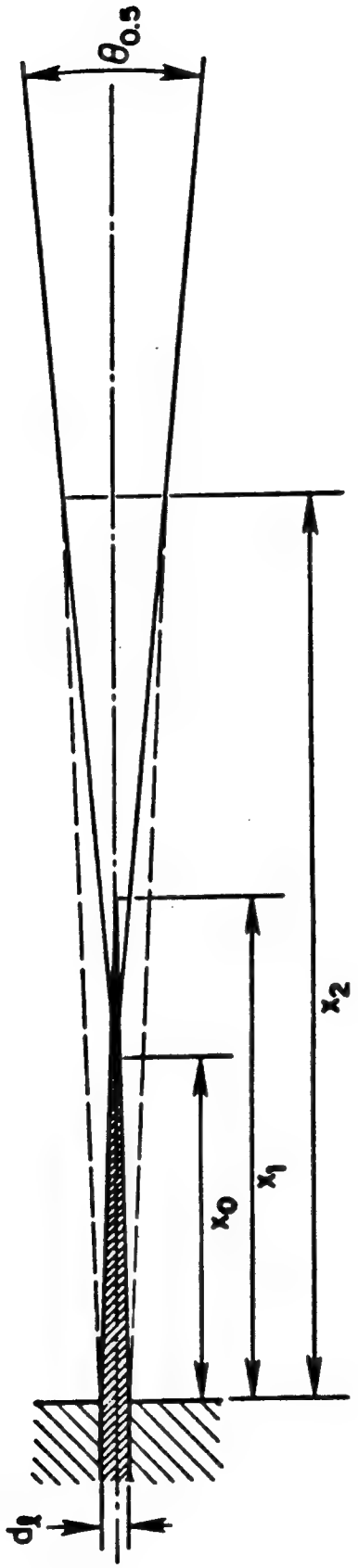

FIG. 10
Bracco

APPENDIX B

COMPUTATIONS AND ANALYSIS OF TRANSIENT HOLLOW CONE SPRAYS

T. Takagi*

Department of Mechanical and Aerospace Engineering
Princeton University
Princeton, NJ 08544

Report MAE 1706

June 1985

* Visiting Professor - Department of Mechanical Engineering,
Osaka University, Japan

Table of Contents

Table of Contents (continued)

1. Abstract

Numerical computations of transient hollow cone sprays are performed to clarify the flow and drop dispersion characteristics in the sprays for various condition and parameters.

The effects are investigated of parameters such as drop size, ambient gas pressure (gas density), injection velocity and injection mass flow rate, and spray cone angle.

Computations of full cone sprays are included for comparison with hollow cone sprays.

Sprays with evaporation and with intermittent injection are also included.

Detailed descriptions are given of the drop dispersion, gas and drop velocity, drop size distribution, drop size-velocity correlation, etc., for each spray condition.

A scaling analysis based on the fundamental equations is developed to get the fundamental parameters that govern the spray flow characteristics. The analysis interprets the spray flow characteristics in terms of unified variables and parameters.

Acknowledgments

This work was performed in cooperation with Dr. A. Chatwani and Professor F.V. Bracco.

Support was provided by the Department of Energy (Contract DE-AC-04-81AL16338), the Army Research Office (DAAG29-85-K-0028), General Motors, Komatsu, and Cummins Engine. Some of the results were presented at the 21st DISC Meeting, U.S. Department of Energy, March, 1985.

APPENDIX C

SAE The Engineering Resource For Advancing Mobility

400 COMMONWEALTH DRIVE WARRENDALE, PA 15096

SAE Technical Paper Series

850394

Modeling of Engine Sprays

F. V. Bracco
Department of Mechanical and Aerospace Engineering
Princeton University
Princeton, NJ

Reprinted from P-156—
Engine Combustion Analysis: New Approaches

International Congress
& Exposition
Detroit, Michigan
February 25 — March 1, 1985

850394

Modeling of Engine Sprays

F. V. Bracco
Department of Mechanical and Aerospace Engineering
Princeton University
Princeton, NJ

ABSTRACT

Atomization and full-cone sprays from single cylindrical orifices are considered. The following subjects are reviewed: the structure of the breakup region; the structure of the far field; modern models that, given the outcome of the breakup process, compute the steady and transient of sprays; some comparisons with detailed measurements; and some practical applications. The following conclusions are reached: the spray breakup and the development regions are the most relevant in engine applications; the inner structure of the breakup region is still largely unknown; two- and three-dimensional spray models are available but remain mostly untested, particularly in their vaporization and combustion components, in part because of a lack of accurate measurements in controlled engine-type environments; engine applications of such models are, nonetheless, recommended for very valuable learning, interpretative, and exploratory studies, but not for predictions.

MANY TYPES OF NOZZLES ARE OF INTEREST for direct fuel injection in engines [1-3], but we will discuss only atomization and sprays from single cylindrical orifices. Moreover, although the title of this review is modeling of such sprays, the real subject is their structure because models simply encode our understanding of the structure. (Hollow-cone sprays, particularly pulsating hollow-cone sprays as used in some open-chamber stratified-charge engines, exhibit interesting properties but their structure has received little attention and will not be reviewed at this time.)

An initial general idea of the configuration of sprays from single cylindrical orifices can be obtained by considering the similar, but better-understood, family of incompressible jets [4-6]. An incompressible jet is obtained when ambient and injected media have the same density and the Mach number is sufficiently low for compressibility effects to be negligible.

Figure 1 shows the initial propagation of a turbulent incompressible jet [7] and of a spray [8] into quiescent environments. The propagation of the incompressible jet is marked by the advancement and growth of a head vortex that is fed, from its upstream side, by the injected medium and the ambient medium that was entrained in the region between the head vortex and the nozzle. Practically, this intermediate region is in its steady state configuration. That is, the head vortex leaves a turbulent, steady, incompressible jet behind itself. In the laboratory frame, the vortex moves at a fraction of the local steady-state centerline velocity. Within the steady part, the shear layer and the potential core can be seen. The length of the potential core is normally less than 10 nozzle diameters. After a development region of at least 50 nozzle diameters, steady turbulent incompressible jets are said to have become fully developed. The radial profiles of fully developed incompressible jets scale with distance from a point that is called the virtual origin.

The lengths that outline the steady-state structure of an incompressible turbulent jet are shown in Fig. 2 where x_0 is the virtual origin, x_1 is the end of the potential core, x_2 is the end of the development region and the beginning of the fully developed region, and $\theta_{0.5}$ is the angle at which the axial component of the mean velocity reaches one half of its centerline value.

Going back to Fig. 1 and looking at the spray, we notice again that the propagation of the spray is also marked by the advancement and growth of a head vortex. Although

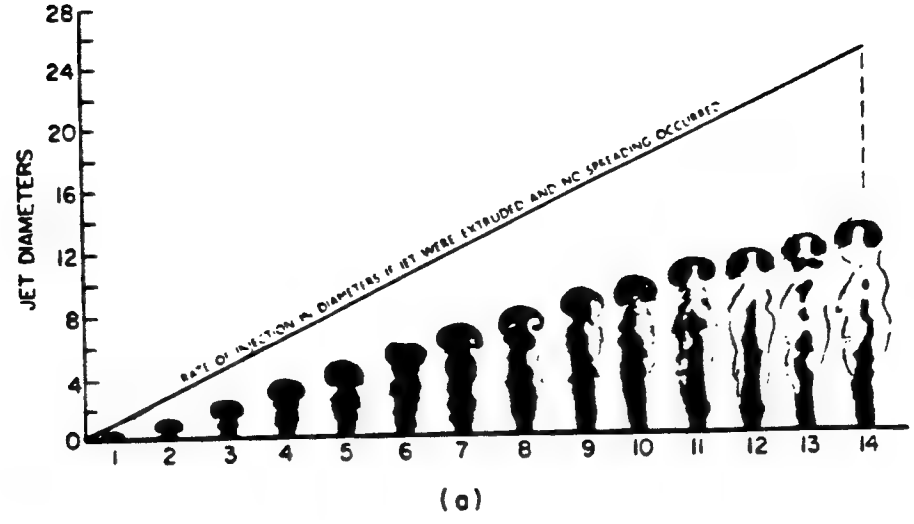

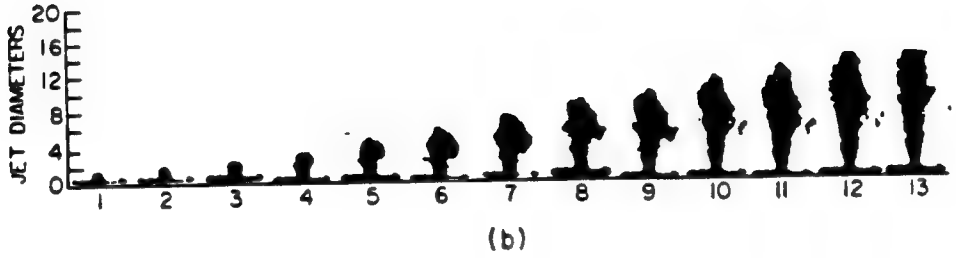

Fig. 1. Development of: a) a turbulent incompressible jet [7] (water in water, Re = 4 10^4); and b) an atomizing spray [8] (50% glycerol + 50% water into N_2).

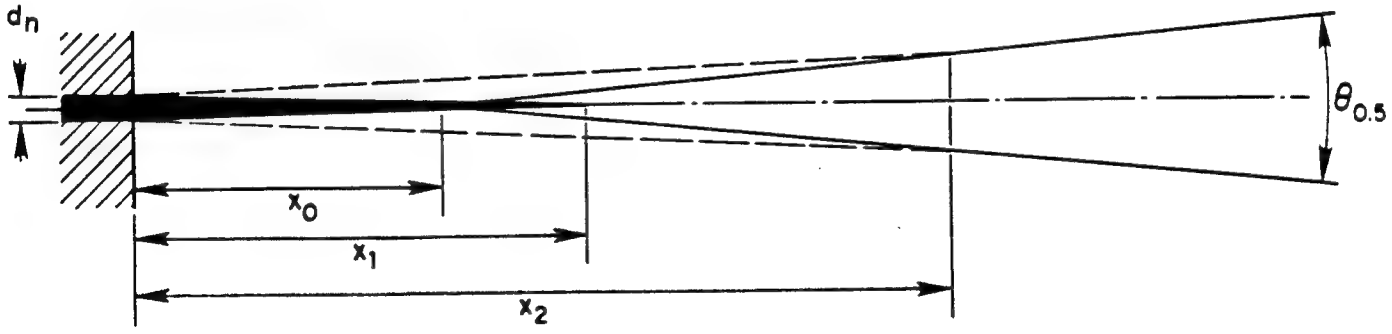

Fig. 2. Schematic structure of incompressible jets and full-cone sprays

the details of its structure are not clear, we expect the head vortex to be fed from its upstream side by the liquid coming from the nozzle and by the gas entrained by the liquid in the region between the head vortex and the nozzle. Again, looking at the spray divergence angle, we observe that this intermediate region appears to be in steady state as if the head vortex left a steady spray behind itself. It has also been argued that, in the laboratory frame, the head vortex travels at a fraction of the local steady state centerline velocity. Within the steady part, we cannot see the shear layer and an intact liquid core that would correspond to the potential core of the incompressible turbulent jet. But, as we shall see, there are reasons to believe that an intact liquid core exists and that its length is much longer than 10 nozzle diameters. Finally, at sufficient distance from the injector, enough ambient gas will have been entrained by the liquid to set up a flow field similar to that of fully developed incompressible jets but the length of the development region can be expected to be much longer than 50 nozzle diameters due to the density of the injected medium being greater than that of the ambient one.

Thus Fig. 2 can be seen also as outlining the steady state structure of sprays except that x_0, x_1, and x_2 are now larger than in incompressible jets by some factor, of which the dominant component is expected to be the liquid-to-gas density ratio. In other words, due to the greater density of the liquid, and the different mechanism by which a spray initially entrains the ambient gas, a spray maintains its momentum better than an incompressible jet and its development requires a longer distance. But, due to the entrainment process, all sprays achieve the structure of fully developed incompressible jets at sufficient distance from the nozzle. As we shall see, in direct injection engines the development length of fuel sprays is of the order of several hundred nozzle diameters, i.e. between 2 and 10 cm for nozzle diameters between 100 and 300 μm. Thus the development region is the one of primary importance in such applications.

To summarize terminology, x_1 is called the intact core length, or the break up length. It defines the end of the break up region after which the steady spray completes its development within the length x_2. Thus the breakup region is a fraction of the development region. Downstream of x_2 there is the fully developed region, also called the far field.

In the following, we will consider successively: the structure of the breakup region; the structure of the far field; modern models that, given the outcome of the breakup process, compute the steady and transient of sprays; some comparisons with detailed measurements; and some practical applications of these models. Much time will be spent on the breakup region because this region, whose length in engine environments may approach 100 nozzle diameters, is the most complex and the least understood quantitatively.

THE BREAKUP REGION

It is important to realize that different forces control the breakup of jets from cylindrical orifices under different conditions, thus defining different regimes for which different correlations, and sometimes opposite trends, are applicable. Some common regimes are listed below in the order in which they are encountered if the injection velocity is increased progressively while all the other parameters are kept constant [9]:

Rayleigh Jet Breakup Regime (Fig. 3a) - The breakup, which occurs many jet diameters downstream of the nozzle, yields drops whose diameter exceeds that of the jet. It is caused by the growth of axisymmetric oscillations of the jet surface, induced by surface tension.

First Wind-Induced Breakup Regime (Fig. 3b) - The breakup, which again occurs many jet diameters downstream of the nozzle, yields drops whose diameter is of the order of the jet diameter. In this case, the surface tension effect is augmented by the relative motion of the ambient gas and the jet which produces a static pressure distribution on the jet surface that accelerates breakup.

Second Wind-Induced Breakup Regime (Fig. 3c) - The breakup of the jet surface, which occurs some jet diameters downstream of the nozzle, yields drops whose average diameter is much smaller than the jet diameter. Droplet formation results from the unstable growth of short wavelength waves on the jet surface and is caused by the relative motion of the jet and the ambient gas. Here surface tension opposes the wave growth.

Atomization Regime (Fig. 3d) - The breakup of the outer surface of the jet occurs at, or before, the nozzle exit plane and results in droplets whose average diameter is much smaller than the nozzle diameter.

The atomization regime is the one of interest in engine applications and its mechanism of breakup is the subject of our discussion.

Since most detailed measurements of atomizing sprays are taken under steady conditions, it is important to establish that in an engine the state of the spray immediating downstream of the nozzle adjusts itself on a time scale that is much shorter than those over which significant changes occur in injection pressure and combustion-chamber gas

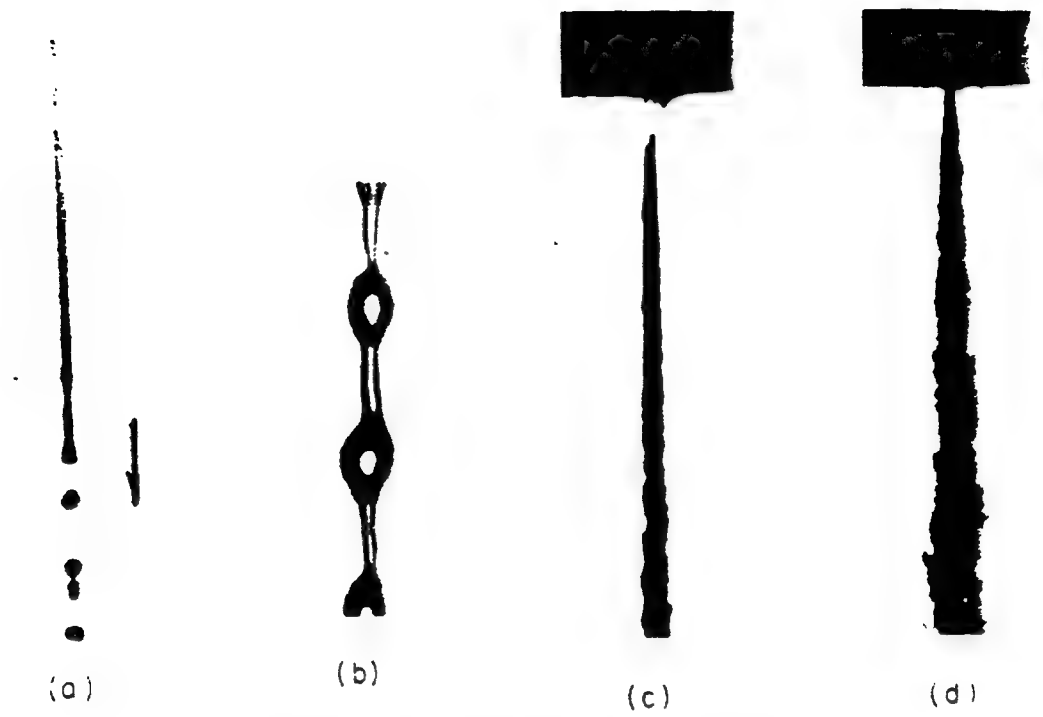

Fig. 3. Four regimes of liquid jet breakup [9]

condition. This quasi-steady situation allows one to use instantaneous injection pressure and chamber gas condition and steady state spray results to get the instantaneous condition of the spray immediately downstream of the nozzle. The quick adjustment of atomizing sprays in the immediate vicinity of the nozzle is demonstrated, for example, by ultrahigh speed films of the inception of atomizing jets such as that of Fig 1b. Stationary pressurized liquid and gas were separated by an electric fuse that closed the nozzle exit. Application of a sudden voltage pulverized the fuse and started the injection [8]. It was found that the stem of the spray near the nozzle achieves its steady configuration in times as short as the residence time of the liquid within the nozzle passage; in fact as soon as such stem could be identified. For velocities of O(100 m/s) and nozzle lengths of O(1 mm), the resident time of the fuel in the nozzle is O(10 μs). In engine applications, the time for the liquid and gas conditions to change significantly generally is no shorter than 100 μs so that the quasi-steady approximation is applicable. One could push the argument a little further and say that the quasi-steady approximation may be acceptable also up to about 10 nozzle diameters from the nozzle exit.

Thus one is justified in analysing steady state information in the vicinity of the nozzle exit and in using it in engine applications.

For engine-type sprays, even steady state measurements are very difficult in the vicinity of the nozzle because of the small lengths (10 to 100 μm) and large velocities (>100 m/s) involved. In fact the only quantity that can be measured with relative ease is the spray angle. Thus we will consider first extensive measurements of the initial spray angle in the immediate vicinity of the nozzle exit and later some data on the drop size and the intact core.

In a series of studies [9,10], spray angles in the immediate vicinity of the nozzle exit were measured from backlighted photographs over broad ranges of conditions and with a variety of nozzle geometries (Table 1 and Fig. 4). First, the influence of the various parameters on this angle was identified and then the most likely mechanism of atomization was deduced from it.

As far as influence is concerned, it was found that: Jet divergence angles increase with increasing chamber gas compression; jet divergence begins progressively closer to the nozzle exit, as the chamber gas is compressed, until it reaches the exit with no evidence of abrupt change; these variations are due to effects related to increases in the gas density, not in the gas pressure; jet divergence angles decrease with increasing liquid viscosity; jet divergence begins at

Table 1 Test Conditions of Steady, Initial Spray Angle Measurements [9,10]

	Ref. 9	Ref. 10
Test liquid	Water, glycerol, and their mixtures	Water, n-hexane, and n-tetradecane
ρ_ℓ (g/cm^3)	0.998 - 1.261	0.665 - 0.998
p_ℓ (MPa)	3.9 - 18.0	11.1 - 107.6
μ_ℓ (g/s•cm)	0.010 - 17.596	0.0032 - 0.0218
σ_ℓ (dyne/cm)	63.0 - 72.8	18.4 - 72.8
T_ℓ(K)	room temp.	room temp.
Ambient Gas	N_2, H_e, and X_e	N_2
$\rho_g x10^3$ (g/cm^3)	1.1 - 51.5	1.2 - 48.7
p_g (MPa)	0.1 - 4.2	0.1 - 4.2
$\mu_g x10^4$ (g/s•cm)	1.70 - 2.26	1.70
T_g (K)	room temp.	room temp.
Nozzle Geometries	9	13
d_n(μm)	343	254,343, and 660
L_n/d_n	0.5 - 85	≈ 0 - 50
Ta	$1.3x10^{-4}$-$1.6x10^3$	0.4 - 420
ρ_g/ρ_ℓ x 10^3	1.1 - 51.6	1.8 - 73.2

the nozzle exit once the liquid viscosity is decreased below a certain level and there is no evidence of abrupt change; for straight-wall nozzles with sharp inlet and outlet, jet divergence angles reach a maximum for length-to-diameter (L_n/d_n) ratios between 10 and 20 and then decrease with increasing nozzle L_n/d_n, for sufficiently small L_n/d_n, rounded inlet nozzles produce less divergent jets than sharp edged inlet nozzles; jet divergence commences at the nozzle exit at different gas density and liquid viscosity levels as the nozzle design is changed; relatively large variations in the injection velocity (or injection pressure) have little influence on the observed trends. In particular, it was found that in the atomization regime the parameters that have the greatest influence on the initial spray angle are the nozzle geometry and the gas-liquid density ratio. For Diesel applications, straight hole nozzles are often used with $3<L_n/d_n<8$ and $15\ 10^{-3} < \rho_g/\rho_\ell < 30\ 10^{-3}$. From Figs. 5 and 6 we see that the initial spray angle, θ, could be between 6° and 16° and that the effect of large variations in injection velocity may not be negligible due to the narrow range of ρ_g/ρ_ℓ. We also see that definite trends are not obvious within narrow ranges of ρ_g/ρ_ℓ and L_n/d_n. (Moreover, the exact distance from the nozzle at which the angle is measured, or different lighting and measuring techniques, may lead different authors to somewhat different values for θ). But the ranges of Figs. 5 and 6 and of Table 1 are much broader than those of immediate interest to engine applications and this breadth was very useful to assess the validity of the many and diverse atomization mechanisms that had been suggested [9].

Castlemen [12] guessed that atomization is due to aerodynamic interaction between the liquid and the gas leading to the growth of unstable waves on the liquid jet surface. Various authors analyzed this model, including Ranz [13] that brought attention to the theory of Taylor [14]. Also Levich [15] reports analyses of several aerodynamic-interaction regimes but mentions only briefly the effect of liquid viscosity that is included in the theory of Taylor.

DeJuhasz [16] proposed that the jet breakup process occurs within the nozzle itself and that liquid turbulence may play an important part. Schweitzer [17] suggested that the radial component of velocity in turbulent pipe flow could cause the immediate disruption of the jet at the nozzle exit. Other mechanisms based on liquid turbulence have been proposed by Holroyd [18] and Sitkei [19]. However, Bergwerk [20] argued that the turbulent velocity components in the Reynolds number range of interest are not of sufficient magnitude to explain the atomization phenomenon. He concluded that liquid cavitation phenomena inside the nozzle could create large amplitude pressure disturbances in the flow leading to atomization. Sadek [21] hypothesized that cavitation bubbles may influence the jet breakup process.

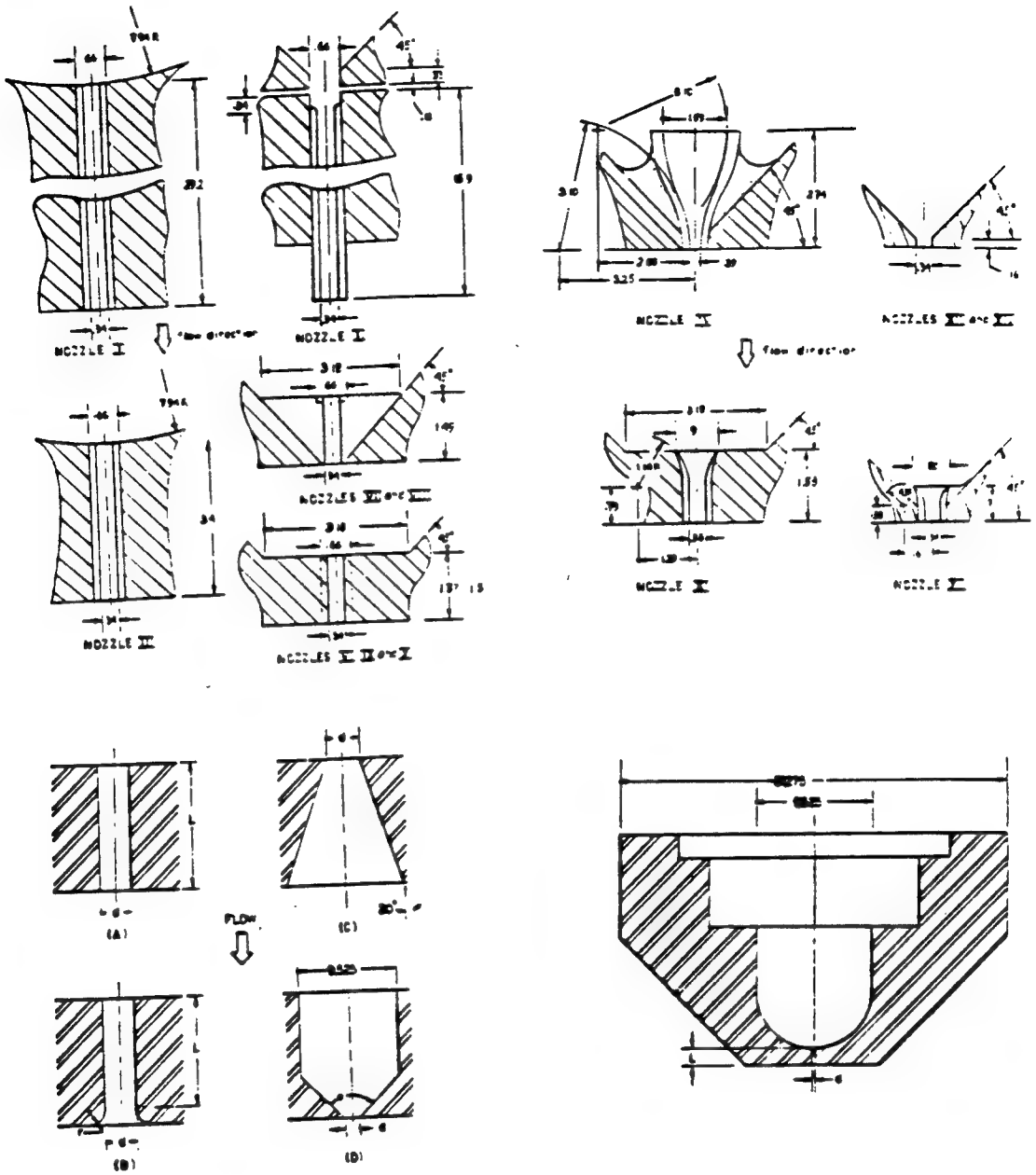

Fig. 4. Nozzle geometries of initial spray angle measurements [9,10]

Other authors have suggested that the jet breakup is due to velocity profile rearrangement. For example, Rupe [22] observed that high-velocity laminar liquid jets could be more unstable than fully developed turbulent jets. He reasoned that this is due to rearrangement in the cross-sectional velocity profile of the laminar jet once the constraint of the nozzle wall is removed at the nozzle exit. This redistribution of energy within the jet gives rise to radial velocity components which were thought to disrupt the jet. This effect is minimal for jets with flat exit velocity profiles which explained the greater stability that was observed for turbulent jets [9].

Another suggested atomization mechanism is the acceleration experienced by the fluid in the boundary layer on the nozzle wall at the nozzle exit caused by the abrupt change in the boundary condition on the flow. Shkadow [23] investigated the effect of changes in interface tangential stresses in a boundary layer stability analysis and confirmed the existence of unstable short wavelength surface waves.

Finally, liquid supply pressure oscillations have been noted by Giffen and Muraszew [1] to have an effect on the outcome of the atomization process. Since these supply pressure oscillations are commonly found in injection systems, it has been suggested that

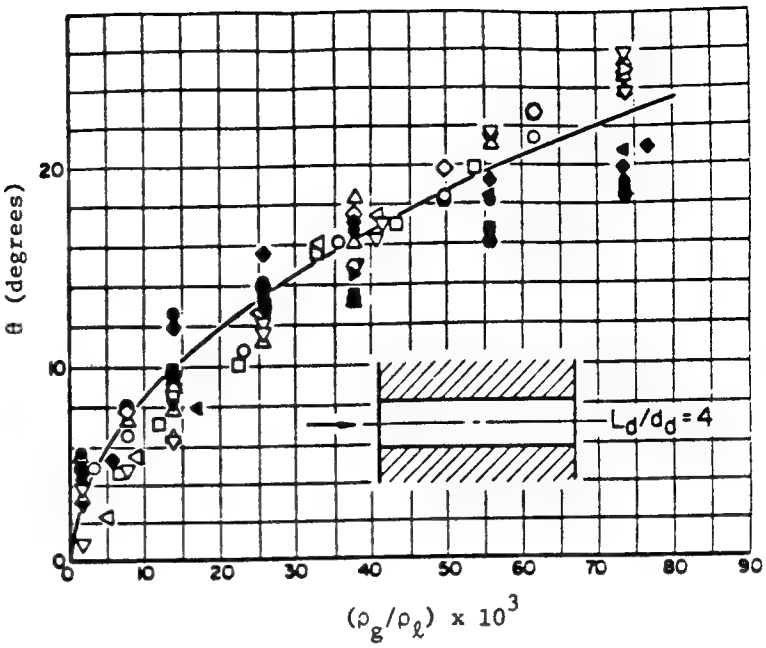

Fig. 5. Initial angle of atomizing jets versus density ratio for fixed nozzle geometry. Injections of glycerol-water, water, hexane, tetradecane into N_2, H_e, X_e, Ar at liquid pressures of 500-13,300 psi and D = 254, 343, and 610 μm. Room temperature. The continuous line is from Eq. 7 with $f_m^* = 3^{1/2}/6$ and $A_\theta = 4.9$ [10].

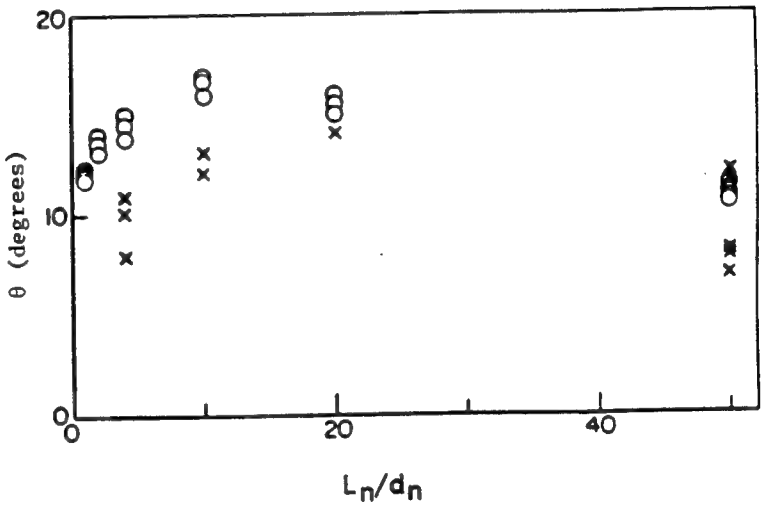

Fig. 6. Initial angle of atomizing jets versus nozzle length-to-diameter ratio: O Ref. 10 (n-hexane into N_2, d_n = 330-343 μm, Δp = 11 MPa, ρ_g/ρ_ℓ = 0.0346); X Ref. 11 (H_2O into N_2, d_n = 300 μm, p_g = 3 MPa, V_a = 120 m/s).

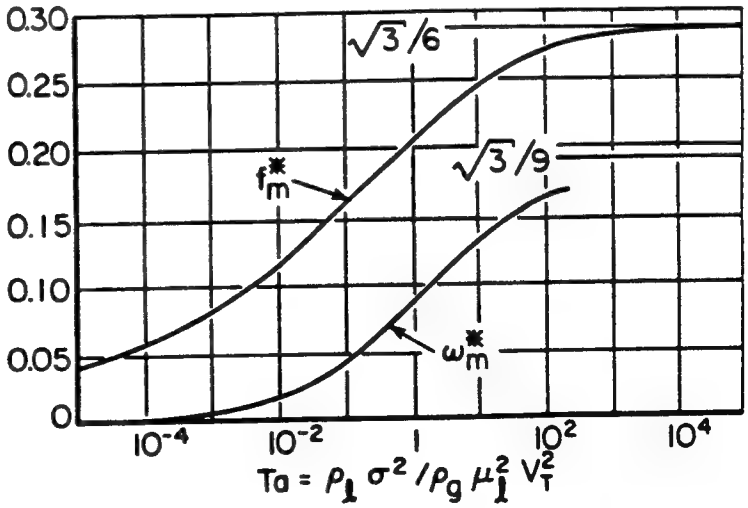

Fig. 7. Two functions [14] for the initial spray angle (Eq. 7), drop size (Eq. 9), and intact core length (Eq. 12).

they play an essential role in the atomization mechanisms itself.

None of the proposed mechanisms was found sufficient to explain the trends exhibited by the spray angle near the nozzle exit. Each hypothesis led to conclusions that were contrary to the measured trends [9,10]: If aerodynamic surface wave growth were the only mechanism controlling the jet divergence, the results shold be independent of the nozzle geometry; if pipe turbulence were the only controlling breakup agency, turbulent jets (from nozzles with large L_n/d_n ratios) should be the most unstable; if the rearrangement of the cross-section axial velocity profile of the jet were the only mechanism of breakup, Poiseuille flows (high viscosity jets) should be the most unstable; if liquid supply pressure oscillations were the only agency, jet atomization should not have occurred in the experiments of Refs. 9 and 10 in which the supply pressure was kept constant; if wall boundary layer exit velocity profile relaxation effects were the only mechanism, the jet breakup phenomena should be independent of the gas density and influenced by the radius of the outer edge of the nozzle; if cavitation were the only mechanism, atomization should not have resulted from cavitation-free nozzles.

However, the measured initial spray angle data did lend support to the hypothesis that aerodynamic interaction at the liquid-gas interface is a major component, but not the only component, of the mechanism of atomization. Indeed, for a fixed nozzle geometry, the measured initial spray angle behaves as predicted assuming that the aerodynamic interaction is the only mechanism of break up. Since aerodynamic interaction causes the breakup of jets at somewhat lower speed, when a short intact surface length is still observable, i.e. in the second wind-induced breakup regime, it is not unreasonable that it may continue to do so at somewhat higher speeds when the jet appears to diverge immediately at the nozzle exit. According to this view, the length of jet surface over which unstable surface waves grow becomes shorter and shorter as the speed is increased, due to the faster growth rate of the unstable waves, until it becomes of $\mathcal{O}$ (0.1 to 1 μm) and is no longer detectable. As previously stated, Castleman [12] was among the earlier supporter of this view, Taylor [14] produced theoretical results for it, and Ranz [13] was among the first to apply Taylor's results. Reitz [9,24] produced a dispersion relationship that covers Taylor's limit and other limits, including those corresponding to the regimes of Fig. 3 and those reviewed by Levich [15]. Since Taylor's theory leads to predictions for the initial angle of the spray, the initial size of the drops, and the length of the intact core, it may be advisable to outline it so as to point out its limitations as well.

Taylor studied the rate of growth of the perturbations of planar liquid surfaces induced by gases flowing over it. He considered the limit $\rho_g \ll \rho_\ell$ and included the effects of liquid viscosity and surface tension, but not those of the gas viscosity. His most relevant equations can be written as follows:

$$\delta = \delta_0 \exp(\omega t) \tag{1}$$

$$\dot{\delta} = d\delta/dt = \delta\omega \tag{2}$$

$$\lambda_m = 2\pi\sigma \lambda_m^* / \rho_g V_T^2 \tag{3}$$

$$\omega_m = 2 \left(\frac{\rho_g}{\rho_\ell}\right)^{1/2} \left(\frac{\rho_g V_T^3}{\sigma}\right) \omega_m^* \tag{4}$$

$$\delta_b = \lambda_m / A_\theta \tag{5}$$

$$\dot{\delta}_b = \delta_b \omega_m \tag{6}$$

$$\tan\frac{\theta}{2} = \frac{1}{A_\theta} 4\pi \left(\frac{\rho_g}{\rho_\ell}\right)^{1/2} f_m^* \tag{7}$$

$$\bar{d}_{d,0} = 2\delta_b/B_d' = 2\lambda_m/A_\theta B_d' \equiv \lambda_m B_d \tag{8}$$

$$= B_d \frac{2\pi\sigma}{\rho_g V_T^2} \lambda_m^* \tag{9}$$

$$\dot{V} = \frac{C_c' B_d^3 \pi \lambda_m \omega_m}{6 \ln(\delta_b/\delta_{b,0})}$$

$$= \left[\frac{2 C_c' B_d^3 \pi^2}{3 \ln(\delta_b/\delta_{b,0})}\right] \left(\frac{\rho_g}{\rho_\ell}\right)^{1/2} V_T f_m^* \tag{10}$$

$$d_j = d_j(0) - 2\dot{V} x/V_T \tag{11}$$

$$\frac{x_l}{d_j(0)} = \frac{V_T}{2\dot{V}} = C_c \left(\frac{\rho_\ell}{\rho_g}\right)^{1/2} f_m^{*-1} \tag{12}$$

Equation 1 relates the instantaneous amplitude of a surface perturbation wave to its frequency and initial amplitude. Equation 2 defines the growth velocity of the wave. Equations 3 and 4 identify the wavelength and frequency of the fastest growing of the unstable surface perturbation waves and λ_m^*, ω_m^* and $f_m^* = \lambda_m^* \omega_m^*$ (in Taylor's symbols respectively equal to x_m, $s/x_m^2\theta^{1/2}$, and $s/x_m\theta^{1/2}$) are functions of $Ta = \rho_\ell \sigma^2/\rho_g \mu_\ell^2 V_T^2$ and are plotted in Fig 7. The assumption is then made that most of the drops are formed by the breakup of the fastest growing of the unstable surface waves and Eq. 5 further states that the amplitude at which those waves break to form drops is a fraction of their

wavelength. Eq. 6 is a restatement of Eq. 2 applied to the waves that break and identifies the velocity of the wave at the moment of breakup. If V_T is the axial velocity of the surface of the liquid relative to the gas, then at breakup the drops have an axial velocity V_T and a radial velocity δ_b. Since $\tan(\theta/2) = \delta_b/V_T$, Eq. 7, that is the equation for the initial angle of the spray, is obtained combining Eqs. 3-6 so that the measurement of the initial angle of the spray can be used to determine the constant A_θ. In the measurements of Refs. 9 and 10, A_θ was found to be a function of the nozzle geometry.

The initial size of the drops is determined through Eq. 8 which states that the average initial drop diameter is proportional to the amplitude of the wave at breakup (combining Eqs. 8 and 3, one finds Eq. 9). If one assumes that the mass of the drop is equal to all the mass contained in a wave of length and width λ_m and amplitude δ_b, then the constant B_d is determined by the constant A_θ as $B_d = (3/\pi A_\theta)^{1/3}$. In general B_d can be regarded as an unknown constant, probably of order unity.

Notice that Taylor's solution is independent of any length scale of the problem, including the jet diameter, and that the effect of the liquid viscosity comes in only through the dimensionless number Ta. Increasing the viscosity of the liquid, ω_m^* and f_m^* decrease while λ_m^* increases so that the initial spray angle decreases while the initial drop size increases. At the other extreme, for inviscid liquids $\omega_m^* \to 3^{1/2}/9$, $f_m^* \to 3^{1/2}/6$, and $\lambda_m^* \to 3/2$.

To get the length of the intact core, Taylor reasoned as follows. The number of most unstable waves per unit area of liquid surface should be proportional to $1/\lambda_m^2$. Say it is C'/λ_m^2, where C' is a constant smaller than unity. From Eq. 1 the time of breakup would be $t_b = (\ln(\delta_b/\delta_{b,0})/\omega_m$, where δ_{b0}, is the initial amplitude of the fastest growing unstable wave and is unknown. Then the number of breakups per unit liquid surface area and time would be $C'/\lambda_m^2\, t_b$ and the volume of the drops formed per unit liquid surface area and time would be given by Eq. 10. Subtracting this time rate of mass loss from the mass flow rate of the liquid, equations are found for the local radius of the intact core (Eq. 11) and for the intact core length (Eq. 12). In Eq. 12 the constant C_c includes all the unkown constants of Eq. 10. To the extent that $B_d = (3/\pi A_\theta)^{1/3}$, C_c would be proportional to A_θ. That is, those processes that make the initial spray angle larger should also tend to make the intact core length shorter.

Thus Taylor's theory predicts the initial spray angle (Eq. 7), the initial average diameter of the drops (Eq. 9), and the shape and length of the intact liquid core (Eqs. 11,12), but some observations are in order. The velocity V_T that appears in Eqs. 1-12 is the velocity of the liquid surface relative to the gas. In the vicinity of the nozzle exit, such velocity should be some fraction of the injection velocity, because of the boundary layer of the liquid on the wall of the nozzle, but the exact value of this velocity is not known. It has a relatively small effect on the initial spray angle and the length of the intact core, because of the insensitivity of f_m^* to Ta, but a strong effect on the initial drop size because of V_T^2 in Eq. 9. All the equations are derived for small perturbations of an infinite planar liquid surface exposed to a gas that contains no drops. Such an ideal situation may be approached by the outer surface of the jet in the vicinity of the nozzle exit but it is not realized inside the spray as its axis is approached. Finally, an increasing number of assumptions are required to obtain Eqs. 7,9,11, and 12. Thus the equation for the initial spray angle should be the most reliable; that for the initial drop size should be applicable to the drops that are formed where the other surface of jet breaks but not necessarily to the drops that are formed when the inner part of jet breaks; and those for the shape and length of the core should be considered only indicative.

The prediction that in the atomization regime the initial value of the spray angle depends almost exclusively on the density ratio and the nozzle geometry is surprising, considering the many parameters that could effect it, but is generally born out by the measurements, as we have already seen (e.g. Figs. 5,6). However, it may be mentioned that, whereas the theory predicts that the spray angle decreases monotonically, if weakly, with increasing injection velocity, the measurements [10] show a mild opposite trend at sufficiently low values of ρ_g/ρ_ℓ (for $\rho_g/\rho_\ell < 35$ in Fig. 5).

Recently [25] the diameter of drops was measured at the edge of atomizing sprays in the immediate vicinity of the nozzle exit using backlighted photographs. The average diameter is given in Fig. 8 for the conditions of Table 2. When compared with Eq. 9, the measured average diameters exhibit the correct trends with respect to injection velocity, liquid properties and nozzle geometry (it should have little effect and none was observed) but the incorrect one with respect to gas density. Moreover the measured diameters are about a factor of 3 greater than reasonably expected. However when drop collisions and coalescence were accounted for, with a model that will be men-

Table 2: Spray Conditions for the Drop Size Measurements of Fig. 8 [25].

Series	Nozzle $d_n(\mu m)$-L_n/d_n	p_g (MPa)	ρ_g (kg/m^3)	Liquid	Δp_n (MPa)	V_a (m/s)	C_D	$Re_{n,a}$ x10^{-4}	$We_{n,a}$ x10^{-4}	No of Drops
1	335-4	1.48	17.0	n-C_6H_{14}	1.38	59.4	0.92	4.14	4.26	119
2	335-4	2.86	33.0	n-C_6H_{14}	1.38	52.4	0.81	3.65	3.32	109
3	335-4	1.48	17.0	n-C_6H_{14}	3.45	79.2	0.78	5.51	7.58	116
4	335-4	2.86	33.0	n-C_6H_{14}	3.45	92.8	0.91	6.46	0.41	111
5	335-4	1.48	17.0	n-C_6H_{14}	6.90	99.0	0.69	6.89	11.85	107
6	335-4	2.86	33.0	n-C_6H_{14}	6.90	111.0	0.77	7.73	14.89	117
7	335-10	1.48	17.0	n-C_6H_{14}	3.45	79.2	0.78	5.51	7.58	119
8	127-4	1.48	17.0	n-C_6H_{14}	3.45	78.1	0.77	2.06	2.79	114
9	335-4	1.48	17.0	n-$C_{14}H_{30}$	3.45	81.2	0.86	0.95	6.31	103

tioned presently, better agreement in trends and magnitudes was found [25]. Indeed between the jet surface where the drops are formed, that is not visible, and the edge of the spray, where the measurements were possible and were made, there is a region of dense spray in which it would be surprising if there were no drop collisions and coalescence. Coalescense was found to lead to the rapid increase in drop size, particularly in high gas densities.

Finally the data of Hiroyasu, et al. [11] support the prediction of Eq. 12 with respect to injection velocity and gas density; for $(C_c f_m^{*-1})$ they arrive at a value of 15.8. However the technique they used, based on measurement of the electrical resistance between the nozzle and a screen that could be moved axially, and the way that reduces their data, by using the signal intermittence and assuming that unconnected sprays carry no current, led them to overestimating the length of the intact core. Recently [26] their technique was applied again but with some modifications in the procedure and the analysis of the data. The initial intent was to measure both the length and the shape of the intact core. Thus a voltage was applied between the nozzle and fine needles, rods, and screens inserted at various axial and radial positions into atomizing full-cone water sprays and the electrical resistance offered by various parts of the spray was measured. The parameters of the experiment are given in Table 3. The results show that current is carried not only by intact liquid columns but also by

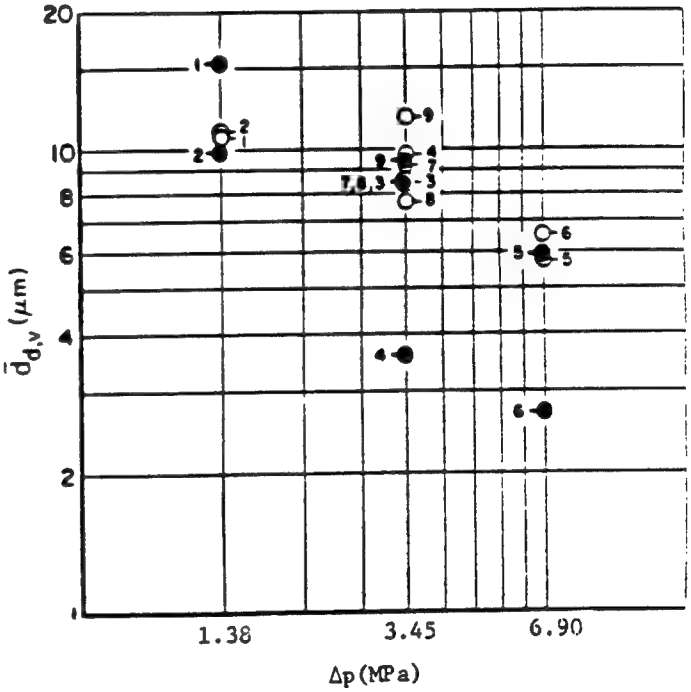

Fig. 8. Volume median diameter of drops in the immediate vicinity of the nozzle exit for the atomizing jets of Table 2: O measured; ● expected trends from Eq. 9 [25].

atomized unconnected sprays and even across such sprays. Thus the shape of the intact core could be deduced only in the vicinity of

the nozzle exit where the current carried by the unconnected spray was assumed to be small in comparison to that carried by the intact core. The length of the intact core was then obtained by extrapolation of the data taken in the vicinity of the nozzle exit and Eq. 12 was again found adequate but the value of $(C_c f_m^{*-1})$ was placed at about 7 (since Ta was 14.4 and 36.6, f_m would be about 1/4 and $C_c = 7/4$). In spite of the many uncertainties associated with this technique, the presence of an intact core and $C_c f_m^{*-1} = 7$ are reasonable statements also in comparison with the corresponding behavior of incompressible jets (but a direct comparison between the intact core of sprays and the potential core of incompressible jets is not obvious due to differences in the controlling forces.) Notice that even with $C_c f_m^{*-1} = 7$, the length of the intact core in Diesel engine sprays is estimated to be more than 50 nozzle diamaters.

To summarize then, any one of the quoted experiments does not provide adequate support for the supplemented-aerodynamic theory of atomization. But together they form a rather consistent picture. By comparison, the support for alternative theories is very meager. Thus one is justified in using Eqs. 7,9. and 12 to estimate the initial angle, drop size, and core length for the computation of engine sprays. However, more experimental information is needed on the size and shape of the intact core and, most of all, on the size of the drops that are formed by the breakup of the interior part of the jet. Unfortunately suitable experimental techniques, either non-perturbing or perturbing, do not seem to have been found for such measurements.

THE STEADY FAR FIELD

In an engine environment sprays do not reach their fully developed configuration because the distance available is too short and the gas is unsteady. However a brief review [27] of the far field of steady sprays is justified because: its equations have been used in engine modelling; understanding its configuration is useful as a limit; measurements are easier in it; and a necessary (but not sufficient) condition for the validity of a spray model is that the spray model accurately reproduces this far field.

The classical point source, boundary layer, similarity solution of Tollmien (see [4]) for incompressible jets is a satisfactory guide to the understanding of the global structure of the far field of full cone sprays. In principle, only one constant, such as C_t, that relates the turbulent diffusivity D_t to the kinematic momentum flow rate $\dot{M}_o^i/\rho^i$, is left undetermined by this solution and must be evaluated from measurements. Then the width of the jet increases as $(x-x_0)$, the centerline velocity decays as $1/(x-x_0)$, and the ratio of the entrained mass to the injected mass increases as $(x-x_0)$:

$$\dot{M}_o^i/\rho^i = C_o \pi V_i^2 d_n^2/4 \tag{13}$$

$$\dot{M}_{a,j}^i/\rho^i = C_D \pi V_i d_n^2/4 \tag{14}$$

$$D_t^i = C_t [C_o \pi V_i^2 d_n^2/4]^{1/2} \tag{15}$$

$$r_{0.5}^i = 8[\pi(2^{1/2}-1)/3]^{1/2} C_t(x-x_0) \tag{16}$$

$$V_{CL}^i = (3 C_o^{1/2}/16 \pi^{1/2} C_t) d_n V_i/(x-x_0) \tag{17}$$

$$\dot{M}_{a,e}^i/\dot{M}_{a,j}^i = (16\pi^{1/2} C_t C_o^{1/2}/C_D)(x-x_0)/d_n \tag{18}$$

In the above equations the constants C_o and C_D are used to relate the kinematic momentum flow rate and the volumetric flow rate to the ideal injection velocity through the injection velocity profile, and x_0 is the virtual origin. (In practice the determination of C_o, x_0 and of a needed additional constant (x_2) is nontrivial even for incompressible jets [28]).

But at this point the growth of the entrained mass and the local characteristic convection and diffusion times are of interest to us. Schlichting [4] gives $C_t = 0.0161$ and Eq. 18 shows that for $C_o = C_D = 1$, the entrained mass is already 10 times the injected one 22 nozzle diameters from the virtual origin. Local convection and diffusion times can be obtained dividing $(x-x_0)$ by V_{CL}^i from Eq. 17 and $r_{0.5}^{i2}$ by D_t^i from Eqs. 16 and 15. The two times are of the same order and increase as $(x-x_0)^2$.

For our sprays the injected medium is a liquid and the entrained medium is a gas, so that the initial entrainment process can be expected to differ from that of incompressible jets. But at sufficient distance from the injector, the injected mass must become negligible in comparison to the entrained one because past a certain distance their ratio grows as x. Downstream of such region, the momentum that leads to the entrainment of more ambient gas resides mostly with the ambient gas that was entrained earlier. That is, the structure of fully developed incompressible jets is recovered.

Imbedded in this far field there are drops that move in equilibrium with the gas. This is because the time for the drop velocity to relax to the local gas velocity, $\rho_\ell d_d^2/18\mu_g$, has an upper limit whereas the

fluid time continues to grow as x^2. Since there is a distribution of drop sizes and of eddy times, equilibration will be selective and dependent on conditions but at some appropriate distance from the injector, all sprays become incompressible jets dominated by the entrained ambient medium and drops move within them as markers of the motion of the ambient medium.

Having accepted the existence of this limit, Eqs. 13-18 can be modified for direct application to the far field of sprays. Following Thring and Newby [29] and Kleinstein [30], we can equate the axial momentum evaluated at the nozzle exit, where the density is ρ_ℓ, to that evaluated in the far field, where the density is ρ_g and the velocity profile is fully developed, and conclude that, as far as the far field is concerned, a liquid spray is an incompressible jet with an equivalent kinematic momentum flow rate of $(C_o \pi V_i^2 d_n^2/4)(\rho_\ell/\rho_g)$. Then Eqs. 13-18 give

$$D_t = D_t^i (\rho_\ell/\rho_g)^{1/2} \tag{19}$$

$$r_{0.5} = r_{0.5}^i \tag{20}$$

$$V_{CL} = V_{CL}^i (\rho_\ell/\rho_g)^{1/2} \tag{21}$$

$$\dot{M}_{a,e}/\dot{M}_{a,j} = (\dot{M}_{a,e}^i/\dot{M}_{a,j}^i)(\rho_g/\rho_\ell)^{1/2} \tag{22}$$

Parallel interpretations are that in the far field a spray is an incompressible jet from an equivalent nozzle diameter [29] of $d_n(\rho_\ell/\rho_g)^{1/2}$ or with an equivalent turbulence diffusivity [30] of $D_t^i(\rho_\ell/\rho_g)^{1/2}$. Notice however that the change in the virtual origin is not identified by this theory since this quantity is determined by the structure of the development region. Also the ratio of the entrained to the injected mass is now reduced by the factor $(\rho_g/\rho_\ell)^{1/2}$ indicating again that the development length will be longer. Finally, the ratio of the turbulent diffusion time to the drop relaxation time becomes

$$\frac{\tau_t}{\tau_{d,o}} = \frac{r_{0.5}^{i\,2}}{D_t^i} \left(\frac{\rho_g}{\rho_\ell}\right)^{1/2} \frac{18\,\mu_g}{\rho_\ell\, d_d^2} \tag{23}$$

The above equation can be used to estimate the distance from the virtual origin at which the velocity of a drop of a given size becomes nearly equal to the gas velocity (if local information is available, a more accurate estimate is obtained using $\tau_t = k/\varepsilon$).

Several authors have realized the existence of this limit and taken good advantage of it [31], but only recently detailed drop velocity measurements within sprays of this family have provided direct evidence of it.

The data of Fig. 9 were taken in the sprays of Table 3 under steady injections, at distances $> 300d_n$, and with the gas contained in a vessel of such size that a wall-free environment was approached [28]. (In Figs. 9-11, $\bar{V}_{inj} \equiv V_a$ and $d = d_n$). These sprays looked very much like those of Figs. 1b and 2d. Up to $r = r_{0.5}$, the radial profiles of the mean axial drop velocity and of the amplitude, skewness, and flatness of the fluctuation of the drop axial velocity are seen to fall within the range of the corresponding fluid quantities measured in incompressible jets by Wygnanski and Fiedler [32] by hot wire anemometry and by others [4-6,33,34] with hot wire anemometry and laser Doppler velocimetry. The same parallel was also found for the radial component of the drop velocity, for the centerline velocity decay and for the width. Also, the drop velocity was measured with various laser power levels, thus weighing the measurements in favor of drops of different sizes, and the results were found to be independent of it for $x > 300d_n$. If the drops had not been in equilibrium with the gas, their velocity would have depended on their size. Thus indications are that, within the error of the velocity measurements of [28], which was <10%, the full cone sprays of Table 3 very nearly achieve the incompressible jet and drop-gas equilibrium limits around $x = 300d_n$ and for $r \leq r_{0.5}$. For spray E, at $x = 200d_n$ the measurements indicate that drops are not in equilibrium with the gas and for $x > 300d_n$ but $r > r_{0.5}$ the evidence is inconclusive because of large errors in both HWA and LDV data [28].

There is no reason to expect that all sprays of Table 3 should reach equilibrium at the same axial distance, but the data were not sufficiently numerous or sufficienty accurate to differenciate. Thus the $300d_n$ location should be considered only indicative. By extrapolating backward the centerline velocity decay, and also checking the growth of the jet width, it was determined that $x_0 = 30d_n$ for $\rho_\ell/\rho_g = 13.7$ and $x_0 = 100d_n$ for $\rho_\ell/\rho_g = 39.1$. If the $300d_n$ range and the two values of x_0 are compared with the corresponding $50d_n$-$70d_n$ and $5d_n$-$10d_n$ values for incompressible jets [5,32], the reasonable conclusion is reached that full-cone sprays develop into incompressible jets but require a longer distance and that the increase is likely to be a function primarily of ρ_ℓ/ρ_g.

The density ratio, ρ_ℓ/ρ_g, which was the main parameter in the atomization process, is seen to be the main parameter also for the achievement and the structure of the far field of full-cone sprays.

As far as future work is concerned, it would be worthwhile to continue and study the structure of fully developed full-cone sprays for the reasons given at the beginning

Table 3: Spray Conditions for the Drop Velocity Measurements of Figs. 9-11 [28].

Series	p_g (MPa)	ρ_g/ρ_ℓ	Δp_n (MPa)	V_a (m/s)	Nozzle $d_n(\mu m)$ - L_n/d_n	x/d_n
A	1.48	0.0256	11.0	127	127-4	300,400,600,800
B	4.24	0.0732	11.0	127	127-4	300,400,500,600
C	4.24	0.0732	26.2	194	127-4	400,500,600
D	4.24	0.0732	11.0	149	76-4	300,600,700,800
E	1.48	0.0256	11.0	125	76-1	300

Liquid : n-hexane, $\rho_\ell = 665$ kg/m^3, $\mu_\ell = 3.2 \times 10^{-4}$ N·s/m^2, $\sigma_\ell = 1.84 \times 10^{-2}$ N/m. Gas : nitrogen. Room temperature.

of this section. For example, simultaneous LDV measurements of drop size and drop and gas velocities would provide more direct information on the equilibration process and would be useful to assess the drop drag equation and drop-turbulence interactions. The same measurements repeated under various rates of drop vaporization i.e. at various gas temperatures, would be useful to evaluate the drop vaporization equation and the effect on vaporization of drop-turbulence interactions.

Detailed measurements are not easy even in the far field. For example, in the region between 300 d_n and 800 d_n, in which the LDV drop velocity measurements of Fig. 9 were taken, the transmissivity of the laser light was less than 10% and nearly constant in the center of the sprays and less than 90% over about 90% of the width of the sprays [35]. However, one can consider just the outer part of non-vaporizing spray, or distances greater than 800 d_n, or vaporizing sprays. Then, for sufficiently dilute sprays, numerous optical techniques have been used to measure drop sizes in the range of 10 μm to 40 μm including imaging techniques [36,37], diffraction techniques [38,39], techniques based on the angular or polarization dependence of Mie scattering [40,41], interferometric or visibility techniques [42,43], and pulse height techniques [44-46]. The pulse height techniques are particularly interesting since they allow one to measure drop size and velocity simultaneously.

COMPUTATIONS

So far in our discussion of atomization and of the far field of full-cone sprays, we have relied almost exclusively on measurements to reach our conclusions. Now we would like to consider the extent to which the behavior of atomizing engine sprays can be reproduced by computations today. After giving some general references and a very brief outline of the background of current models, we will consider computations designed to assess the validity and accuracy of the models and then come application-oriented calculations.

The literature on modeling of sprays is very extensive. For an historic perspective and a broad view of the subject the reader may consult [31,47-53]. In particular, some analytical approaches are outlined in [47], a variety of physical and numerical modeling techniques in [47-53], details of some droplet processes in [50], and progress from one-dimensional to two-dimensional engine spray models in [51-52]. In short, concerning engine sprays with combustion, one-dimensional computations were performed in the early 70's [54]; initial two-dimensional calculations appeared in the late 70's [55]; and three-dimensional results have been obtained since early 80's [56-58]. This evolution parallels the increased speed and size of computers in the same time span.

Today, the prevailing numerical formulation for engine applications is based on

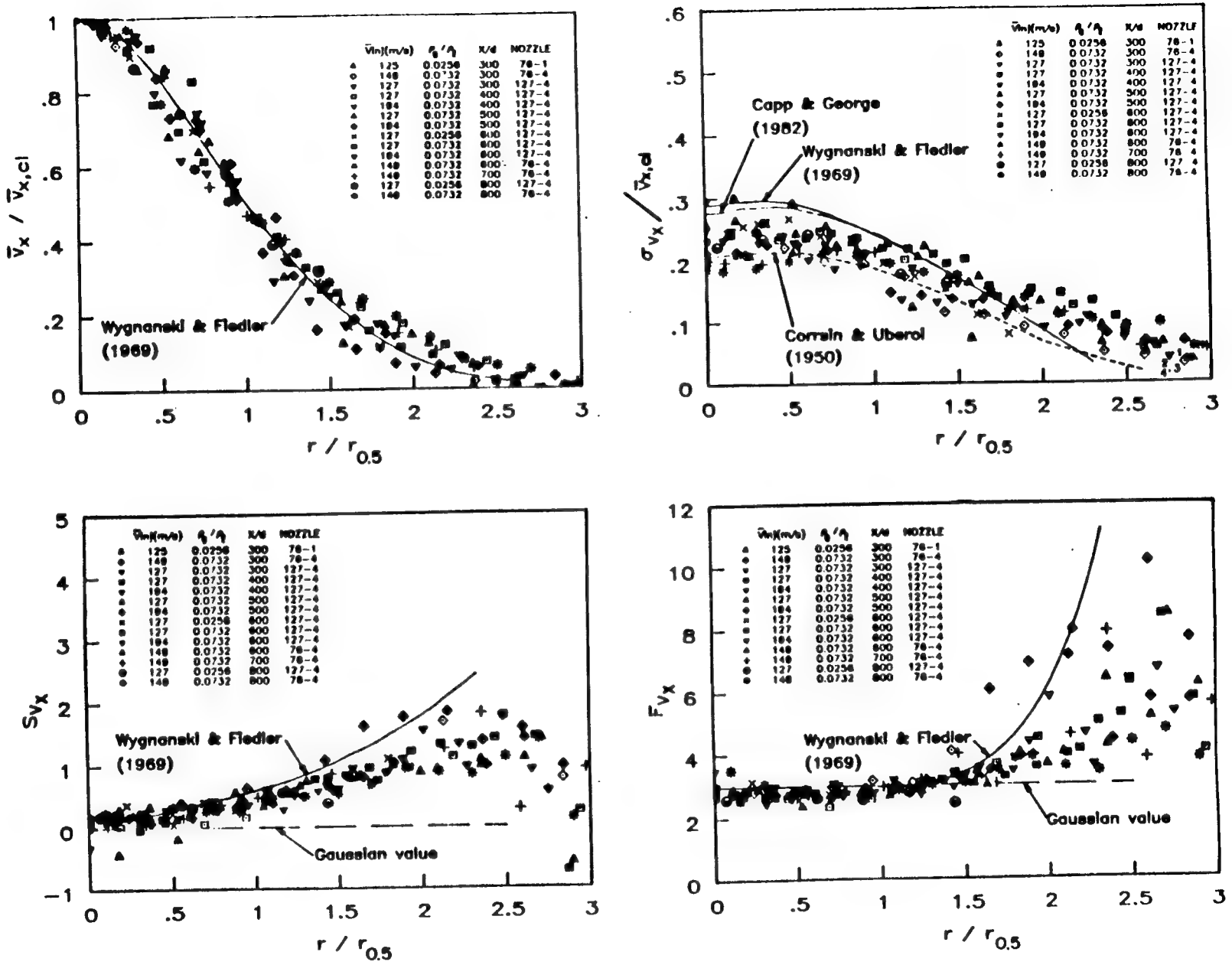

Fig. 9. Mean axial drop velocity and amplitude, skewness, and flatness of the fluctuation of the axial drop velocity for the atomizing sprays of Table 3 [28].

a Lagrangian treatment of the liquid phase and an Eulerian one of the gas phase. Early contributions to this approach go back at least to the late 50's [59,60]. The most significant recent improvements are the introduction of a stochastic treatment of the drop parcels by Dukowicz [61] and the inclusion of drop collisions and coalescence by O'Rourke [62,63].

Testing of Models

Comparisons with quantities measured in simplified controlled environments are better suited to assess the accuracy of multi-dimensional spray models than comparisons with engine quantities. In simplified environments the measurements can be more numerous, more accurate, and can be designed to test the various parts of the model separately. For example, the dynamic part of a model can be tested independently of its vaporization and combustion components using data from sprays injected in gases at suitably low temperature. Moreover, successful comparisons with a small number of engine data are not conclusive since they can always be obtained by adjusting injection or model parameters, and unsuccessful comparisons leave one to wonder which of the many model components that are active in an engine environment is at fault.

Thus Dukowicz [55,61] compared his two-dimensional results with tip penetration rates of non-vaporizing Diesel sprays measured by Hiroyasu and Kadota [64], O'Rourke and Bracco [62], and Kuo and Bracco [65] made comparisons with the same tip penetration rates and with the drop size distributions measured far downstream from the injector [64], and O'Rourke [63] also made comparisons of drop size and velocity distributions with those measured by Groeneweg [66] at several locations within a spray from a swirl atomizer. These early comparisons were encouraging but not very conclusive, as far as the validity of the models are concerned, because the experimental data were either not space-resolved, as in the case of tip penetration and downstream drop size, or incomplete. Also, these models were affected by several limitations, including the use of the incorrect constant diffusivity for the gas turbulence, given by Eq. 15, instead of the correct one (at least for the far field) given by Eq. 19. Nonetheless, this work was sufficient to demonstrate the importance of drop collisions and coalescence [62,65], to indicate substantial differences between the structure of continuously injected sprays and pulsating sprays [65], and to point out again that considerable errors may result if sprays are treated as gaseous jets under all engine conditions [65]. Most importantly, it was clearly realized that more precise, space-resolved measurements are needed to assess the accuracy of the models.

Unfortunately, well-documented, accurate, space-resolved measurements in Diesel-type sprays in controlled environments are still largely missing. The far field measurements of drop velocities of Fig. 9, taken in the sprays of Table 3 [28], already considered in the previous section, may constitute a beginning. Using the model described in the Appendix, that is as advanced and comprehensive as any available today, detailed comparisons were made with those measured drop velocities [67]. All mean quantities were reproduced with adequate accuracy but the amplitude of the fluctuations of the axial component of the drop velocity was underestimated by a factor of two. Typical comparisons are given in Figs. 10 and 11 [67]. The reason for the disagreement is still unknown but is probably related to the way the drop motion and turbulence are coupled in the model. The physics of this coupling is not well understood [31] but current work on particle-laden jets should be helpful [68-70].

On the positive side, efforts are often being made to check the individual components of spray models, that eventually are to be applied to engines, so that the causes of shortcomings are more readily identified. Thus, for example, the gas part of the spray model of the Appendix has reproduced with acceptable accuracy (with the same set of model constants) steady and transient pipe flows [71], steady and transient laminar, and turbulent incompressible jets [72], gas compression in valved and ported engines without and with swirl [73], and combustion in premixed charge engines [74]. But, as we have seen, as far as sprays are concerned, there are still difficulties even in reproducing non-vaporizing, non-combusting conditions.

Additional difficulties are expected when vaporization, and then combustion, are considered. One known problem is associated with the numerical method of introducing the drops into the gas. The original approach of injecting drops into the gas directly from the nozzle exit may be useful to get a general feel for the problem, but is inadequate to reproduce the structure of a spray with any accuracy, even for non-vaporizing sprays, because the exchange of momentum between drops and gas is functionally different from that between jets and gas. For the same reason, the success of ad hoc modifications is also bound to be very limited. For example, if one adjusts the initial drop size to match, and then only partially, such global parameters as the tip penetration rate, large drops results that do not agree with downstream drop size measurements. Howeever, it is interesting that if one starts the computations with the correct injection momentum flow rate, and uses the far field drop size (without coalescence) and gas turbulence, then one will recover the proper mean quantities of the steady-state far field at suf-

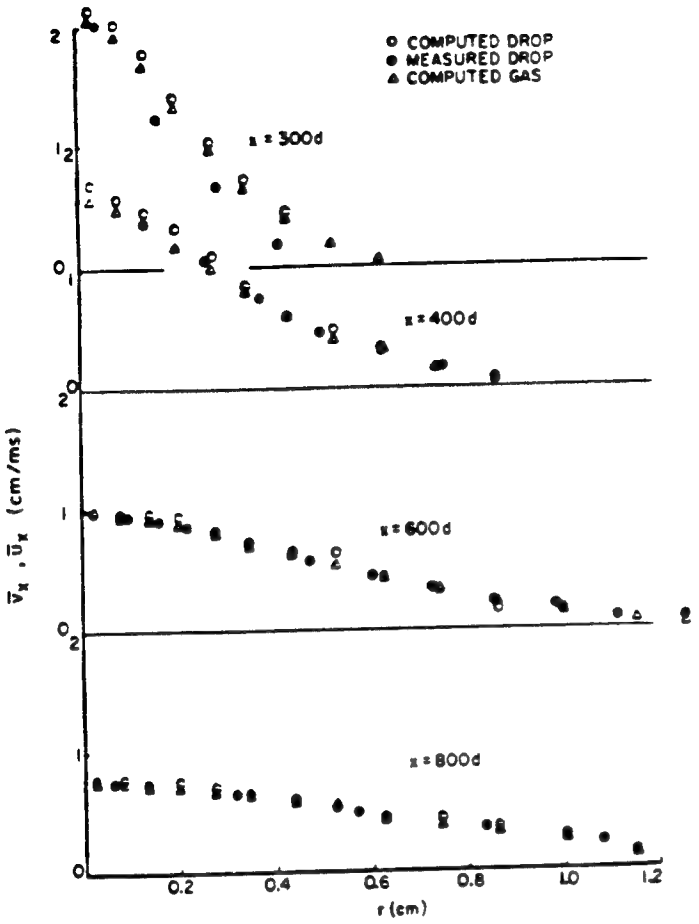

Fig. 10. Measured [28] mean axial drop velocity and computed [65] mean axial drop and gas velocity for spray A of Table 3.

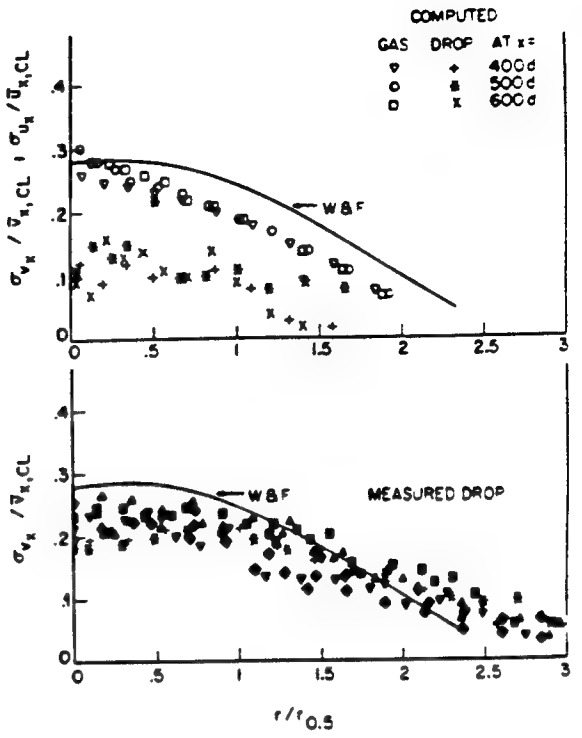

Fig. 11. Measured [28] amplitude of the fluctuation of the axial drop velocity and computed [65] amplitudes of the fluctuations of the axial drop and gas velocity for spray C of Table 3.

ficient distance from the nozzle because of the properties of the far field discussed earlier. But this positive affect is of no use in engine applications.

To lessen this problem, computations were started some 10 nozzle diameters downstream of the actual nozzle exit plane and by injecting a mixture of small drops (their size being given by Eq. 9) and entrained chamber gas, with both phases moving at the same velocity [62]. Using the experimental initial angle given by Eq. 7, it can be estimated that at such location the average center-to-center interdrop distance would be about two drop diameters in Diesel sprays and the gas volume-fraction would be about 90% if the liquid jet were already broken up into drops. Then the numerical injection velocity, which is somewhat lower than the actual one, is calculated from conservation of momentum. The advantages of this technique is that computations start with a jet and with a gas volume-fraction for which the equations of the Appendix can be applied (for lower gas volume-fractions, no useful constitutive equations seem to be available). Again, one recovers the proper mean quantities of the steady-state far field [67] including, it would appear, the far field drop size when drop collisions and coalescence are accounted for [65]. Because one starts from a jet, one comes closer to reproducing the development region but even for non-vaporizing sprays, sufficiently close to the injector, this approach fails too because it does not account for the intact liquid core.

When vaporization and combustion are present, the technique of starting from a mixture of drop and entrained ambient gas gives excessive vaporization near the nozzle and is particularly inadequate to reproduce the ignition delay of Diesel engines even if proper chemical kinetics is used. The original technique of injecting drops directly into the gas domain is even worse. Near the injector, the essential feature of an actual spray is its unmixed core and the small amount of drops available for mixing and vaporizations at its periphery. To come closer to simulating this situation, a line-source drop injection technique was developed [75] in which the length of the intact core is assumed to be long in comparison to the nozzle radius and drops are injected into the gas from a line source along the axis of the spray. During the transient, the tip of the line source penetrates the gas at a fraction

of the ideal injection velocity until it reaches the steady-state length given by Eq. 12. The idea of injecting drops into the gas from their generating surface was used with some success in the reproduction of the measured drop size in the immediate vicinity of the nozzle exit [25]. Although preliminary results are encouraging, there remain at least two serious limitations: since the inner structure of a spray is not known, we still do not know how to specify the size of the drops formed there; even allowing for good numerical resolution computations can only consider cells in which the gas volume-fraction is greater than 90%, because, as previously stated, useful constitutive equations are not available for lower gas volume-fractions. At this time it is not known the extent to which practical applications will be handicapped by such limitations.

Applications

Given that several essential aspects of the structure of the development region of solid-cone sprays are not known, that difficulties exist in simulating correctly what is known, and that multi-dimensional spray models have undergone only minute controlled testing, it would appear that applications to engines are premature, but this is not the case.

First and foremost, they are the best computational tools engineers have and engineers have always made do with what they have. But also engine applications, such as those of [76-80,57], although imprecise, serve many useful general purposes: they increase the awareness of modellers to the sensitivity of their results to the many model assumptions and numerical parameters; they present the engine designer qualitative, if distorted, pictures of complex chamber events he cannot see otherwise; they stimulate experimentalists to obtain more detailed and accurate in-cylinder measurements; and they encourage engine research departments to consider these new tools. Most of all they force everybody to think of chamber processes with increased resolution and sophistication.

Finally, in some cases their contributions are already more specific. For example, Gosman and Johns [76] brought to the attention of everyone that sprays induce velocities and turbulence levels that are comparable to those produced by other chamber motions such as intake, compression, swirl and squish. This property should always be kept in mind when interpreting chamber events and selecting strategies to control the combustion process. At a more detailed level, Kuo et. al [78-80] have studied the possible contributions of some potential sources of unburned hydrocarbons in direct-injection Diesel engines and the effects of injection characteristics on vaporization and mixing, which are the heart of the Diesel combustion process.

However, it is imperative that engine research groups be aware of the untested, and often inadequate, aspects of available engine spray models and look at their computed results more to stimulate their own critical thinking and to get suggestions for the interpretation of complex experimental trends than as reproductions of reality.

CONCLUSIONS

For full-cone sprays, the breakup and the development regions are the most relevant to engine applications. The inner structure of the breakup region is still largely unknown. For non-vaporizing sprays, but in Diesel-type environments, the modeling of drop and gas processes is just beginning to be tested versus controlled experiments and there are questions particularly about drop-turbulence interactions. For vaporizing and combusting engine-type sprays, testing of the models versus measurements in controlled environments appear to be mostly missing. Nonetheless, while the development and testing of the models continue, engineering applications of available two- and three-dimensional spray models are to be encouraged because they provide information that would not be available otherwise, and force everyone to think of chamber processes with increased resolution and sophistication. Even though progress in the last decade has been impressive, engine spray models today must still be considered exploratory and learning, not predicting, tools.

NOMENCLATURE

A_θ	constant of the initial spray angle equation
B_d	constant of the initial drop size equation
c_p	average specific heat at constant pressure of gas
$c_{p,i}$	specific heat at constant pressure of species i in ga
c_ℓ	specific heat of liquid
C_c	constant of the intact core length equation
C_1, C_2, C_3, C_4	turbulence model constants, $C_1 = 1.5$; $C_2 = 1.9$; $C_3 = -1$; $C_4 = 0.09$
C_d	drop drag coefficent
C_D	nozzle discharge coefficient
C_o	constant relating kinematic momentum flow rate to ideal injection velocitv in jets

C_t constant relating turbulent diffusivity to kinematic moment flow rate in incompressible jets

d_d drop diameter

$\bar{d}_{d,v}$ $\int_0^{\bar{d}_{d,v}} dV_d/V_d = 0.5$ drop volume median diameter

d_j intact jet diameter at nozzle exit

$d_j(x)$ axially varying intact core diameter, $d_j(0) = d_j$

d_n nozzle diameter

D_t turbulent mass diffusivity

f drop number distribution, $f(\underline{x},\underline{v},r,T_d,t)$

f_m^* $\lambda_m^* \omega_m^*$ a dimensional function of Ta in Taylor's drop formation theory

F_{v_x} flatness of the fluctuation of the axial component of the drop velocity, $\overline{v_x'^4}/\overline{v_x'^2}^2$

$\underline{g}$ gravity acceleration

G source term for turbulence kinetic energy

h_g specific enthalpy of gas

$h_{g,i}$ specific enthalpy of species i in gas

h_ℓ specific enthalpy of liquid

$h_{\ell g,i}$ enthalpy of vaporization of species i

$\underline{\underline{I}}$ unit tensor

k turbulent kinetic energy

K_d drop transfer number

L_n nozzle length

$\dot{M}_{a,e}$ total entrained mass flow rate

$\dot{M}_{a,j}$ total injected mass flow rate

$\dot{M}_o$ total momentum flow rate

p static pressure

p_ℓ injector upstream liquid pressure

p_g injector downstream gas pressure

Pr_k = 1.0 constant of the turbulence model

Pr_ε = 1.3 constant of the turbulence model

r_d drop radius (= $d_d/2$)

$\dot{r}_d$ Lagrangian time rate of change of drop radius

$r_{0.5}$ jet half width at half the average axial centerline velocity

R universal gas constant

$Re_{n,a}$ $\rho_\ell V_a d_n/\mu_\ell$ jet Reynolds number based on the mass-mean injection velocity and the nozzle diameter

Re_d $\rho_\ell |\underline{u}-\underline{v}| d_d/\mu_g$ drop Reynolds number

S_{v_x} skewness of the fluctuation of the axial component of the drop velocity, $\overline{v_x'^3}/\overline{v_x'^2}^{3/2}$

t time

T temperature

Ta $\rho_\ell \sigma^2/\rho_g \mu_\ell^2 V_T^2$ liquid viscosity parameter in Taylor's theory of drop formation

T_d drop temperature

$\dot{T}_d$ Lagrangian time rate of change of drop

$T_{d,s}$ drop surface temperature

T^o reference temperature

$\underline{u}$ gas velocity

$\underline{v}$ drop velocity

V_a $C_D V_i$ mass-mean liquid injection velocity

V_{CL} centerline velocity

V_d drop volume

V_i $[2 \Delta p_n/\rho]^{1/2}$ ideal injection velocity

V_T relative liquid-gas velocity in Taylor's theory of drop formation

W_i molecular weight of species i

$We_{n,a}$ $\rho_\ell V_a^2 d_n/\sigma$ Weber number based on the mass-mean injection velocity and the nozzle diameter

x_0 location of virtual origin

x_1 end of potential or intact core

x_2 end of development region

x_j^o $d_j (\rho_\ell/\rho_g)^{1/2}$ reference jet axial length

Y_i mass fraction of gaseous species i

$Y_{gd,i}$ mass fraction of species i on the gas side of the drop surface

δ dirac delta function
wave amplitude

δ_D $C_4^{3/4} k^{3/2}/\epsilon$ turbulence dissipation length scale

Δp_n pressure drop across the nozzle

ϵ rate of dissipation of turbulence kinetic energy
liquid volume-fraction

η_{ab} collision efficiency of drops (or particles) a,b

η_c coalescence efficiency

θ spray full angle
gas volume-fraction

λ_g thermal conductivity of gas

λ_ℓ thermal conductivity of liquid

λ_m^* dimensionless wave length of fastest growing surface wave in Taylor's theory of drop formation. It is a function of Ta

μ_g gas viscosity

μ_ℓ liquid viscosity

ν_{ab} collision frequency of drops (or particles) a,b

ρ_g gas density (mass of gas per unit volume of gas)

ρ_ℓ liquid density (mass of liquid per unit volume of liquid)

β_g mass of gas per unit volume of mixture = $\theta\rho_g$

σ surface tension

σ_{ab} transition probability function for collisions of drops a and b.

σ_{v_x} standard deviation of the fluctuation of the axial component of the drop velocity, $\overline{v_x'^2}^{1/2}$

$\tau_{d,o}$ $\rho_\ell d_d^2/18\ \mu_g$ drop velocity relaxation time

τ_t turbulence characteristic time

$\underline{\underline{\tau_t}}$ turbulence stress tensor

τ_c drop-turbulence correlation time

ω_m^* dimensionless growth rate of fastest growing surface wave in Taylor's theory of drop formation. It is a function of Ta

ACKNOWLEDGMENTS

Support for this work was provided by the Department of Energy (Contract DE-AC-04-81AL16338), the Army Research Office (DAAG29-85-K-0028), General Motors, Komatsu, and Cummins Engine.

REFERENCES

1. Giffen, E. and Muraszw, A., "The Atomization of Liquid Fuels", John Wiley and Sons, N.Y., N.Y., 1953.
2. Taylor, C.F., "The Internal-Combustion Engine in Theory and Practice", M.I.T. Press, Cambridge, MA, 1968.
3. Obert, E.F., "Internal Combustion Engines", Inter. Textbook Co., Scranton, PA, 1970.
4. Schlichting, H., "Boundary-Layer Theory", McGraw-Hill Book Co., N.Y., N.Y., 1968.
5. Hinze, J.O., "Turbulence", McGraw-Hill Book Co., N.Y., N.Y., 1975.
6. Abramovich, G.N., "The Theory of Turbulent Jets", The M.I.T. Press, Cambridge, MA, 1963.
7. Rizk, W., "Experimental Studies of the Mixing Processes and Flow Configurations in Two-Cycle Engine Scavening", Proc. Inst. Mech. Eng., Vol. 172, pp. 417-437, 1958.
8. Reitz, R.D. and Bracco, F.V., "Ultra-High-Speed Filming of Atomizing Jets", Phys. Fluids, Vol. 22, pp. 1054-1064, 1979.
9. Reitz, R.D. and Bracco, F.V., "Mechanism of Atomization of a Liquid Jet", Phys. Fluids, Vol. 25, pp. 1730-1742, 1982.
10. Wu, K.-J., Su, C.C., Steinberger, R.L.,

Santavicca, D.A., and Bracco, F.V., "Measurements of the Spray Angle of Atomizing Jets", J. of Fluids Engineering, Vol. 105, pp. 406-413, 1983.
11. Hiroyasu, H., Shimizu, M., and Arai, M., "The Breakup of High Speed Jet in a High Pressure Gaseous Atmosphere", ICLASS-82, Madison, WI, 1982.
12. Castleman, R.A., Jr., "The Mechanism of Atomization Accompanying Solid Injection", NACA Report No. 440, 1932.
13. Ranz, W.E., "Some Eperiments on Orifice Sprays", Can. J. Chem. Eng., Vol. 36, 175-181, 1958.
14. Batchelor, G.K. (Editor), "Collected Works of G.I. Taylor", Cambridge Univ. Press, Cambridge, MA, 1958.
15. Levich, V.G., "Physicochemical Hydrodynamics", Prentice-Hall, Englewood Cliffs, NJ, 1962.
16. DeJuhasz, K.J., "Dispersion of Sprays in Solid Injection Oil Engines", Trans. A.S.M.E. (OGP), Vol. 53, p. 65, 1931.
17. Schweitzer, P.H., "Mechanism of Disintegration of Liquid Jets", J. Applied Physics, Vol. 8, p. 513, 1937.
18. Holroyd, H.B., "On the Atomization of Liquid Jets", J. Franklin Inst., Vol. 215, p. 93, 1933.
19. Sitkei, G., "On the Theory of Jet Atomization", ACTA Tech. Acad. Sci. Hungaricae, Vol. 25, p. 87, 1959.
20. Bergwerk, W., "Flow Pattern in Diesel Nozzle Spray Holes", Proc. Instn. Mech. Engrs., Vol. 173, p. 655, 1959.
21. Sadek, R., Communication to Bergwerk, Proc. Instn. Mech. Engrs., Vol. 173, p. 671, 1959.
22. Rupe, J.H., "On the Dynamic Characteristics of Free-Liquid Jets and a Partial Correlation with Orifice Geometry", J.P.L. Tech. Report No. 32, p. 207, 1962.
23. Shkadov, V.Ya., "Wave Formation on the Surface of a Viscous Liquid due to Tangential Stress", Fluid Dynamics, Vol. 5, p. 473, 1970.
24. Reitz, R.D. and Bracco, F.V., "Mechanisms of Breakup of Round Liquid Jets", Encyclopedia of Fluid Mechanics (N.P. Cheremisinoff, Editor), Gulf Publ, in press.
25. Wu, K.-J., Reitz, R.D., and Bracco, F.V., "Drop Sizes of Atomizing Jets", submitted for publication.
26. Chehroudi, B., Onuma, Y., Chen, S.-H., and Bracco, F.V., "On the Intact Core of Full-Cone Sprays", SAE Paper 850126, 1985.
27. Bracco, F.V., "Structure of High-Speed Full-Cone Sprays", Recent Advances in Gas Dynamics (C. Casci, Editor), AIAA Publication, in press.
28. Wu, K.-J., Coghe, A., Santavicca, D.A., and Bracco, F.V., "LDV Measurements of Drop Velocity in Diesel-type Sprays", AIAA J., Vol. 22, pp. 1263-1270, 1984.
29. Thring, M.W. and Newby, M.P., "Combustion Length of Enclosed Turbulent Jet Flames", 4th Symposium on Combustion, Willians and Wilkins Co., Baltimore MD, pp. 789-796, 1953.
30. Kleinstein, G., "Mixing in Turbulent Axially Symmetric Free Jets", J. Spacecraft, Vol. 1, pp. 403-408, 1964.
31. Faeth, G.M., "Evaporation and Combustion of Sprays", Progress in Energy and Combustion Science, Vol. 9, pp. 1-76, 1983.
32. Wygnanski, I. and Fiedler, H., "Some Measurements in the Self Preserving Jet", J. Fluid Mech., Vol. 38, pp. 577-612, 1969.
33. Corrsin, S. and Uberoi, M.S., "Further Experiments on the Flow and Heat Transfer in a Heated Turbulent Air Jet", NACA TR998, 1950.
34. Capp, S.P. and George, W.K., Jr., "Measurements in an Axisymmetric Jet Using a Two-Color LDA and Burst Processing", Int. Symp. on Appl. of LDA to Fluid Mech., Lisbon, Portugal, 1982.
35. Wu, K.-J., "Atomizing Round Jets", Princeton University, Department of Mechanical and Aerospace Engineering, Ph.D. Thesis 1612-T, 1983.
36. McCreath, C., Roett, M., and Chigier, N., "A Technique for Measurement of Velocities and Size of Particles in Flames", J. Phys., Vol. E5, pp. 601-604, 1972.
37. Takeuchi, K., Murayama, H., Senda, J., and Yamada, K., "Droplet Size Distribution in Diesel Fuel Sprays", Bulletin of the JSME, Vol. 26, pp. 797-804, 1983.
38. Swithenbank, J., Beer, J.M., Taylor, D.S., Abbot, D., and McCreath, G.C., "A Laser Diagnostic Technique for the Measurement of Droplet and Particle Size Distribution", AIAA Paper No. 76-69, AIAA 14th Aerospace Sciences Meeting, Washington, DC, 1976.
39. Ruscello, L.V. and Hirleman, E.D., "Determining Droplet Size Distributions of Sprays with a Photodiode Array", WSS/CI-81-49, 1981.
40. Jones, A.R., "Scattering of Electromagnetic Radiation in Particle Laden Fluids", Prog. Energy Combustion Sci., Vol. 5, p. 73, 1979.
41. Kerker, M., The Scattering of Light, Academic Press, N.Y., N.Y., 1969.
42. Farmer, W.M., "Measurement of Particle Size, Number Density and Velocity Using a Laser Interferometer", Applied Optics, Vol. 11, p. 2603, 1972.
43. Durst, F., "REVIEW - Combined Measurements of Particle Velocities, Size Distributions, and Concentrations", ASME Transactions, Vol. 104, p. 284, 1982.
44. Ungut, A., Ereaut, P., Yule, A.J., and

Chigier, N.A., "Measurement of Drop Size and Velocity in Vaporizing Sprays", ICLASS-82, Madison, WI, 1982.
45. Allano, D., Gouesbet, G., Grehan, G., and Lisiecki, D., "Comparative Measurements of Calibrated Droplets Using Gabor Holography and Corrected Top-Hat Laser Beam Sizing, with Discussion of Simultaneous Velocimetry", International Symposium on Applications of Laser Doppler Anemometry to Fluid Mechanics, Liston, Portugal, 1982.
46. Hishida, K., Maeda, M., Imasu, J., Hironaga, K., and Kano, H., "Measurements of Size and Velocity of Particle in Two-Phase Flow by a Three Beam LDA System", International Symposium on Application of Laser Doppler Anemoemtry to Fluid Mechanics, Lisbon, Portugal, 1982.
47. Williams, F.A., "Combustion Theory", Addison-Wesley, Reading, MA, 1965.
48. Harrje, D.T. (editor), "Liquid Propellant Rocket Combustion Instabilities", NASA SP-194, 1972.
49. Faeth, G.M., "Current Status of Droplet and Liquid Combustion", Progress in Energy and Comb. Science, Vol. 3, pp. 191-224, 1977.
50. Sirignano, W.A., "Fuel Droplet Vaporization and Spray Combustion Theory", Progress in Energy and Comb. Science, Vol. 9, pp. 291-322, 1983.
51. Bracco, F.V., "Introducing a New Generation of More Detailed and Informative Combustion Models", SAE Paper 741174, 1974, or SAE Transactions, Vol. 84, pp. 3317-3340, 1975.
52. Bracco, F.V., "Modeling of Two-Phase, Two-Dimensional, Unsteady Combustion for Internal Combustion Engines", Institution of Mechanical Engineers, Publication 1976-11, 1976.
53. Haselman, L.C. and Westbrook, C.K., "A Theoretical Model for Two-Phase Fuel Injection in Stratified Charge Engines", SAE Paper 780318, 1978.
54. Bracco, F.V., "Theoretical Analysis of Stratified, Two-Phase Wankel Engine Combustion", Combustion Science and Technology, Vol. 8, pp. 69-84, 1973.
55. Butler, T.D., Cloutman, L.D., Dukowicz, J.K, Ramshaw, J.D., and Krieger, R.B., "Towards a Comprehensive Model for Combustion in a Direct-Injection Stratified-Charge Engine", Proceedings of the GM Symposium on Combustion Modeling in Reciprocating Engines (1978), Plenum Press, NY, NY, 1980.
56. Markatos, N.C. and Mukerjee, T., "Three-Dimensional Computer Analysis of Flow and Combustion in Automotive Internal Combustion Engines, Trans. IMACS, Vol. 23, p. 354, 1981.
57. Duggal, V.K., Kuo, T.W., Mukerjee, T., Przekwas, A.J., and Singhal, A.K., "Three-Dimensional Modeling of In-Cylinder Processes in DI Diesel Engines", SAE Paper 840227, 1984.
58. Butler, T.D., Amsden, A.A., O'Rourke, P.J., and Ramshaw, J.D., "KIVA: A Comprehensive Model for 2-D and 3-D Engine Simulations", SAE Paper 850554, 1985.
59. Lambiris, S., Combs, L.P., and Levine, R.S., "Stable Combustion Processes in Liquid Propellant Rocket Engines", Fifth Colloquium of the Combustion and Propulsion Panel, AGARD, 1962.
60. Borman, G.L. and Johnson, J.H., "Unsteady Vaporization Histories and Trajectories of Fuel Drops Injected into Swirling Air", SAE 598C, 1962.
61. Dukowicz, J.K., "A Particle-Fluid Numerical Model for Liquid Sprays", J. Comp. Phys., Vol. 35, pp. 229-253, 1980.
62. O'Rourke, P.J. and Bracco, F.V., "Modeling of Drop Interactions in Thick Sprays and a Comparison with Experiments", The Institution of Mechanical Engineers, Publication 1980-9, 1980.
63. O'Rourke, P.J., "Collective Drop Effects on Vaporizing Liquid Sprays", Princeton University, Department of Mechanical and Aerospace Engineering, Ph.D. Thesis 1532-T, 1981.
64. Hiroyasu, H. and Kadota, T., "Fuel Droplet Size Distribution in Diesel Combustion Chamber", SAE Paper 74015, 1974.
65. Kuo, T.-W. and Bracco, F.V., "Computations of Drop Sizes in Pulsating Sprays and of Liquid-Core Length in Vaporizing Sprays", SAE Paper 820133, 1982.
66. Groeneweg, J.F., "The Statistical Description of a Spray in Terms of Drop Velocity, Size and Position", University of Wisconsin at Madison, Department of Mechanical Engineering, Ph.D. Thesis, 1967.
67. Martinelli, L., Reitz, R.D., and Bracco, F.V., "Comparisons of Computed and Measured Dense Spray Jets", 9th Int. Coll. on Dyn. of Expl. and Reactive Systems, Poitiers, France, 1983; AIAA Progress in Astr. and Aero. Series, Vol. 95, pp. 484-512, 1984.
68. Elghobashi, S.E. and Abou-Arab, T.W., "A Two-Equation Turbulence Model for Two-Phase Flows", Physics of Fluids, Vol. 26, pp. 931-938, 1983.
69. Modarress, D., Wuerer, J., and Elghobashi, S.E., "An Experimental Study of a Turbulent Round Two-Phase Jet", Chem. Eng. Commun., Vol. 28, pp. 341-354, 1984.
70. Mostafa, A.A. and Elghobashi, S.E., "A Two-Equation Turbulence Model for Jet Flows Laden with Vaporizing Droplets", to appear in the Inter. J. of Multiphase

Flow.
71. Kuo, T.-W., "On the Scaling of Transient Laminar, Turbulent, and Spray Jets", Princeton University, Department of Mechanical and Aerospace Engineering, Ph.D. Thesis 1538-T, 1982.
72. Kuo, T.-W. and Bracco, F.V., "On the Scaling of Impulsively Started Incompressible Turbulent Round Jets", J. Fluids Eng., Vol. 104, pp. 191-197, 1982.
73. Hayder, E., Varma, A.K., and Bracco, F.V., "A Limit to TDC Turbulence Intensity in Internal Combustion Engines", submitted for publication.
74. Abraham, J., Reitz, R.D., and Bracco, F.V., "Comparisons of Computed and Measured Pre-Mixed Charge Engine Combustion", submitted for publication.
75. Chatwani, A.U. and Bracco, F.V., "Computation of Dense Spray Jets", ICLASS-85, London, U.K., 1985.
76. Gosman, A.D. and Johns, R.J.R., "Computer Analysis of Fuel-Air Mixing in Direct-Injection Engines", SAE Paper 800091, 1980.
77. Gosman, A.D. and Harvey, P.S., "Computer Analysis of Fuel-Air Mixing and Combustion in an Axisymmetric D.I. Diesel", SAE Paper 820036, 1982.
78. Yu, R.C., Kuo, T.-W., Shahed, S.M., and Chang, T.W., "The Effect of Mixing Rate, End of Injection, and Sac Volume on Hydrocarbon Emissions from a D.I. Diesel Engine", SAE Paper 831294, 1983.
79. Kuo, T.-W., Yu, R.C., and Shahed, S.M., "A Numerical Study ofthe Transient Evaporating Spray Mixing Process in the Diesel Environment", SAE Paper 831735, 1983.
80. Kuo, T.-W. and Yu, R.C., "Modeling of Transient Evaporating Spray Mixing Processes - Effect of Injection Characteristics", SAE Paper 840226, 1984.

APPENDIX: A DENSE-SPRAY MODEL

The equations of the model for the transient and steady state of dense sprays are those of Refs. 62 and 67:

Spray Equation (1)

$$\frac{\partial f}{\partial t} + \nabla\cdot(f\underline{v}) + \nabla_{\underline{v}}\cdot(f\dot{\underline{v}}) + \frac{\partial}{\partial r}(f\dot{r}) + \frac{\partial}{\partial T_d}(f\dot{T}_d)$$

$$= \frac{1}{2}\iint_{ab} \nu_{ab}\, n_{ab} \{\sigma_{ab} - \delta(r-r_a)\delta(\underline{v}-\underline{v}_a)\,\delta(T_d-T_{d,a})$$

$$-\delta(r-r_b)\delta(\underline{v}-\underline{v}_b)\delta(T_d-T_{d,b})\}dr_a d\underline{v}_a dT_{d,a} dr_b d\underline{v}_b dT_{d,}$$

Gas Mass Equation (2)

$$\frac{\partial \hat{\rho}_g}{\partial t} + \nabla\cdot(\hat{\rho}_g\underline{u}) = -\iiint 4\pi r^2 \dot{r}\,\rho_\ell\, f dr d\underline{v} dT_d$$

Species Mass Equation

for volatile component (i = 1) (3a)

$$\frac{\partial \hat{\rho}_g Y_1}{\partial t} + \nabla\cdot(\hat{\rho}_g Y_1\underline{u}) = \nabla\cdot(\hat{\rho}_g D_t \nabla Y_1)$$

$$-\iiint 4\pi r^2 \dot{r}\rho_\ell\, f dr d\underline{v} dT_d + S_1$$

for non-volatile component (i=2,I) (3b)

$$\frac{\partial}{\partial t}\hat{\rho}_g Y_i + \nabla\cdot(\hat{\rho}_g Y_i\underline{u}) = \nabla\cdot(\hat{\rho}_g D_t \nabla Y_i) + S_i$$

Gas Momentum Equation (4)

$$\frac{\partial \hat{\rho}_g \underline{u}}{\partial t} + \nabla\cdot(\hat{\rho}_g \underline{u}\,\underline{u}) + \nabla p = \nabla\cdot\underline{\underline{\tau}}_t - \iiint[4\pi r^2 \dot{r}\underline{v}$$

$$+ \frac{4}{3}\pi r^3 \dot{\underline{v}}\,]\,\rho_\ell\, f dr d\underline{v} dT_d$$

where $\underline{\underline{\tau}}_t = \hat{\rho}_g D_t\,[\nabla\underline{u} + \nabla\underline{u}^T - \frac{2}{3}\nabla\cdot\underline{u}\,\underline{\underline{I}}\,]$

Gas Energy Equation (5)

$$\frac{\partial \hat{\rho}_g h_g}{\partial t} + \nabla\cdot(\hat{\rho}_g h_g \underline{u}) = \theta\left(\frac{\partial p}{\partial t} + \underline{u}\cdot\nabla p\right) + \nabla\cdot[\hat{\rho}_g c_p D_t \nabla T_g]$$

$$+ \underline{\underline{\tau}}_t : \nabla\underline{u} - \iiint f\rho_\ell \{4\pi r^2 \dot{r}[h_\ell(T_d) + \frac{1}{2}(\underline{v}-\underline{u})^2]$$

$$-\frac{4}{3}\pi r^3 [\dot{\underline{v}}_a\cdot(\underline{u} + \underline{u}' - \underline{v}) - c_\ell \dot{T}_d]\}\, dr d\underline{v} dT_d$$

Turbulence Kinetic Energy (6)

$$\frac{\partial \hat{\rho}_g k}{\partial t} + \nabla\cdot(\hat{\rho}_g \underline{u}k) = \nabla\cdot\left(\frac{\hat{\rho}_g D_t}{Pr_k}\nabla k\right) + G - \hat{\rho}_g\varepsilon$$

Rate of Turbulent Energy Dissipation (7)

$$\frac{\partial \hat{\rho}_g \varepsilon}{\partial t} + \nabla\cdot(\hat{\rho}_g \underline{u}\varepsilon) = \nabla\cdot\left(\frac{\hat{\rho}_g D_t}{Pr_\varepsilon}\nabla\varepsilon\right)$$

$$+ \frac{\varepsilon}{k}(C_1 G - C_2\,\hat{\rho}_g\varepsilon) + C_3\,\hat{\rho}_g\varepsilon\nabla\cdot\underline{u}$$

where

$$G = \underline{\underline{\tau}}_t : \nabla \underline{u} - \frac{2}{3} \rho_g k \nabla \cdot \underline{u}$$

and $D_t = D + C_4 k^2/\varepsilon$

Equations Determining Exchange Rates (8a-8e)

$$-\rho_\ell \dot{r} = \frac{\lambda_g}{c_p} \frac{Nu_g}{2r} \frac{Y_{gd,l} - Y_l}{1 - Y_{gd,l}}$$

$$-\rho_\ell \dot{r} = \frac{\lambda_g}{c_p} \frac{Nu_g}{2r} \left\{ \frac{c_p}{h_{\ell g,l}(T_{d,s})} \left[(T_g - T_{d,s}) - \frac{Nu_\ell \lambda_\ell}{Nu_g \lambda_g} (T_{d,s} - T_d) \right] \right\}$$

$$(Y_{gd,l}/W_l)/(Y_{gd,l}/W_l + Y_{g,I}/W_I) = p_l(T_{d,s})/p$$

where $W_I^{-1} = \sum_{i \neq l} (Y_i/W_i) / \sum_{i \neq l} (Y_i)$ and $Y_{g,I} = 1 - Y_{gd,l}$

$$\dot{T}_d = \frac{3}{2} \frac{\lambda_\ell}{\rho_\ell c_\ell r^2} Nu_\ell (T_{d,s} - T_d) + 3 \frac{\dot{r}}{r} (T_{d,s} - T_d)$$

$$\dot{\underline{v}} = \dot{\underline{v}}_a - \frac{1}{\rho_\ell} \nabla p - \underline{g}$$

where $\dot{\underline{v}}_a = \frac{3}{8} \frac{\rho_g}{\rho_\ell} \frac{|\underline{u} + \underline{u}' - \underline{v}|}{r} (\underline{u} + \underline{u}' - \underline{v}) C_d$

Equations of State (9a-9d)

$$p = \rho_g R T_g \sum_i (Y_i/W_i)$$

$$h_g = \sum_i Y_i h_{g,i}$$

$$h_\ell (T_d) = h_{g,l}(T_d) - h_{\ell g,l}(T_d)$$

$$h_{\ell g,l}(T_d) = h_{\ell g,l}(T^o) + h_{g,l}(T_d) - h_{g,l}(T^o) - c_\ell (T_d - T^o)$$

Equation 1 is Williams' spray equation [47] plus two terms that account for the possibility that otherwise-identical drops may have different temperature and for drop collisions and coalescence (the integral on the right hand side). The collision frequency between drops with subscript a and those with subscript b is

$$\nu_{ab} = f_a f_b \pi (r_a + r_b)^2 |\underline{v}_a - \underline{v}_b| . \qquad (10)$$

In Equation 1, the portion of the integrand within the brackets gives the sources (given by the transition probability function, σ_{ab}) and the sinks (given by the delta functions, δ) of drops of velocity $\underline{v}$ and radius r due to collisions between drops of classes a and b. In most applications, the collision efficiency η_{ab} is very nearly unity.

The transition probability function σ_{ab} determines whether the outcome of a collision is coalescence or separation. Its mathematical expression is given by O'Rourke [63]. The criterion for drop separation after collision is that the rotational energy of the coalesced drop pair exceeds the surface energy required to reform the original drops from the coalesced pair. For the resulting coalescence efficiency, η_c, which is the probability of coalescence given that collision has occurred, O'Rourke and Bracco [62] give the expression

$$\eta_c = \min (2.4 g(\xi)/We_{d,c}, 1.0) \qquad (11)$$

where

$$We_{d,c} = \rho_\ell |\underline{v}_a - \underline{v}_b|^2 r_a/\sigma, \; r_a < r_b, \; \xi = r_b/r_a$$

and $g(\xi) = \xi^3 - 2.4\xi^2 + 2.7\xi$.

In the present application, most of the colliding drops have radii of similar magnitudes so that $We_{d,c}$ is important, the coalescence efficiency is generally < 1.0, and drop re-separation (grazing collision) is significant.

In the gas phase, mass, momentum and energy conservation equations, the integrals on the right-hand sides represent the exchange functions. They are the sum over all drops at point $\underline{x}$ and time t of the time rates of mass, momentum and energy exchanges between each drop and the gas; thus they involve the time rate of drop radius change $\dot{r}$, velocity change $\dot{\underline{v}}$, and temperature change $\dot{T}_d$.

The time rate of drop radius change is found by solving simultaneously equations 8a-8c for $T_{d,s}$, $Y_{gd,l}$, and $\dot{r}$. Then $\dot{T}_d$ is obtained from (8d).

The drop acceleration $\dot{\underline{v}}$, given by equation 8e, has a contribution due to aerodynamic drag and one due to the mean pressure gradient which has been shown to be important in some applications [63]. In equations 8a-8e there are three unknown functions: the gas and liquid phase Nusselt numbers, Nu_g and Nu_ℓ, and the drag coefficient C_d. After a detailed survey of experimental and theoretical studies, O'Rourke and Bracco proposed the following correlations to account for the effect of the gas volume-fraction, θ,

$$C_d(\theta, Re_r) = 24 (\theta^{-2.65} + Re_r^{2/3} \theta^{-1.78}/6)/Re_r \qquad (12)$$

$$Nu_g = [2\theta^{-1.75} + 0.6(Re_r/\theta)^{1/2} Pr^{1/3}] (\ell n(1+K_d))/K_d \qquad (13)$$

where $K_d = (Y_{gd,l} - Y_l)/(1 - Y_{gd,l})$ is the drop transfer number, $Nu_\ell = 1$, $Pr = 0.7$, and

$$Re_r = 2\rho_g \mid \underline{u}+\underline{u}'-\underline{v} \mid r_d/\mu_g.$$

The effect of turbulence on the gas phase is accounted for by the terms involving D_t in equations 3-5, where D_t is the turbulent diffusivity which is found from the turbulent kinetic energy and its rate of dissipation as shown in equations 6 and 7 [67]. The turbulence effects on the drops are calculated by adding to the mean gas velocity, $\underline{u}$, a fluctuating component, $\underline{u}'$, when computing the aerodynamic drag force and the gas phase Nusselt number. $\underline{u}'$ is chosen randomly from an isotropic Gaussian distribution with mean square deviation k2/3, where k is the turbulence kinetic energy. For each drop, after a turbulent correlation time τ_c, a new value of $\underline{u}'$ is chosen and τ_c is given by

$$\delta_D = \int_t^{t+\tau_c} \mid \underline{v}(t') - \underline{u}\ (t') \mid dt' \qquad (14)$$

where $\underline{u}\ (t')$ is the mean gas velocity at the drop position at time t' and δ_D is the dissipation length scale

$$\delta_D = C_4^{3/4}\ k^{3/2}/\epsilon. \qquad (15)$$

A detailed derivation and discussion of the equations of the dense spray model is [63]. It should be noted that the above equations are expected to be valid only for gas volume-fractions greater than 90%.

For the numerical solution of the above equations, it is necessary to specify the initial size, velocity, and temperature of the drops and the point, line, or surface from which they enter the gas. The correlations most often used are those derived from the supplemented aerodynamic-interaction theory of jet breakup [9,10].

APPENDIX D

LDV Measurements of Axial Drop Velocity in Evaporating, Dense Sprays

P. G. Felton,* B. Chehroudi,* and F. V. Bracco†
Princeton University, Princeton, New Jersey
and
Y. Onuma‡
Toyohashi University of Technology, Toyohashi, Japan

The axial component of the drop velocity was measured by laser Doppler velocimetry (LDV) within steady hexane-into-nitrogen sprays from a cylindrical nozzle at gas temperatures from 300 to 500 K. Also varied were the injection velocity and the gas-to-liquid density ratio. It was found that the gas temperature had no effect on the mean centerline velocity for distances smaller than 200 and greater than 650 nozzle diameters. At short distances, the core of the spray is not sensitive to the gas temperature; at long distances, the large amount of entrained gas renders inconsequential the degree of vaporization. Beyond 300 nozzle diameters, so much gas has been entrained that the mean axial velocity approaches the fully developed incompressible jet structure. The approach is accelerated by higher gas temperatures and gas-to-liquid density ratios. The axial drop velocity fluctuation amplitude responds to variations in gas temperature similarly to the mean axial drop velocity. Skewness and flatness indicate nearly Gaussian distributions near the axis and rapid increases beyond the half-radius and differ somewhat from those of incompressible jets, possibly because small drops vaporize fast and large ones do not follow the flow as closely as the small ones.

Nomenclature

C, C_l, C_g = constants of Eqs. (1) and (2)
d = nozzle orifice diameter, μm
L = nozzle passage length, μm
P = pressure, MPa
$r_{0.5}$ = half-radius of the drop axial velocity profile (radius at half peak velocity), m
T = temperature, K
U = gas velocity, m/s
V = liquid velocity, m/s
V_i = ideal injection velocity, m/s
X = axial distance from nozzle exit, m
X_0 = virtual origin, m
ΔP = effective injection pressure, MPa
ρ = density, kg/m^3

Superscript
$(\bar{\ })$ = mean value

Subscripts
cl = centerline value
g = gas property
j = jet property
l = liquid property
rms = root mean square
x = axial component

Received Sept. 2, 1986; revision received Sept. 30, 1987.

*Research Staff, Department of Mechanical and Aerospace Engineering.
†Professor, Department of Mechanical and Aerospace Engineering. Member AIAA.
‡Professor, Department of Energy Engineering.

Introduction

THE breakup of liquid jets is achieved through a large variety of atomizers for a large variety of applications.[1,2] The breakup increases the surface-to-volume ratio of the liquid and, thus, increases the rates of mass, momentum, and heat transfer, and the vaporization rate. In the case of diesel engines, poppet, pintle, and multihole nozzles are used, the most common being the latter, which usually consists of a group of cylindrical holes from 100 to 300 μm in diameter.[3,4]

When a liquid is forced through a cylindrical hole into a gas, many modes of breakup are observed. In the one relevant to internal combustion engines, no outer intact length is observed and the jet starts to diverge at the nozzle exit. This regime, which has been termed the atomization regime, is reached at high injection velocities, on the order of 100 m/s for the fuels and conditions of engine applications.[5]

Due to their practical importance, many aspects of atomizing jets have been studied extensively. In the 1930s, significant data were gathered on global quantities, such as downstream drop size distribution, tip penetration rates, and average spray angles. More recent efforts have attempted to determine the structure of atomizing jets. For example, the outer part in the immediate vicinity of the nozzle exit[5,6] and the inner part in the same region[7,8] have been studied in detail. Recently, laser techniques have been used to measure drop velocity, drop size distribution, and liquid volume concentrations in sprays from air-blast atomizers, but so dilute as to transmit more than 90% of the light.[9-13]

The application of laser techniques to diesel-type sprays is made difficult by the high number density of droplets. Nevertheless, measurements of drop velocity by laser Doppler velocimetry (LDV) in nonvaporizing, steady, diesel-type, dense sprays produced by single-hole cylindrical nozzles injecting into compressed nitrogen atmospheres at room temperature have recently been reported.[14] In experiments by Wu et al.,[14] measurements were made in regions of the spray where the light transmission was as low as 2%. However, successful simultaneous measurements of drop size distribution have not yet been possible in such sprays due to the high drop number density.

drop number density in this region, the signals were much less noisy and increased laser power resulted in an increased data rate. The best position at which this change should be made was difficult to determine accurately; but, if the change was made at the wrong position, a sudden step was observed in the velocity profile. More recently, we have used two Bragg cells at different frequencies to give the required frequency shift rather than a down-mixer. This change resulted in less noisy signals and, thus, a smaller change in laser power was required, which substantially reduced this problem. Only axial velocity measurements were made.

The optical system was mounted on a traversing table, which could be moved in three dimensions while the spray chamber remained stationary. The probe volume could be positioned to ± 25 μm in each direction, and the spray axis was determined to ± 250 μm by locating the maximum velocity position; all subsequent positions were then made with reference to this point. The axial distance from the nozzle tip was determined to within ± 125 μm from photographs of the crossed beams and the nozzle tip. The data reported were measured along the diameter coplanar with the laser beams.

The Doppler frequency was measured with a TSI 1990 counter processor interfaced to a Hewlett-Packard 21MX minicomputer. The number of fringes set on the counter processor over which the time was measured was 8, except near the centerline close to the injector, where 16 fringes were sometimes used to reduce the noise. The use of such a small proportion of the available fringes ($\sim 10\%$) was, in part, to reduce trajectory bias,[15] which is particularly important at the spray edge. Also, the use of fewer fringes resulted in an increased data rate.

All of the measurements reported were made with steady sprays. The choice of LDV system parameters described earlier resulted in data rates less than 5 kHz, which guaranteed a total data acquisition time (> 0.4 s) significantly longer than the characteristic fluctuation time of the spray. Flash photography and stroboscopic observation showed spray structures at exposure times of 0.03 ms at distances from the nozzle on the order of 300 nozzle diameters, whereas such structures were not observed at exposure times of 1 ms. For each position, 2048 validated data points were collected, a small fraction of which ($< 1\%$) were rejected on the criterion that they did not fall within 3.5σ of the mean. No measurement of the drop size distribution yet has been made in these sprays and, therefore, no correlation between drop size and velocity could be made directly.

Error Analysis

An extensive analysis of the experimental errors was carried out; details are given in Ref. 16 and a summary is reported in Ref. 14. With the exception of velocity biasing, the overall error is expected to be $\leq 5\%$ of the mean values.

The quantity measured by LDV is the average drop velocity, weighted by the frequency of arrival of the drops in the contour volume (drop flux). Therefore, the higher velocity drops give a higher data rate.[17-19] In the case of the seeded gas flow this is referred to as velocity biasing. Conversion from the flux-weighted average to the number-weighted average can be performed if the drop arrival rate is known. When the relative fluctuation amplitude is small, a simplified a posteriori conversion can be performed by weighting each realization by the inverse of the major velocity component.[17] This conversion is acceptable only as long as the relative fluctuation of the drop velocity is less than 30%, as the residence time can no longer be approximated by a single velocity component when this value is exceeded. An indication of this problem in our experiments occurred when drops having zero axial velocity passed through the measurement volume; in this case, a weighting factor of infinity would be used, leading to a singularity in the velocity distribution that greatly distorts the statistics of the distribution. For our sprays, the relative fluctuation intensity of the drop velocity was usually greater than 20% at the centerline and exceeded 30% a short distance from the axis, therefore, the conversion cannot be made. However, the multidimensional models used today for these sprays[20] yield the same flux-weighted drop velocity distributions as measured by LDV. Therefore, corrections for velocity biasing are unnecessary and were not made.

Results and Discussion

The experimental conditions examined are listed in Table 2. The same nozzle was used throughout the experiments, the discharge coefficient of which was determined from the measured ΔP and volumetric flow rate and was found to be 0.7. Two gas-to-liquid density ratios, two injection pressures, and three gas temperatures were used in the main series of tests, and three additional gas temperatures were used in one case. The gas pressure was varied to ensure constant gas density when the temperature was changed. In the experiments, at the lower value of the density ratio (0.0144), it was impossible to obtain data at some of the axial distances due to the high optical density of the spray, this was particularly so in the case of the high injection pressure (33 MPa). Also at the furthest axial distance ($X/d = 650$) and the highest temperature (550 K), insufficient droplets were present to obtain meaningful data.

First, we shall consider the mean drop velocities followed by the fluctuation of the drop velocity. As in Ref. 14, the incompressible jet data of Wygnanski and Fiedler[21] are included for reference and comparison only.

The effect of gas temperature on the centerline mean velocity is shown in Fig. 3. Close to the nozzle ($X/d = 200$) little effect is seen; at the medium distances ($X/d = 300$ and 400), the mean velocity decreases as the gas temperature is increased. Further downstream ($X/d = 650$), the drop velocity is again almost independent of gas temperature. If these velocities are normalized by the centerline injection velocity and plotted against the axial distance normalized by the jet diameter multiplied by the square root of the liquid-to-gas density ratio, the plot shown in Fig. 4 results. At sufficient distance from the injector, the velocity ratio depends only on $X/d_j\ (\rho_l/\rho_g)^{1/2}$. The initial diameter of the liquid jet, d_j, was 106 μm, as measured by Chehroudi et al.,[8] and the straight line is the incompressible jet limit.[21] The approach to the incompressible jet limit agrees well with the data on isothermal sprays by Wu et al.[14] and previous work on other types of jets.[21-24] It should be noted that the jet injected at the higher density ratio approaches the straight line earlier than the one injected at the lower density ratio, and higher gas temperatures also favor an early approach to the limit.

Table 2 Spray conditions

ρ_g/ρ_l	T_g, K	P_g, MPa	ΔP, MPa	X/d
0.025	350	1.726	11	200, 300, 400, 650
0.025	450	2.219	11	200, 300, 400, 650
0.025	550	2.713	11	200, 300, 400
0.0144	300	0.854	11	400
0.0144	350	0.996	11	300, 400, 650
0.0144	400	1.137	11	400
0.0144	450	1.281	11	300, 400, 6.
0.0144	500	1.425	11	400
0.0144	550	1.566	11	300, 400, 650
0.0144	350	0.996	33	650
0.0144	450	1.281	33	400, 650
0.0144	550	1.566	33	400
Liquid temperature 320 K ± 5 K				

The effect of temperature on the mean drop velocity profile is shown in Fig. 6 for a density ratio of 0.0144 at an axial distance of 400 diameters. In the central portion of the spray, from the centerline to a radius of approximately 2 mm, the mean velocity decreases as the gas temperature is increased. From a radius of 2 mm to the edge of the spray, the mean velocity increases as the gas temperature is increased; thus, we find again that the effect of increased gas temperature is to give a more fully developed spray. Two causes for this effect can be identified that the current experiments are unable to distinguish. First, the higher gas temperatures promote vaporization of the liquid and the gas formed loses its momentum to the surrounding gas more rapidly than a spray. Second, the gas entrained into the spray is cooled by the injected liquid, thus increasing the density of the gas near the spray core. In the isothermal spray, an increase in gas density was found to lead to an increase in the spray angle and a reduction in the centerline drop velocity[14,16,28] since the increased gas density again leads to more rapid momentum transfer. We can now go back to the trends pointed out in Fig. 3 and say that, sufficiently near the injector the spray centerline, velocity is influenced little by the gas temperature because most of the momentum is still with the spray. Sufficiently far from the injector, most of the momentum has been transferred to the entrained gas (whether the spray has vaporized or not), and the temperature difference within the spray has decreased so that the gas temperature is unimportant again. It is the intermediate development region of the spray that is influenced by the gas temperature, in that higher temperature promotes faster vaporization and quicker development of the spray.

The fluctuating components show similar effects with temperature. For the same experimental conditions as given earlier, the radial profile of the fluctuation amplitude of the drop axial velocity is plotted for several gas temperatures in Fig. 7. The profile is characterized by a local minimum on the centerline rising to a maximum at a radius of 2 mm followed by a steady decay toward the outer edge of the spray. Similar behavior was observed by Capp and George[25] for incompressible jets, which they attributed to the production of turbulent kinetic energy by the mean shear stress. As the gas temperature is increased, the fluctuation amplitude decreases and the minimum becomes less pronounced. Increase in the temperature beyond 450 K results in little further change in the fluctuation amplitude.

If the mean velocity profiles are normalized by their respective centerline velocities and the radial distance scaled by the half-radius of the velocity profile, then a self-similar profile results (Fig. 8). This profile agrees with that obtained by Wu et al.[14] for isothermal sprays and the results of Wygnanski and Fiedler[21] for incompressible jets. At dimensionless radial distances up to 1.2, the scatter of the points is small, but further out, where the effects of evaporation would be expected to be greatest, the scatter increases noticeably. The relative fluctuation amplitude also shows self-similar profiles as observed by Wu et al.[14] (Fig. 9). At the outer edge of the spray, the relative fluctuation amplitude exceeds that observed by Wygnanski and Fiedler[21] and comes closer to the observations of Baker[29] who used LDV in an incompressible jet. The

Table 3 Virtual origin as a function of T_0 and ρ_g/ρ_l

$X_0/d_j(\rho_g/\rho_l)^{1/2}$	T_0, K	ρ_g/ρ_l
25 ± 1	350	0.0144
14 ± 1	550	0.0144
17 ± 1	350	0.025
5 ± 1	550	0.025
16	300	0.0256[14]

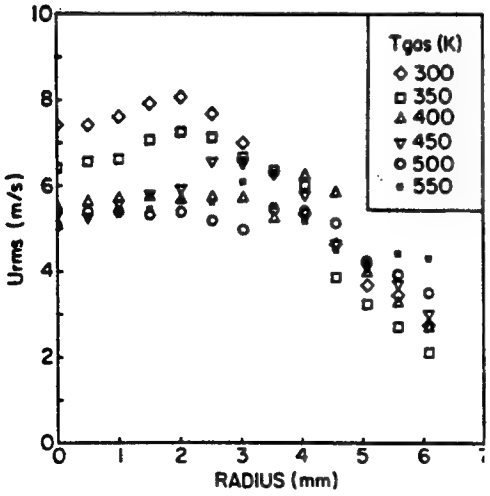

Fig. 7 Fluctuation amplitude of the drop axial velocity vs radius for various gas temperatures: $X/d = 400$; $\rho_g/\rho_l = 0.0144$.

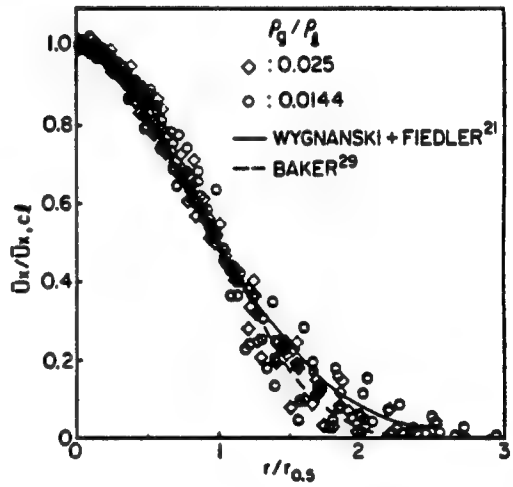

Fig. 8 Self-similar profile of the mean drop axial velocity for all the data of Table 2.

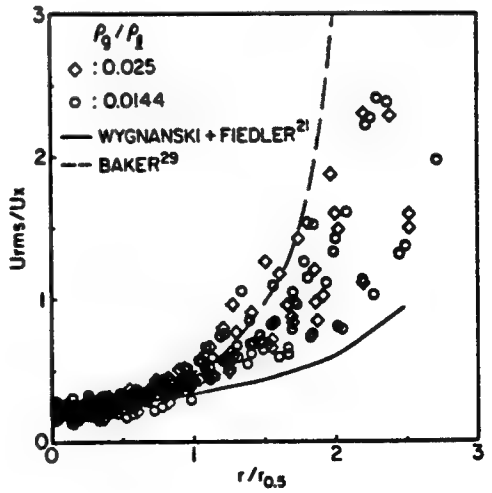

Fig. 9 Self-similar profile of the relative fluctuation amplitude for all the data of Table 2.

[10]Jackson, T. A. and Samuelson, G. S., "Detailed Characterization of an Air Assist Atomizer and Its Use in a Swirl Stabilized Combustor," AIAA Paper 85-1811, July 1985.
[11]Jackson, T.A. and Samuelson, G.S., "Spatially Resolved Droplet Size Measurements," *Journal of Engineering for Gas Turbines and Power*, Vol. 108, Jan. 1986, pp. 196–203.
[12]Bachalo, W.D. and Houser, M.J., "Spray Drop Size and Velocity Measurements Using the Phase/Doppler Particle Analyzer," *Proceedings of the International Conference of Liquid Atomization and Spray Systems—85*, July 1985.
[13]Bachalo, W.D., Houser, M.J., and Smith, J.N., "Evolutionary Behavior of Sprays Produced by Pressure Altomizers," AIAA Paper 86-0296, Jan. 1986.
[14]Wu, K-J., Santavicca, D.A., Bracco, F.V., and Coghe, A., "LDV Measurements of Drop Velocity in Diesel-Type Sprays," *AIAA Journal*, Vol. 22, Sept. 1984, pp. 1263–1270.
[15]Buchave, R., George, W.K., Jr., and Lumley, J.L., "The Measurement of Turbulence with the Laser Doppler Anemometer," *Annual Review of Fluid Mechanics*, 1979, pp. 443-503.
[16]Wu, K-J., "Atomizing Round Jets," Ph.D Thesis 1612-T, Dept. of Mechanical and Aerospace Engineering, Princeton Univ., Princeton, NJ, Aug. 1983.
[17]McLaughlin, D.K. and Tiederman, W.G., "Biasing Correction for Individual Realization of Laser Anemometer Measurements in Turbulent Flows," *Physics of Fluids*, Vol. 16, 1973, pp. 2082–2088.
[18]Dimotakis, P.E., "Single Scattering Particle Laser-Doppler Measurements of Turbulence," Advisory Group for Aerospace Research and Development, Neuilly sur Seine, AGARD CP-193, 1976.
[19]Buchave, P., "Biasing Errors in Individual Particle Measurements with the LDA Counter Signal Processor," *Proceedings of the LDA Symposium*, 1975, pp. 258–278.
[20]Martinelli, L., Reitz, R.D., and Bracco, F.V., "Comparisons of Computed and Measured Dense Spray Jets," *AIAA Progress in Astronautics and Aeronautics Series*, "Dynamics of Flames and Reactive Systems," edited by J.R. Bowen, N. Manson, A.K. Oppenhein, and R. I. Soloukhin, Vol. 95, AIAA, New York, 1984, pp. 484–512.
[21]Wygnanski, I. and Fiedler, H., "Some Measurements in the Self-Preserving Jets," *Journal of Fluid Mechanics*, Vol. 38, Sept. 1969, pp. 577–612.
[22]Shearer, A.J. and Faeth, G.M., "Evaluation of a Locally Homogeneous Model of Spray Evaporation," NASA CR-3198, 1979.
[23]Corrsin, S. and Uberoi, M.S., "Further Experiments on the Flow and Heat Transfer in a Heated Turbulent Air Jet," NACA TR998, 1950.
[24]Tross, S.R., "Characteristics of a Submerged Two-Phase Free Jet," M.S. Thesis, Pennsylvania State Univ., University Park, PA, 1974.
[25]Capp, S.P. and George, W.K., Jr., "Measurements in an Axisymmetric Jet using a Two-Colour LDA and Burst Processing," *Proceedings of the International Symposium on Applied LDA to Fluid Mechanics*, 1982.
[26]Hoesel, W. and Rodi, W., "New Biasing Elimination Method for Laser-Doppler Velocimeter Counter Processing," *Review of Scientific Instruments*, Vol. 48, July 1977, pp. 910–919.
[27]Schlicting, H., *Boundary Layer Theory*, 7th ed., McGraw-Hill, New York, 1979.
[28]Reitz, R.D. and Bracco, F.V., "Mechanisms of Breakup of Round Liquid Jets," *Encyclopedia of Fluid Mechanics*, Vol. 3, edited by N.P. Cheremisinoff, Gulf Publishing, Houston, TX, 1986.
[29]Baker, R.J., "The Application of a Filter Bank to Measurements of Turbulence in a Fully Developed Jet Flow," *2nd International Workshop on Laser Velocimetry*, 1984, pp. 355–396.

APPENDIX E

COMPUTATIONS OF TURBULENT DENSE SPRAY JETS

By

M.J.Andrews

MAE Report No. 1788-MAE

Department of Mechanical and Aerospace Engineering

Princeton University

Princeton, NJ 08544

August 1987

ABSTRACT

This report describes work performed in the Engine Laboratory at Princeton University to improve the accuracy of the computed drop fluctuation velocities of dense sprays. The drops are generated when a liquid is injected from a nozzle into a compressed gas at high velocity. The nozzle geometry, injection velocity and gas density are similar to those of fuel injection in Diesel engines, but our sprays are steady and vaporization is negligible.

The work has involved investigation of many elements of the computer code that solves the model equations, and several key details of the model. Our efforts have resulted in an analytical solution to the model for drop-gas velocity equilibration, several improvements to the model, and new observations from the experimental data about the suitability of an isotropic model of turbulence for the gas phase of the jet.

Reported here are the outcomes of the various studies performed. Is is concluded that both gas and drop fluctuations in dense spray jets are strongly anisotropic and therefore cannot be satisfactorily reproduced with a k-ϵ model. However such a model has reproduced all mean quantities and the total turbulence kinetic energy of both gas and drops.

CONTENTS

6. ACKNOWLEDGEMENTS

The advice, suggestions and encouragement of Professor F.V.Bracco throughout the work has been invaluable. Also, the many interesting conversations with Dr J.Abraham of John Deer should be mentioned. Support for this work was provided by the Department of Energy, Office of Energy Utilization Research, Energy Conservation and Utilization Technologies Program (contract DE-AS-04-86AL33209), the Army Research Office (grant DAAG 29-85-K-0028), General Motors Corp and Cummins Engine Co. Thanks are also due to the John Von-Neuman Computing Center (NSF) and to the Los Alamos National Laboratory (DOE) for the use of their computers for many of the computations.

APPENDIX F

Encyclopedia of Fluid Mechanics

VOLUME 8

Aerodynamics and Compressible Flows

N. P. Cheremisinoff, Editor

in collaboration with—

A. L. Addy
M. J. Andrews
K. A. Ansari
P. S. Ayyaswamy
N. C. Baines
F. V. Bracco
R. Chevray
H. W. Coleman
E. Dick
J. C. Dutton
A. Ecer
P. Freymuth
W. Genxing
K. N. Ghia
U. Ghia
A. A. M. Halim
H. Hayami
M. Hayashi
B. K. Hodge
N. E. Huang
S.-I. Iida
Y. Joshi
K. Kamijo
Z. Kazimierski
J. A. Liburdy
P. M. Ligrani
K. A. Mansour
M. Moheban
M. J. Morris
S. Murad
Y. Ohya
A. Okajima
S. Okamoto
R. Ruderich
M. Salikuddin
T. Sattelmayer
B. L. Sawford
Y. Senoo
C. K. W. Tam
R. P. Taylor
D. Vandenberghe
S. Wittig
W. Wysocki
M. Xiao

CHAPTER 26

ON THE STRUCTURE OF TURBULENT DENSE SPRAY JETS

M. J. Andrews and F. V. Bracco

Department of Mechanical and Aerospace Engineering
Princeton University
Princeton, New Jersey, USA

CONTENTS

ABSTRACT

Computations have been performed to study the fluctuations of drops in dense spray jets. Previous computations of axial drop velocity fluctuations had not agreed well with the measurements, and no satisfactory explanation had been provided. In this work we have studied the effect of "added mass," drop collisions and coalescences, grid distribution, residence time of drops in eddies, injection velocity, k-ϵ model constants, and gas phase anisotropy. It is concluded that both gas and drop fluctuations in dense spray jets are strongly anisotropic and therefore cannot be satisfactorily reproduced with a k-ϵ model. However, such a model has reproduced well all mean quantities and the total turbulence kinetic energy of both gas and drops.

INTRODUCTION

The use of multi-dimensional models to understand and then improve combustion in steady and unsteady energy-conversion devices is spreading rapidly [16, 23, 25], even though detailed assessments of the accuracy of the computed results are still limited.

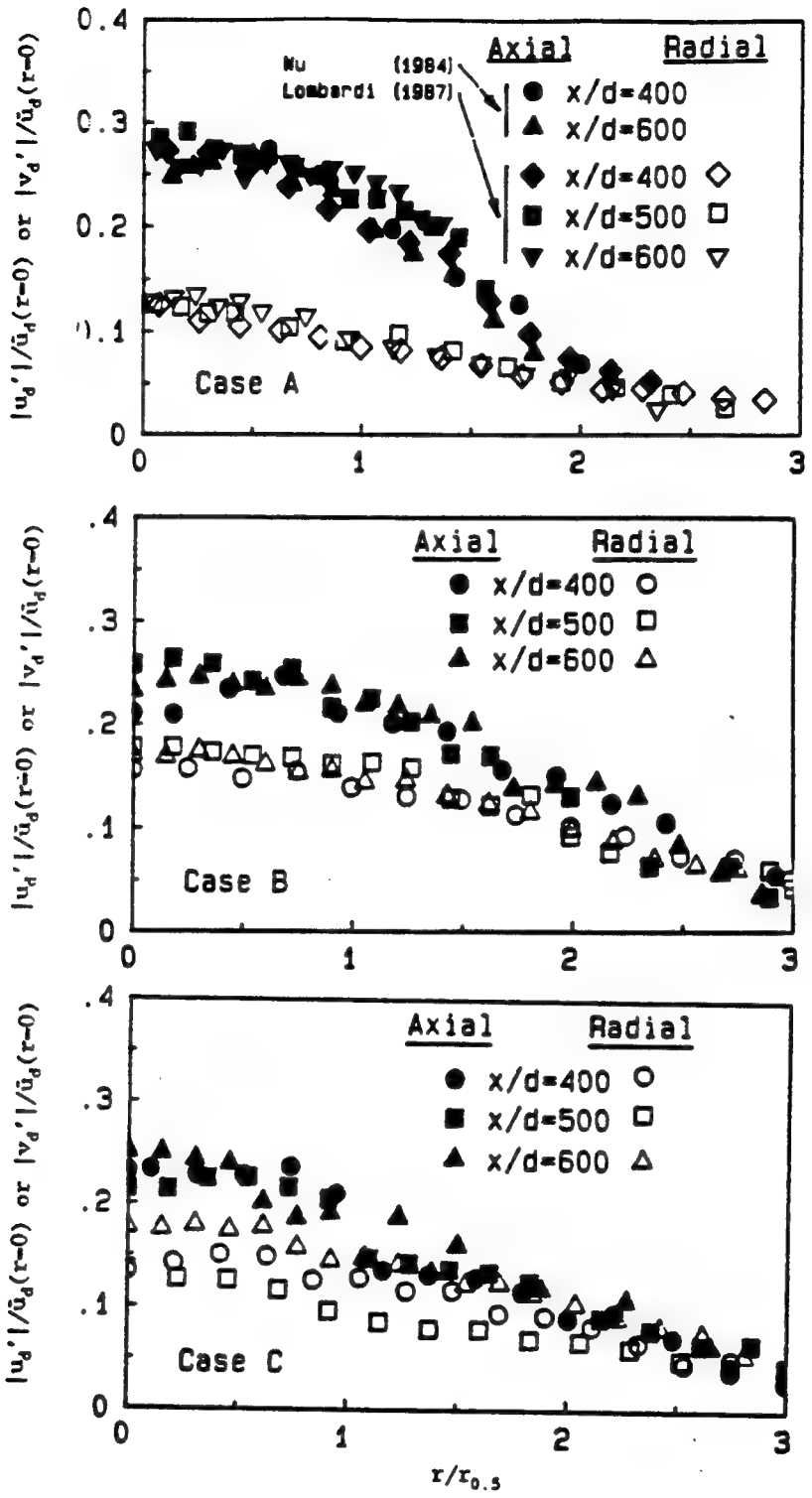

Figure 1. Measurements of axial and radial drop velocity fluctuation intensity for Cases A, B, and C of Table 1 [14, 27].

Table 2
k-ε Model Constants

Author	C_1	C_2	C_μ	σ_k	σ_ϵ
Launder [13]	1.44	1.92	0.09	1.0	1.3
Martinelli [15]	1.5	1.9	0.09	1.0	1.3
Reitz [21]	1.45	1.92	0.09	1.0	1.3
Elgobashi [8]	1.44	1.92	0.09	1.0	1.3
Kuo [12]	1.5	1.9	0.09	1.0	1.3
Shuen [24]	1.44	1.87	0.09	1.0	1.3

where $\Delta\underline{u} = (\underline{\bar{u}}_g + \underline{u}'_g - \underline{u}_d)$ and the drag coefficient is given by:

$$C_D(\theta, Re_r) = 24(\theta^{-2.65} + Re_r^{2/3}\theta^{-1.78}/6)/Re_r \qquad \text{with } Re_r = 2\rho_g|\Delta\underline{u}|r_d/\mu_g \tag{4}$$

As drops travel downstream, they traverse gas eddies and the residence time of a drop within an eddy, t_r, is calculated from:

$$L_e = \int_t^{t+t_r} |\underline{\bar{u}}_g - \underline{u}_d|\,dt \tag{5}$$

where L_e is the eddy size, taken as the dissipation length-scale:

$$L_e = C_\mu^{3/4}k^{3/2}/\epsilon \tag{6}$$

After a time t_r, the model assumes the drop leaves the eddy and enters a new one. A new value for the gas velocity fluctuation is then computed assuming a Gaussian velocity distribution with zero mean, and variance 2k/3.

Drop Injection by Spray Atomization

Atomization of the injected liquid is assumed to take place at the surface of an intact liquid core. Separate equations are used to describe the initial angle of the spray, the mean size of the drops, and the length of the core, respectively:

$$\tan\frac{\phi}{2} = \frac{1}{A}4\pi\left(\frac{\rho_g}{\rho_l}\right)^{1/2} f_m^*$$

$$d_0 = B\frac{2\pi\sigma_l}{\rho_g U_r^2}\lambda_m^* \tag{7}$$

$$\frac{x_L}{D_n} = C\left(\frac{\rho_l}{\rho_g}\right)^{1/2} f_m^{*-1}$$

The boundary conditions imposed are those of Martinelli et al. with open top and RHS boundaries at the ambient pressure to simulate a spray in a semi-infinite gas, a symmetry line at the center-line, and a solid boundary at the LHS. The initial conditions assumed a static gas field at the experimental pressure and temperature (care was taken to ensure the initial pressure and temperature fields satisfied the equation of state), a small initial value for k of $1.7 * 10^{-8}$ cm^2/ms^2 to prevent under-flow errors, and similarly a small initial value for ϵ of $1.7 * 10^{-8}$ cm^2/ms^3.

Computations began at the start of injection, and were continued until a steady-state was achieved, typically some 1.5 times the jet transit time $J_t \simeq 8$ ms. A check of steady-state conditions observed constant mean axial gas velocity, and turbulence energy when averaged over time intervals of typically $J_t/5$. At steady-state, samples were collected to furnish data. A typical sample taken over J_t for one computational cell contained 200 data, and typically 700 parcels of drops were within the computational field at the steady-state.

The computations of Martinelli et al. [15] show the poorest computed axial drop velocity fluctuation intensities for Case A, which has the highest liquid/gas density ratio, and so the coupling of gas and drop velocities by drag is weakest. We first concentrate on trying to obtain the correct axial drop velocity fluctuation intensities for Case A; results for Cases B and C are reported later.

A Reference Case

The first result repeats the calculation of Martinelli et al. for Case A. This calculation serves as a reference for the following work. Figure 3a compares the computed axial drop mean velocity with the measured one at x/d = 400 and 600, and they are seen to be in good agreement. Figure 3b compares the computed self-similar structure of the axial drop velocity fluctuation intensity with the measurements at x/d = 400 and 600 and shows more than a factor 2 discrepancy.

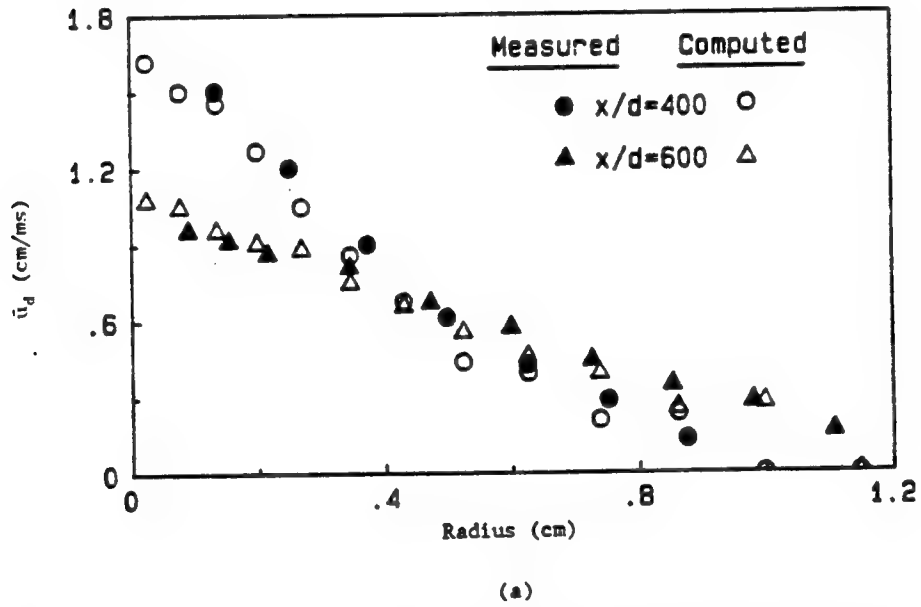

Figure 3. Measured and computed (reference) axial drop mean velocity (a) and drop velocity fluctuation intensity (b) for Case A.

The Gaussian Distribution for a Gas Velocity Fluctuation

The computer program generates a Gaussian distribution of random numbers, that should have a mean of 0, and a standard deviation of 1, using an inverse error function calculation. A gas velocity fluctuation is then modeled by multiplying a generated random number by $(2k/3)^{1/2}$ for each component of the gas fluctuation velocity. The Gaussian generator was found to produce numbers with a standard deviation of $1/\sqrt{2}$, instead of the correct value of 1. The error was traced to the transformation of the error function to a Gaussian distribution function that required a $\sqrt{2}$ as a multiplication factor to give the desired Gaussian random number.

Figure 4 compares the computed axial drop velocity fluctuation intensities with the ones measured at x/d = 400 and 600 when using the corrected Gaussian generator. Comparison of Figure 4 with the reference results of Figure 3 shows that the improvement is marginal at best. This result may be explained by the drop residence time calculation that is considered next.

The Residence Time of a Drop in an Eddy

One way of improving the agreement would be to increase the residence time t_r of a drop in an eddy. The residence time is calculated with Equation 5. If the separation velocity between a parcel of drops and the gas is equal to zero, $\Delta\underline{u} = 0$, then the parcel moves with the gas and so is captured by the eddy. But when $\Delta\underline{u} = 0$, Equation 5 predicts that the parcel still traverses the eddy with a speed $|\underline{u}'_g|$, so for a fixed eddy size a drop spends less time in the eddy and equilibrates less to the eddy velocity (this may explain why raising the magnitude of a gas fluctuation by $\sqrt{2}$ made little difference to the calculated drop fluctuation). The possibility of capture has now been included in the model by using the relative velocity in the residence time calculation:

$$L_e = \int_t^{t+t_e} |\underline{\bar{u}}_g + \underline{u}'_g - \underline{u}_d| \, dt \tag{8}$$

where L_e is calculated with Equation 6. This calculation of the transit time is the same as that used by Gosman and Ioannides [10].

To clarify the difference between the transit time formulations of Equations 5 and 8, the equilibration of a drop and the gas velocity is considered. We assume a constant uniform mean gas velocity in the axial direction, at constant pressure. For initial conditions we assume that an isolated ($\theta = 1$) drop experiences an axial fluctuation of u'_g, and $v'_g = w'_g = 0.0$, and such that $\Delta u = (u_g + u'_g - u_d) > 0$. Under these conditions the drop motion equation becomes:

$$\frac{d\,\Delta u}{dt} = -\gamma(1 + \beta\,\Delta u^{2/3})\,\Delta u \quad \text{and} \quad \frac{dZ}{dt} = \Delta u \tag{9}$$

where Z is the distance moved by the drop relative to the gas with $\gamma = 4.5\mu_g/r_d^2\rho_d$, and $\beta = (2r_d\rho_g/\mu_g)^{2/3}/6$.

The Equations 9 have the following solutions:

$$\Delta u = \left(\frac{1-\eta}{\beta\eta}\right)^{3/2} \quad \text{and} \quad Z = \frac{3}{\gamma\beta^{3/2}}\left[\tan^{-1}\left(\frac{1-\eta}{\eta}\right)^{1/2} - \left(\frac{1-\eta}{\eta}\right)^{1/2}\right] + Z_\infty \tag{10}$$

where $\eta = 1 - \beta K^{2/3} e^{-2\gamma t/3}$

$$K = \frac{\Delta u_0}{(1 + \beta\,\Delta u_0^{2/3})^{3/2}}$$

$$Z_\infty = \frac{3}{\gamma\beta^{3/2}}\left[\left(\frac{1-\eta_0}{\eta_0}\right)^{1/2} - \tan^{-1}\left(\frac{1-\eta_0}{\eta_0}\right)^{1/2}\right] \tag{11}$$

$$\eta_0 = \eta(t = 0)$$

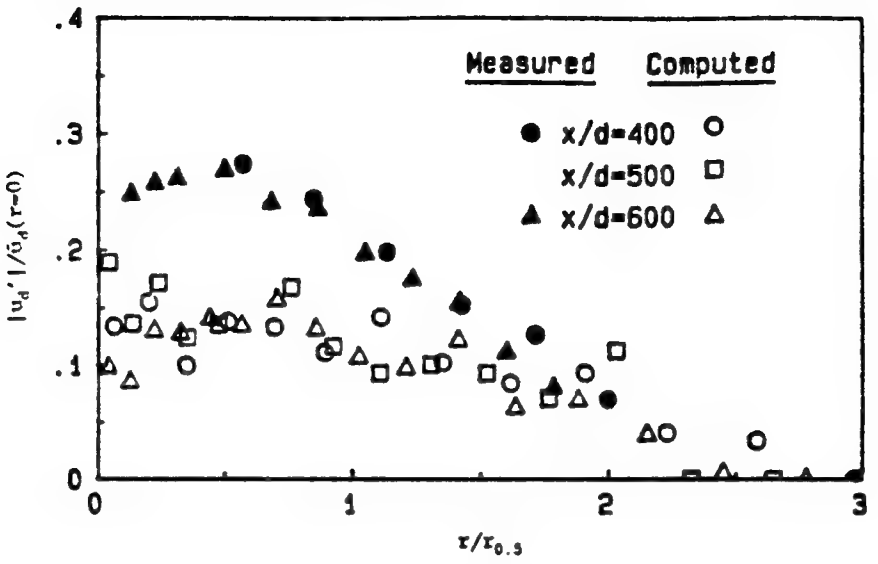

Figure 6. Measured and computed axial drop velocity fluctuation intensity for Case A using $\sqrt{2}$, and Equations 8 and 12.

In the present calculations, it was found that the transit time t_e controlled the residence time, but t_L may be expected to dominate as the spray extends to $x/d = \infty$.

Finally, Figure 6 shows the computed axial drop velocity fluctuation intensities obtained using Equation 8. When they are compared with the corresponding results obtained using Equation 5, shown in Figure 3, there is a slight improvement but not a dramatic one. This is because, for the particular sprays of the present study, the degree of capture given by the two formulations is about the same.

Drop Injection Velocity

Chehroudi et al. [6] photographically measured the diameter of the jet as it emerges from the nozzle and found it to be 106 microns. The nozzle diameter was 127 microns. Martinelli et al. did not know of this contraction and the injection velocity in their computations, U_n, was determined from the time taken to discharge a known mass of liquid through the nozzle area. Since the mass discharges through the contracted jet diameter, a more accurate measure of the velocity of the liquid in the core of the jet is:

$$U_j = U_n \frac{D_n^2}{D_j^2} \tag{13}$$

A computation was performed using U_j in place of U_n to determine the initial spray conditions of Equation 7. The computed axial drop mean velocity and axial drop velocity fluctuation intensities are shown in Figures 7a and 7b. The computations show the center-line drop mean velocity some 20% above its measured value. This result is because of the increase in the injection momentum.

The k-ε Model Constants

Increase of the axial drop mean velocity above the measured value when increasing the injection velocity suggests that we might reconsider the values assigned to the k-ε model constants. The

values used above were those determined by Kuo and Bracco [12] for transient and steady incompressible jets, and used by Martinelli et al. [15]. However, Table 2 shows a range of values assigned to these constants by other workers with round-jets. It is known that the k-ϵ model is sensitive to the values of C_1 and C_2, and it may be observed that if the value of C_1 is reduced or C_2 increased, then the generation of ϵ is decreased and an increase in k is expected. Thus by adopting the original values [13] of $C_1 = 1.44$ and $C_2 = 1.92$ the turbulent diffusivity and jet width are increased, and the jet velocity is decreased.

Indeed, Figures 8a and 8b show the mean velocities now compare better but lack of data near the center-line of the spray prevents a conclusive result. Despite the scatter, a small improvement in the drop velocity fluctuation intensities may be observed.

It was at this juncture that Lombardi and Chehroudi [14] repeated Case A retaking the measurements of Wu et al. but with more data closer to the center-line, and new radial drop velocity fluctuation measurements.

Anisotropic Turbulence

In this final topic, we return to the review of the experimental measurements that revealed unequal drop velocity fluctuation intensity in the axial and radial directions. Figure 9 shows the axial and radial drop velocity fluctuation intensities obtained from the computations performed for Case A of Wu et al. using the contracted jet diameter and the k-ϵ model constants of Launder and Spalding [13]. The figure shows that the computed axial and radial drop intensities are equal. Thus we attribute the anisotropy in the measured drop intensities shown in Figure 1 to anisotropy of the gas velocity fluctuations. With an isotropic k-ϵ model of gas-phase turbulence, we compute isotropic drop velocity fluctuations in agreement with the near equilibrium of gas and drop velocities

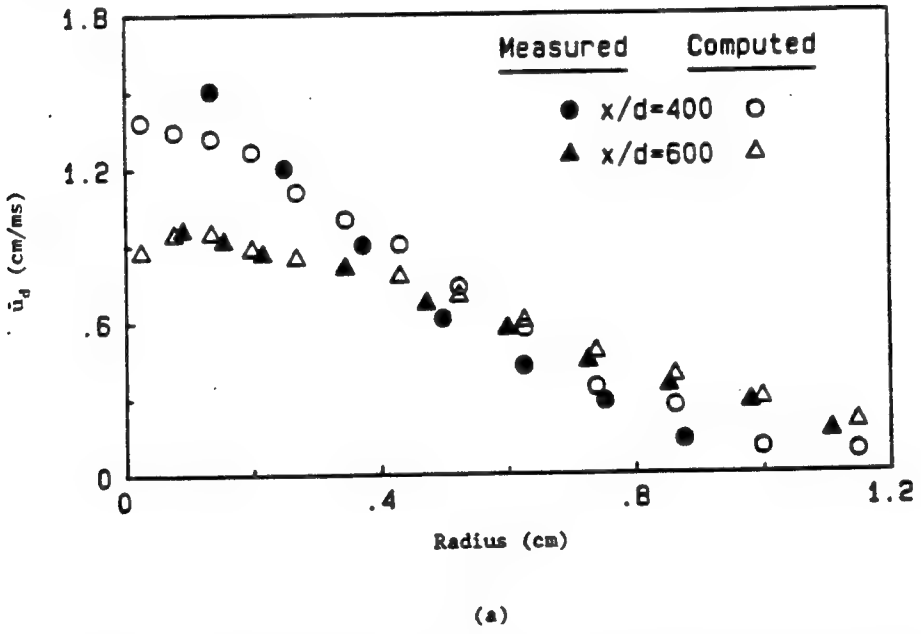

(a)

Figure 8. Measured and computed axial drop mean velocity (a) and drop velocity fluctuation intensity (b) for Case A when using D_j, $C_1 = 1.44$, and $C_2 = 1.92$.

of our sprays. This result contrasts with the findings of Shuen et al. [24] and Faeth [9] who computed anisotropic particle fluctuations when using an isotropic k-ϵ model of gas phase turbulence. However, their particles were much larger than our hexane drops (a particle smd of 79 to 207 microns and density of 2.6 g/cm^3 versus a drop smd of 20 to 40 microns and density of 0.66 g/cm^3) and not likely to have been nearly in equilibrium with the gas. With much larger drops, we also compute larger axial than radial drop velocity fluctuation. Thus non-equilibrium drops in an isotropic gas field can exhibit anisotropic fluctuations. But near equilibrium, drops in an isotropic gas field must undergo near-isotropic fluctuations.

For the sole purpose of checking our conclusion we decided to partition the computed gas turbulence energy, when selecting the gas fluctuation associated with an eddy, according to:

$$(\overline{v_g'^2}) = (\overline{w_g'^2}) = C_\alpha(\overline{u_g'^2}) \text{ and } (\overline{u_g'^2}) = C_\beta k \tag{14}$$

where C_α is a redistribution coefficient determined from the experimental measurements of the drop fluctuations as $C_\alpha = (\overline{v_d'^2})/(\overline{u_d'^2})$, and C_β is chosen so that $(\overline{u_g'^2}) + (\overline{v_g'^2}) + (\overline{w_g'^2}) = 2k$.

The measurements for Cases A, B, and C of radial and axial drop velocity fluctuation intensities at the center-line of the spray suggest a redistribution coefficient, C_α, of 1/2 for Cases B and C, and 1/6 for Case A. Thus C_β was 1 for Cases B and C, and 3/2 for Case A.

A few minor modifications were made at this point. Additional dissipation terms were added to the k-ϵ model equations to represent dissipation of turbulence energy by the passage of drops through an eddy, even though Reitz and Diwakar [21] have shown that these terms are negligible in the dilute region of the spray that is the focus of our attention. The formulation of these terms has been taken from Amsden et al. [1]:

$$S_k = -\int f\rho_g \frac{4}{3}\pi r^3 \underline{F} \cdot \underline{u}_g' \, dr \, du \tag{15}$$

$$S_\epsilon = C_3 \frac{\epsilon}{k} S_k \tag{16}$$

Elgobashi and Abou-Arab [8] developed a more detailed model of the drop dissipation process and assigned a model constant of $C_3 = 1.3$; Reitz and Diwakar [21] used a value of 1.5. We used 1.3, and found that the computed axial drop mean velocities were slightly lower than those measured by Lombardi and Chehroudi [14] whose data had become available by that time. Thus, changing the k-ϵ model constants was unnecessary and we reset $C_1 = 1.5$ and $C_2 = 1.9$, determined to be the best values for transient and steady incompressible jets by Kuo and Bracco.

Figures 10a and b show that partitioning the gas turbulence energy as suggested by the drop fluctuations leads to satisfactory reproduction of the measured drop fluctuations. This exercise proves conclusively that the measured anisotropy of the drop fluctuations is because of the anisotropy of the gas turbulence, and therefore cannot be reproduced with the isotropic k-ϵ model.

According to Capp and George [4] and Wygnanski and Fiedler [28], in fully developed incompressible jets the value of the redistribution coefficient C_α is between 2/3 and 3/4. For the drops of our sprays, it is 1.2 for $\rho_g/\rho_l = 0.0732$ and 1/6 for $\rho_g/\rho_l = 0.0256$. The requirements to obtain the incompressible jet value of C_α for the drops of our sprays are that: (1) the entrained gas totally dominates the structure of the sprays; (2) the gas has achieved the fully developed stage; (3) the drops are in complete equilibrium with the gas. Such limit is being approached but has not yet been achieved. The gas has 92% to 96% of the axial momentum for $\rho_g/\rho_l = 0.0732$ and 86% to 92% for $\rho_g/\rho_l = 0.0256$ [15], and the drops are closer to equilibrium for the higher gas density than for the lower gas density. It is interesting that the distributions of the axial and radial drop fluctuations are more sensitive gauges of the approach to the limit than the self-preserving profiles of Figure 1. Thus, the value of the redistribution coefficient can be expected to be a function not only of ρ_g/ρ_l and of axial distance, but also of the radial distance and of the parameters that influence the drop-gas momentum exchange.

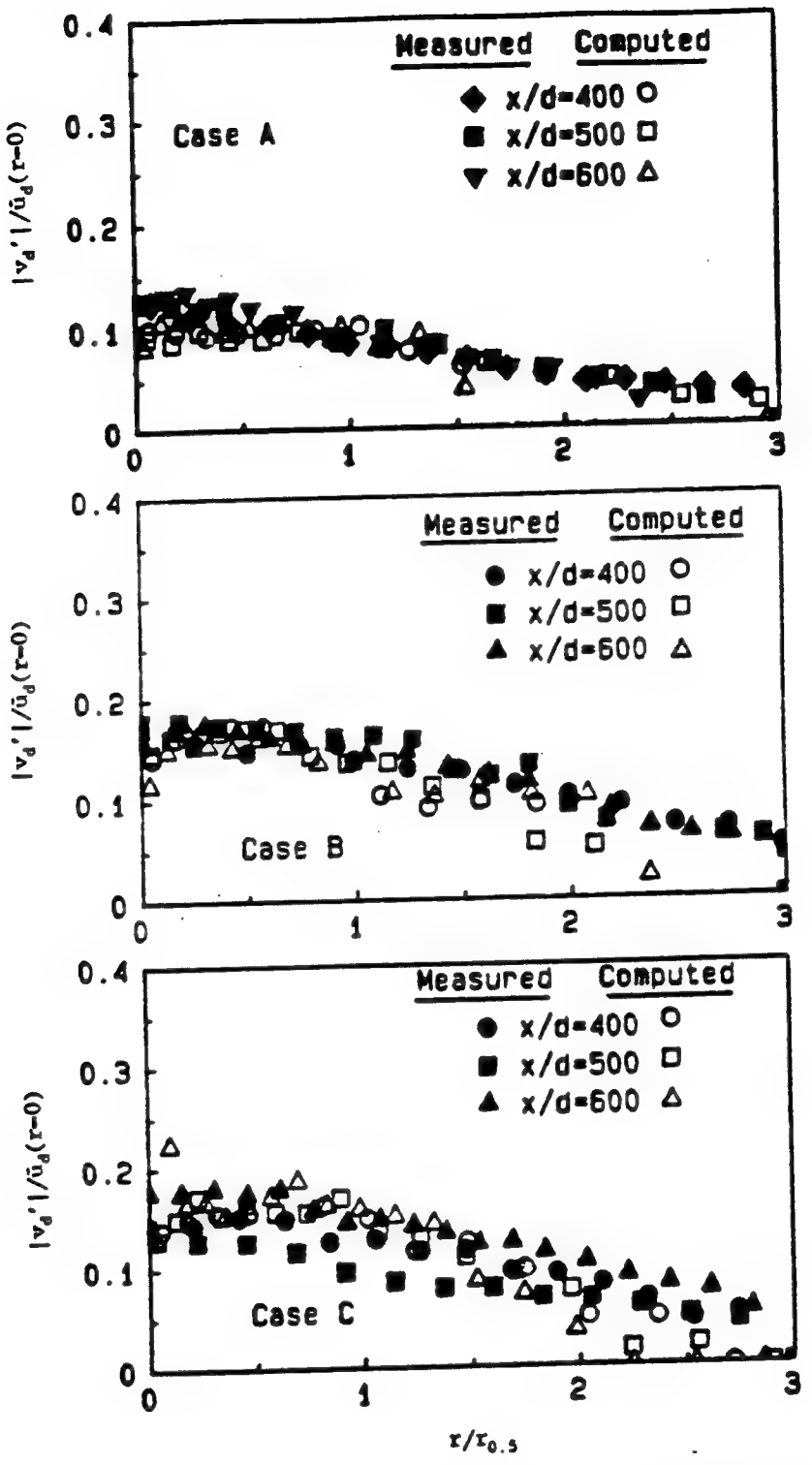

Figure 10b. Measured and computed radial drop velocity fluctuation intensities, partitioning the gas turbulence energy with $C_s = \frac{1}{2}$, $C_\beta = 1$ for Cases B, C; and $C_s = \frac{1}{6}$, $C_\beta = \frac{3}{2}$ for Case A.

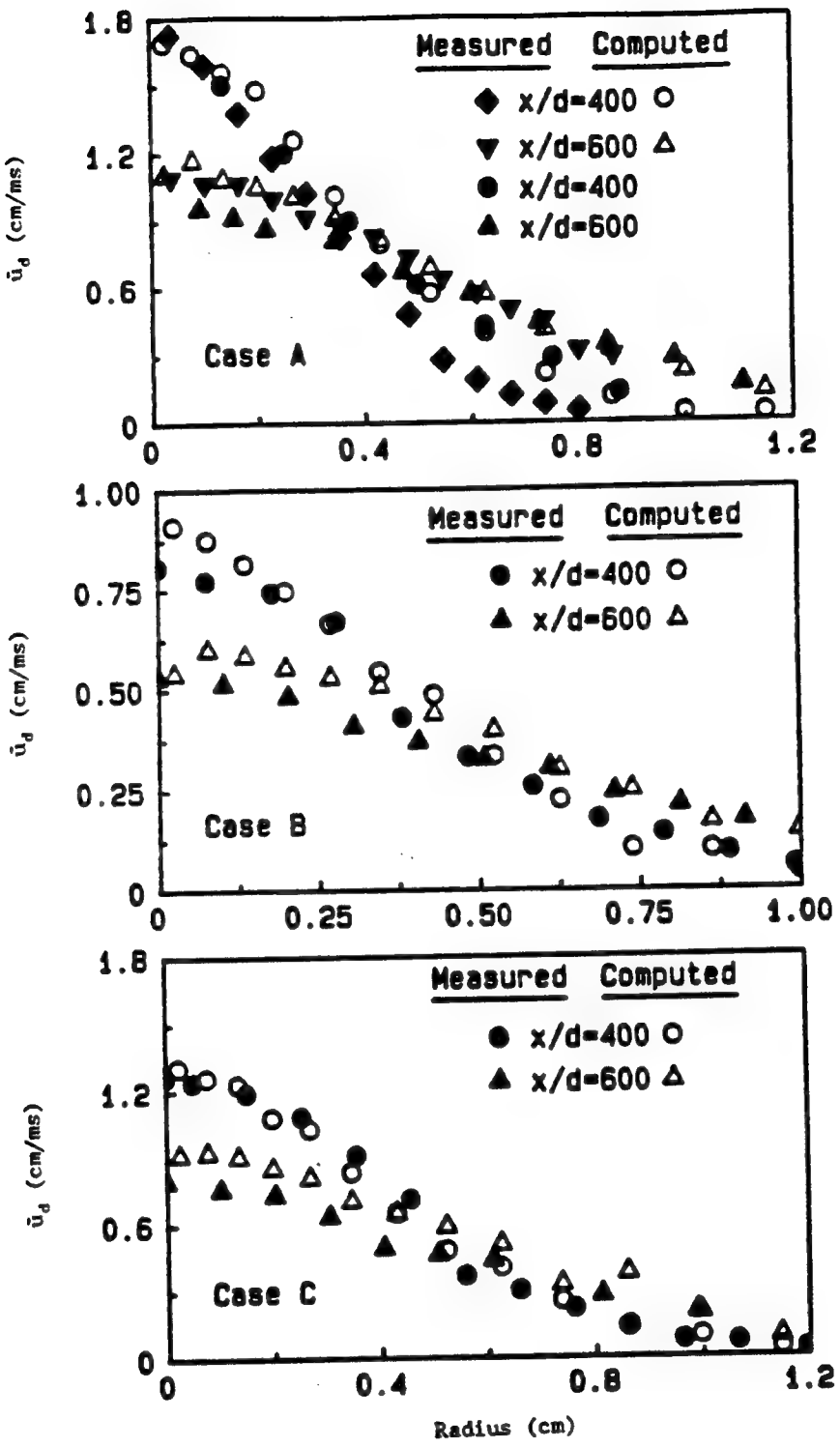

Figure 11a. Measured and computed axial drop mean velocities for Cases A, B, and C using the finalized isotropic model.

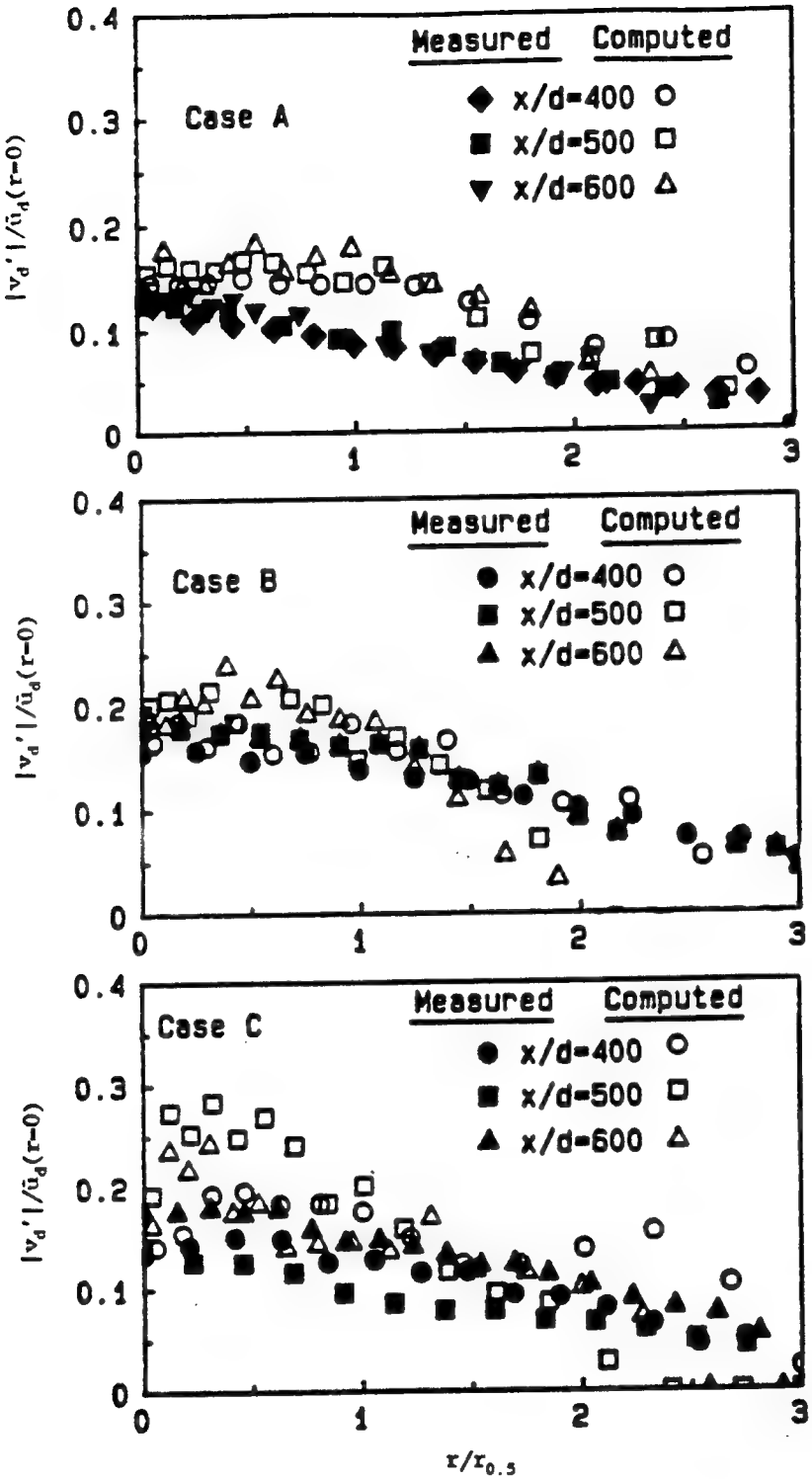

Figure 11c. Measured and computed radial drop velocity fluctuation intensities for Cases A, B, and C using the finalized isotropic model.

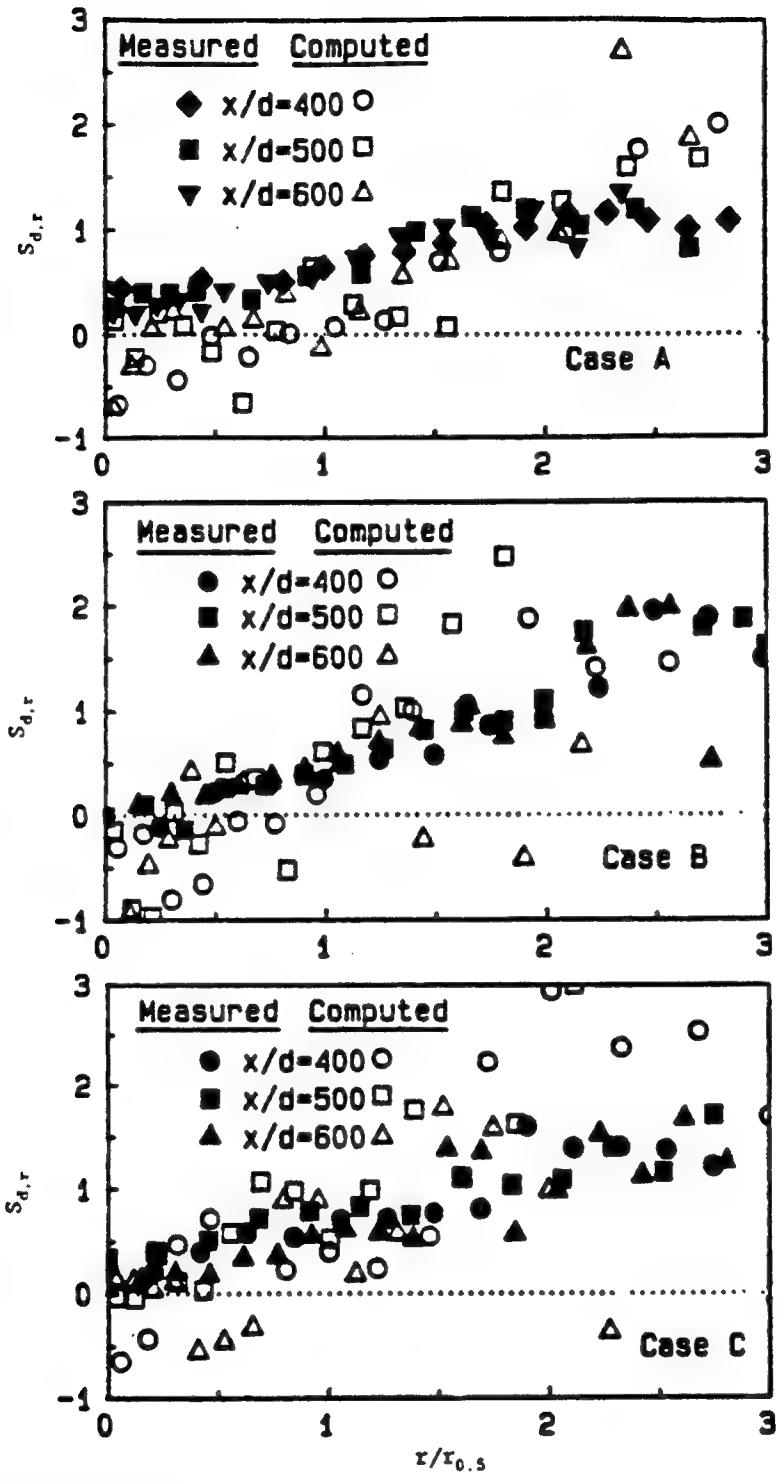

Figure 11e. Measured and computed radial drop velocity skewness for Cases A, B, and C using the finalized isotropic model.

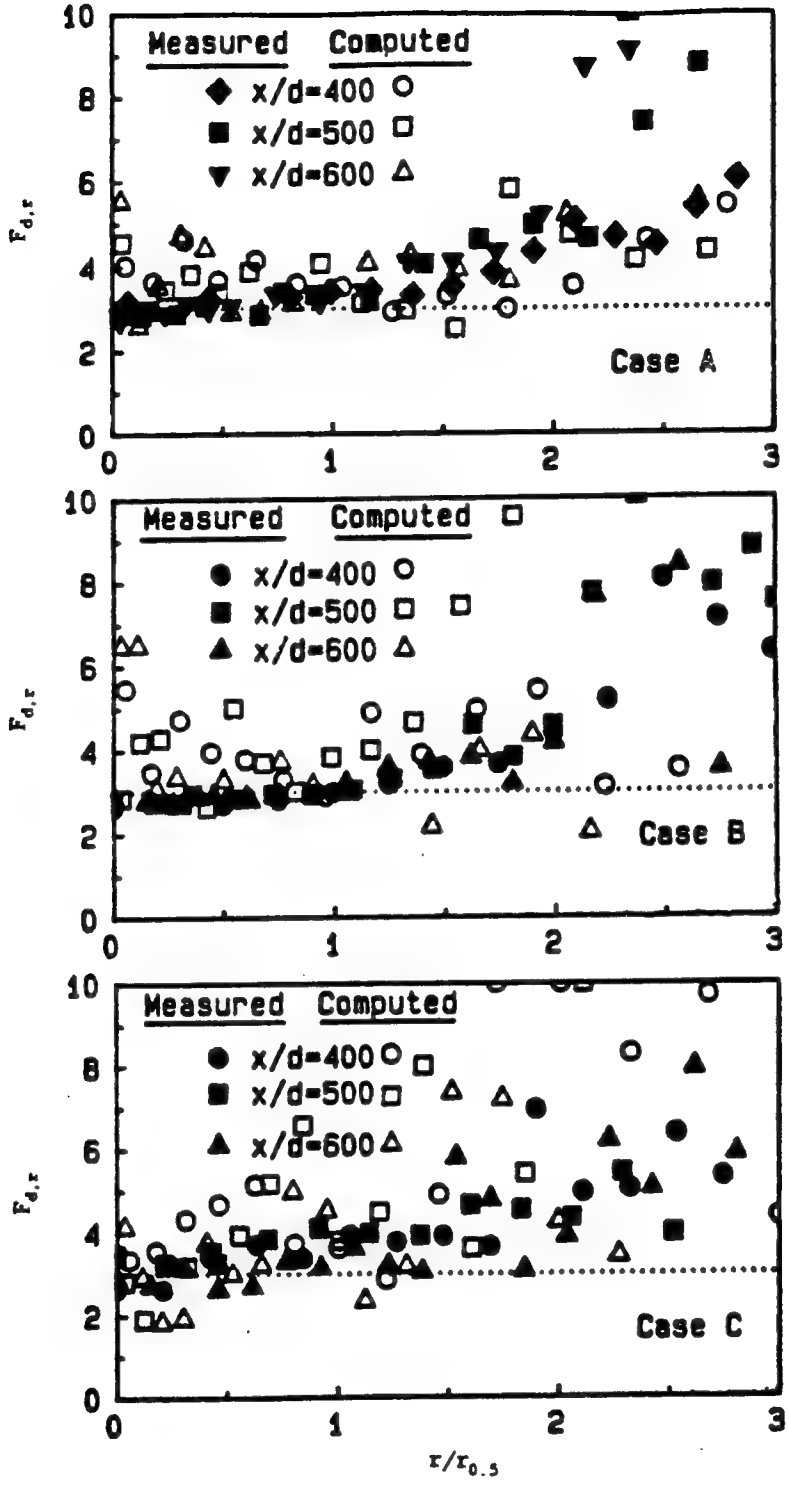

Figure 11g. Measured and computed radial drop velocity flatness for Cases A, B, and C using the finalized isotropic model.

10. Gosman, A. D., and Ioannides, E., "Aspects of Computer Simulation of Liquid-Fueled Combustors," AIAA Paper 81-0323, 1981.
11. Hiroyasu, H., and Kadota, T., "Fuel Droplet Size Distribution in Diesel Combustion Chamber," General Motors Symp. on Combustion Modeling in Reciprocating Engines, 1980.
12. Kuo, T.-W., and Bracco, F. V., "On the Scaling of Impulsively Started Incompressible Turbulent Round Jets," *J. Fluids Eng., 104*, pp. 191–197, 1982.
13. Launder, B. E., and Spalding, D. B., "The Numerical Computation of Turbulent Flows," *Computer Methods in Applied Mechanics and Engineering, 3*, pp. 269–289, 1974.
14. Lombardi, P., and Chehroudi, B., private communication, 1987.
15. Martinelli, L., Bracco, F. V., and Reitz, R. D., "Comparisons of Computed and Measured Dense Spray Jets," *Progress in Astronautics and Aeronautics, 95*, pp. 484–512, 1985.
16. Mattavi, J. N., and Amann, C. A., (Editors), *Combustion Modelling in Reciprocating Engines*, Plenum Press, N.Y., 1980.
17. O'Rourke, P. J., and Bracco, F. V., "Modeling of Drop Interactions in Thick Sprays and a Comparison with Experiments," Institute of Mechanical Engineers, Publication 1980-9, London, England, 1980.
18. O'Rourke, P. J., "Collective Drop Effects on Vaporizing Liquid Sprays," Ph.D. thesis, MAE Dept. Princeton University, 1981.
19. Reitz, R. D., and Bracco, F. V., "Mechanisms of Atomization of Liquid Jets," *Physics of Fluids, 25*, pp. 1730–1742, 1982.
20. Reitz, R. D., and Bracco, F. V., "Mechanisms of Breakup of Round Liquid Jets," *Encyclopedia of Fluid Mechanics*, Vol. 3, pp. 233–249, N. P. Cheremisinoff (Editor), Gulf Publishing Co., Houston, TX, 1986.
21. Reitz, R. D., and Diwakar, R., "Structure of High-Pressure Fuel Sprays," SAE Paper No. 870598, 1987.
22. Reynolds, W. C., and Cebeci, T., "Calculation of Turbulent Flows," In *Turbulence*, P. Bradshaw (Editor), Springer-Verlag, 1978.
23. Shahed, S. M. (Editor), "Engine Combustion Analysis: New Approaches," SAE, Publication P-156, Warrendale, PA, 1985.
24. Shuen, J.-S., Solomon, A. S. P., Zhang, Q.-F., and Faeth, G. M., "Structure of Particle-Laden Jets: Predictions and Measurements," *AIAA J., 23*, pp. 396–404, 1985.
25. So, R. M. C., Whitelaw, J. H., and Mongia, H. C., (Editors), "Calculations of Turbulent Reactive Flows," ASME, AMD-Vol. 81, 1986.
26. Solomon, A. S. P., Shuen, J.-S., Zhang, Q.-F., and Faeth, G. M., "Structure of Nonevaporating Sprays, Part II: Drop and Turbulence Properties," *AIAA Journal, 23*, pp. 1724–1730, 1985.
27. Wu, K.-J., Santavicca, D. A., Bracco, F. V., and Coghe, A., "LDV Measurements of Drop Velocity in Diesel-Type Sprays," *AIAA Journal, 22*, pp. 1263–1270, 1984.
28. Wygnanski, I., and Fiedler, H., "Some Measurements in the Self-Preserving Jet," J. Fluid Mech., *38*, pp. 577–612, 1969.
29. Andrews, M. J., "Computations of Turbulent Dense Spray Jets," MAE Report No. 1788-MAE, 1987.

APPENDIX G

The Engineering Society For Advancing Mobility Land Sea Air and Space®
INTERNATIONAL

400 COMMONWEALTH DRIVE, WARRENDALE, PA 15096-0001 U.S.A.

SAE Technical Paper Series

901673

Preliminary Drop Size and Velocity Measurements in a Dense Diesel-Type Spray

Chehroudi Behrouz
University of Illinois
Chicago, IL

International Off-Highway & Powerplan
Congress and Exposition
Milwaukee, Wisconsin
September 10-13, 199(

Preliminary Drop Size and Velocity Measurements in a Dense Diesel-Type Spray

Chehroudi Behrouz
University of Illinois
Chicago, IL

ABSTRACT

A single-holed round nozzle with diameter of 127 μm, length-to-nozzle diameter ratio of 4, and fuel differential pressure of 13.6 MPa was used to generate a narrow, fast, steady Diesel - type spray of hexane into nitrogen at 1.46 MPa and 65.C. Effects of instrument variables of a Phase Doppler Particle Analyzer (PDPA) on the mean and rms of the drop axial velocity and SMD at a distance-to-diameter ratio of 410 were investigated. It was found that a seemingly good choice of instrument parameters based on SMD may not necessarily be appropriate for velocity measurements. Although all measured quantities tended to level out at sufficiently high values of the photo multiplier voltage, no such tendency was exhibited by changes in the shift velocity. Optical arrangements with smaller measurement volume showed less sensitivity to the instrument parameters and produced mean and rms velocities in agreement with 8% with those obtained with a single-component, dual Bragg-cell LDV system. The SMD decreased radially from 26 μm at the axis to 24 μm and then increased to about 32 μm where the mean velocity was virtually zero. Further drop size (and velocity) measurements are necessary at various axial locations, particularly closer to the nozzle where the spray becomes denser, possibly using different instruments such as the PDPA, the Malvern particle analyzer, the pulse height and visibility: technique (and LDV).

THERE HAS BEEN considerable progress in laser techniques for drop size and velocity measurements in the past 15 years. Currently there are two instruments, the Malvern diffraction particle seizer and the Phase Doppler Particle Analyzer, that are commonly used for spray characterization. The Malvern instrument measures the size distribution of the drops that are within the entire path of the laser beam, thus called line-of-sight measurements, but provides no information about the drop velocity. The PDPA measures simultaneously individual drop size and velocity within a small volume.

Simultaneous drop size and velocity measurements were initiated by W.M. Farmer (1) who suggested that the shape (visibility) of the LDV signal could be used for particle sizing. Further theoretical works by Robinson and Chu (2), Adrian and Orloff (3), Roberds (4), Bachalo (5), and Negus and Drain (6), and experimental works by Roberds, et al. (7), Bachalo et al. (8), Durst (9), Negus (10), and Yeoman et al. (11) with the visibility technique revealed more information on its limitations and the range of practical applications. It was shown that the visibility in general depends on particle size, fringe spacing, number density, detector aperture size and shape, index of refraction, and detector location relative to the probe volume. Some of the dependencies could be relaxed with proper design of the optics. The scattered light should be collected at about 30 to 90 degrees off-axis and in forward scattering. The entire system needs to be calibrated with the same liquid of the spray to eliminate index of refraction effects and one can detect at most a practical range of 8 to 1 in drop size (dynamic range). A different technique for the measurement of the particle size was introduced by Yule et al. (12) who used the observed relationship between the intensity (DC-component of the LDV burst; pulse-height) of the scattered light and the drop size. This technique is well suited for particles of diameter larger than LDV fringe particles of diameter larger than LDV fringe spacing. Although some reasonable results were obtained, it was later shown that the trajectories of the particles in the measurement volume must be known in order to uniquely and unambiguously measure their size. Later a top-hat profile for the laser beams at the measurement volume was introduced by Allano et

al. (13) and Lee (14) which, to some extent, relaxed the intensity-size ambiguity problem. However, this led to a larger probe volume and significantly limited the ability to make measurements in dense sprays. A different approach was taken by Holve and Self (15) to resolve the trajectory ambiguity by using what was called the intensity deconvolution. However, the simultaneous measurement of size and velocity was lost.

A hybrid technique in which both features of pulse-height and visibility are considered was investigated by Hess (16) and Jackson and Samuelson (17, 18). Although repeated runs and careful alignment were necessary, reasonably good results were obtained in the spray of an air-assist nozzle with SMD of less than 35 microns.

The third technique for simultaneous drop size and velocity measurement, Phase Doppler Particle Analysis, was first realized by relating the phase difference between signals obtained by two (or three) photo multipliers (Bachalo and Houser (19,20). The main advantages of this technique are its wide dynamic range (35 to 1) and ease of operation. Comparisons were made between the hybrid technique and PDPA by Jackson and Samuelson (17,18) that showed fair agreement on SMD after proper corrections were made to the measured data.

In the past six years comparisons were made between results obtained with the PDPA and the Malvern in dilute sprays after proper conversion of the instantaneous point measurements of the PDPA to the line-averaged measurements of the Malvern. Dodge et al. (21) reported that the spatially sampled SMD's were very similar, but the PDPA values were higher in some cases. The D10 (number diameter) values from PDPA were generally significantly larger than from the Malvern. The number densities were similar, but the volume fraction of the PDPA was significantly larger than that of the Malvern. The volume flow rate measured by PDPA was inconsistent at different axial locations and significantly larger than the actual value except close to the nozzle, where it was too low. Dodge and Schwalb (22) repeated this experiment after improvements in the PDPA instrument and in operating procedures. They reported significantly improved results for both drop-size and volume flux measurements. Since the Malvern is unable to measure drop velocities, the PDPA velocities were assumed to be the correct velocities. However, Chehroudi and Bracco (23) reported some concerns in application of PDPA and Malvern in dense and high-speed sprays such as Diesel sprays. Hence, the correct comparison should include both velocity and size statistics.

Measurements in dense sprays have been tried using the Malvern with obscuration of up to 95%. Felton et al. (24) suggested a correction formula for Rosin-Rambler parameters that was developed by measurements with latex particles of known size distribution in a flow cell as the number density was progressively increased. Dodge and Bigalow (25) also proposed a correction procedure for Malvern-measured data of high obscuration by measuring effects of the progressive addition of identical sprays in the line of sight of the laser beam. Each spray was measured and characterized separately. Generally these corrections should be applied for obscuration above 50%.

Chehroudi and Bracco (23) demonstrated the sensitivity of some of the measurements by PDPA to the setting of its variables. Dodge and Schwalb (22) also reported variability of results with instrument setting. In this paper, preliminary results about the effects of some PDPA variables on size and velocity measurements in dense and fast Diesel-type sprays are reported. Drop size and velocity were measured by PDPA and the drop velocity was measured also by LDV.

EXPERIMENTAL SETUP AND CONDITION

A single-hole round nozzle with diameter of 127 μm and length-to-diameter ratio of 4 was used for all of the results reported here. Similar nozzle geometries and conditions have been extensively used in our efforts to characterize dense, high speed sprays (e.g. case A of Wu et al. (26)). The fuel was n-hexane which was pressurized by a Haskel fuel pump to generate a differential pressure of 13.6 MPa across the nozzle. Chamber pressure was 1.46 $\pm$ 0.03 MPa. Chamber temperature was 65 $\pm$ 1 C in order to keep the chamber windows free of droplets. All experiments were conducted at a distance of 52 $\pm$ 0.5 mm from the nozzle (x/d = 410).

The experimental rig consisted of a spray chamber, a pressurization system, a nozzle assembly, and instrumentation. A diagram of the system is shown in Fig. 1. The spray chamber was constructed from several cylindrical steel sections, 19 cm I.D. and 90 cm in total length. The window section had four quartz windows 10 cm in diameter. The pressurization system consisted of an air compressor and two booster pumps; one for the fuel and the other for the chamber gas (nitrogen). An accumulator and a reservoir were used to damp oscillations. The apparatus could be run continuously in steady state for extended periods of time. The liquid and gas pressures were measured with Borden Pressure test gauges. Simultaneous drop size and velocity measurement was made with an Aerometric, Inc. Phase Doppler Particle Analyzer (Processor No. 3100.5). In the transmitting optics, it uses a He-Ne Laser with rotating diffraction grating frequency shifter for velocity directional sensitivity. The receiving optics was the standard compact module provided with this model number. Two optical arrangements were used as shown in Figs. 2 and 3.

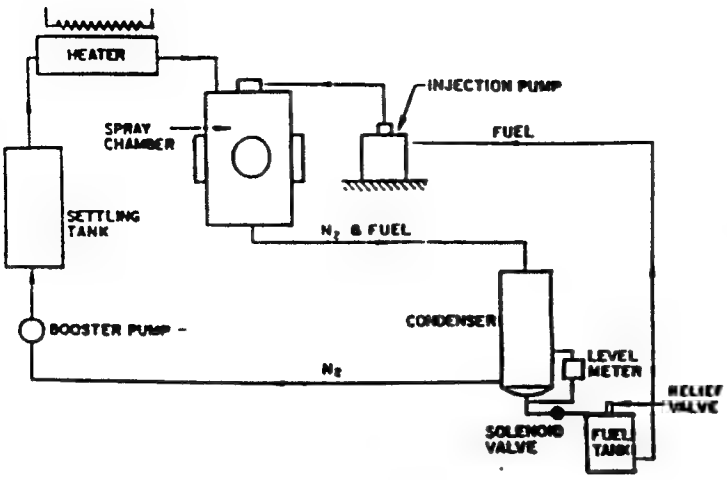

Fig. 1 Schematic of Spray Rig

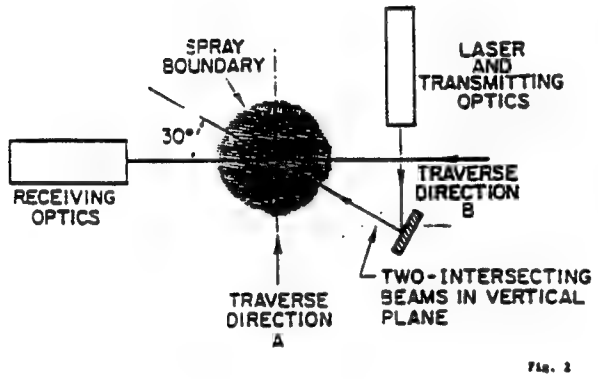

Fig. 2 Optical arrangement I

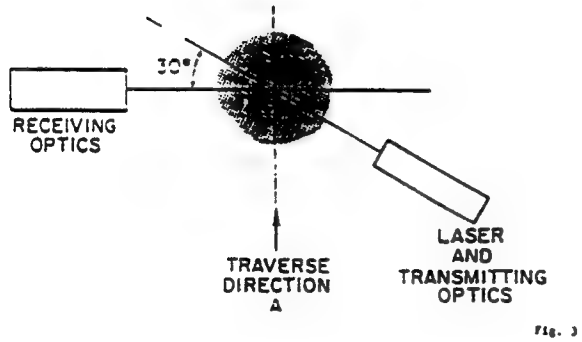

Fig. 3 Optical arrangement II

Arrangement I used a 495 mm f.l. transmitting lens while arrangement II used 200 mm f.l. In either case, the collimating lens was 300 mm f.l. The 200 mm f.l. lens provides a smaller measurement volume (waist diameter of 71 μm) than the 500 mm (waist diameter of 176 μm) which is in principal preferable. Note that a longer focal length collimator or another transmitting lens with a focal length in between 200 mm and 495 mm (which is not available with standard PDPA system) or smaller slit width could have been used to construct a better effective measurement volume diameter (in between 71 and 176 μm). However, this suggestion requires a priori knowledge of the spray drop size distribution and the results, as far as the size is concerned, should lie in between those of arrangements I and II reported in this paper. The PDPA comes with certain set of transmitting and collimating lenses from which arrangements I and II appear to be the better ones to choose. Also, there are cases where the geometrical dimension of the spray chamber restricts the use of the 200 mm f.l. transmitting optics. The slit width in front of the PM tubes was 100 μm for both arrangements.

RESULTS AND DISCUSSION

Table 1 presents the ranges of the variables that were considered. The measurements were made within a three month period. Results of size and velocity as functions of radial position at a distance of 52 mm from the nozzle are presented. This distance was chosen because the central region of the spray is dense while the outer 2/3 of the spray exhibits dilute behavior. Results from test PDA.1 are presented in Fig. 4. The general shape of the radial profile of the mean axial drop velocity is the typical one for full value at the periphery and it increases to a maximum at the axis of the spray. The traverse direction "A" passed through the axis of the spray (Fig. 2) and was identified initially by traversing in the "B" direction until the location of the maximum mean axial velocity was determined, and then locking at this value the traverse mechanism of the "B" direction. A line passing through the maximum mean axial velocity (center line axis) was considered as the reference for all comparisons including symmetry judgments. Traverse direction in all of the figures is from left to right. The rms of the velocity fluctuations also rises from a small value at the periphery to the axis of the spray but it has a broader peek than the mean velocity. The SMD is large (32 μm to 38 μm) where the mean velocity is negative, decreases to about 24 μm halfway to the axis of the spray, and then increases slightly to about 28 μm at the axis. As the measurement volume approaches the axis of the spray, more and more of the transmitting beams is exposed to the spray, the maximum being just after the axis of the spray For the receiving optics, the maximum length through the spray is when the measurement volume

TABLE 1

EXPERIMENTAL DATA

Experiment Code	Shift Vel. m/s	PM Volt Volts	Dia. Measure	Trans. Lens	Arrange-Ment	Drop. Dia Range μm	Drop Vel. Range m/s	Fringe Spacing, μm	No. of Fringes
PDA.1	10	400	ON	495	I	2.1–75	-6.27–45.5	6.55	27
PDA.2	5	350	ON	495	I	2.9–100	-1.3–45.5	6.55	27
PDA.3	15	400	ON	495	I	2.9–100	-11.3–45.5	6.55	27
PDA.4	5	400	ON	495	I	2.9–100	-1.3–45.5	6.55	27
PDA.5	5	400	OFF	495	I	——	-1.3–45.5	6.55	27
PDA.6	15	400	ON	495	I	2.9–100	-11.3–45.5	6.55	27
PDA.7	15	400	OFF	495	I	——	-11.3–45.5	6.55	27
PDA.9	10	360	ON	200	II	2.0–70	-4.13–36.4	9.88	13
PDA.10	10	360	ON	200	II	1.3–44.2	-4.13–36.4	2.66	26

is at the spray axis. Based on this asymmetric behavior, one expects similar asymmetry in Fig. 4, but this figure exhibits reasonably good symmetry. However, all other measurements showed clear asymmetric shapes and one should rely more on the data of the first half of the traverse (left half, in the figures).

Figs. 5 to 7 present some histograms of size, velocity, and volume fractions. There are two observations. First, the histogram of the percent-volume-of-liquid-in-each-band suggests that the maximum cutoff size of 75.0 μm should be increased to obtain a more reliable SMD since large drops contribute more to the SMD than small ones. For this reason, the maximum cut-off size was increased for later tests except for the case PDA.10 as shown in Table 1. Second, a bimodal behavior is shown in Fig. 6 and 7 for the number distribution but not for the percent volume fraction distribution due to larger contribution of the large drops. The origin of this bimodal behavior is not clearly know and it may be due to eddies at the edge of the spray.

There are two important parameters of the PDPA that deserve special attention: the photo multiplier voltage (or gain) and the shift frequency (or velocity). The effects of the two variables on the magnitudes of the drop mean axial velocity, the rms of velocity fluctuations, and the SMD were studied for the conditions of the test PDA.1 at the two radial locations. One location was chosen at the axis of the spray with high number density and spray interference, and the other, half-way from the axis, where dilute spray behavior is expected. Fig. 8 shows the effects of the PM-tube voltage (300, 350, 400, 450 V) on the mean velocity, rms, and SMD at the two locations. At the axis, results for PM-tube

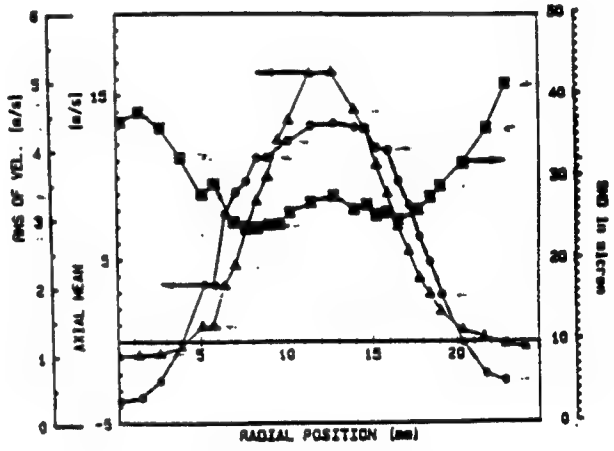

Fig. 4 Mean and rms of the drop axial velocity of radial and SMD as functions of radial positions for setting PDA.1. Triangle symbol is for axial mean velocity. The reference for the radial position is arbitrary but fixed.

voltages of 500, 550, and 650 V are also shown. For voltages greater than 650 V at the axis, and 450 V half-way from the axis, warning lights indicated PM-tube saturation. For this reason, the PM-tube voltage was not increased beyond those values. From Fig. 8, two measurement procedures can be considered: adjust the gain to the local plateau value at each measurement location or choose constant compromise value for all locations. The latter approach was adopted for convenience. A value of 400 V was selected not to saturate the PM-tubes in the outer dilute region of the spray while being sufficient in the inner dense region. According to Fig. 8, 400 V yield somewhat higher values than the plateau values of the rms of the velocity fluctuation and of SMD at the axis and, probably, at the outer location too.

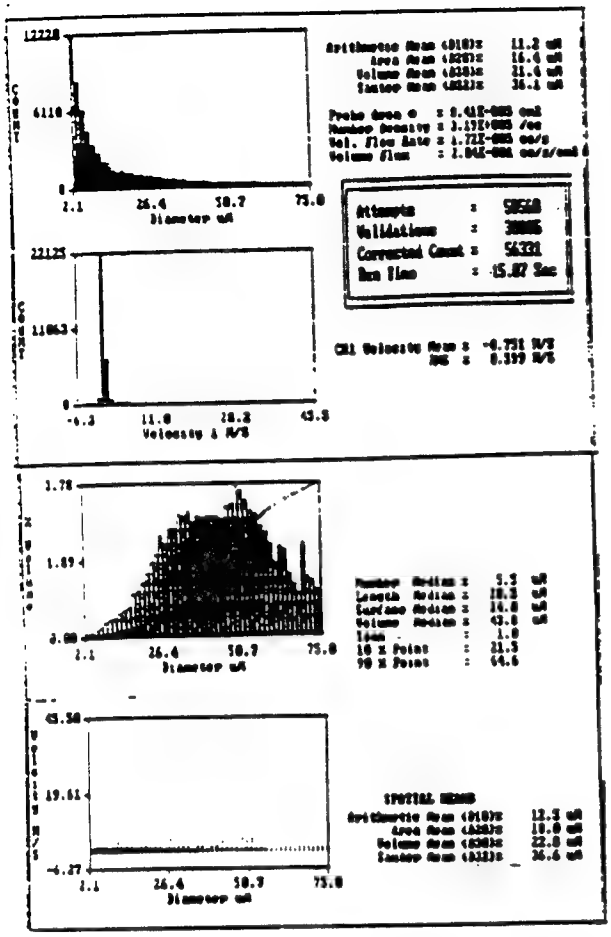

Fig. 5 Print-out from PDPA's software for setting PDA.1 showing size (number and volume) and velocity histograms, and size-velocity correlations for a point at the edge of the spray where the velocity is negative.

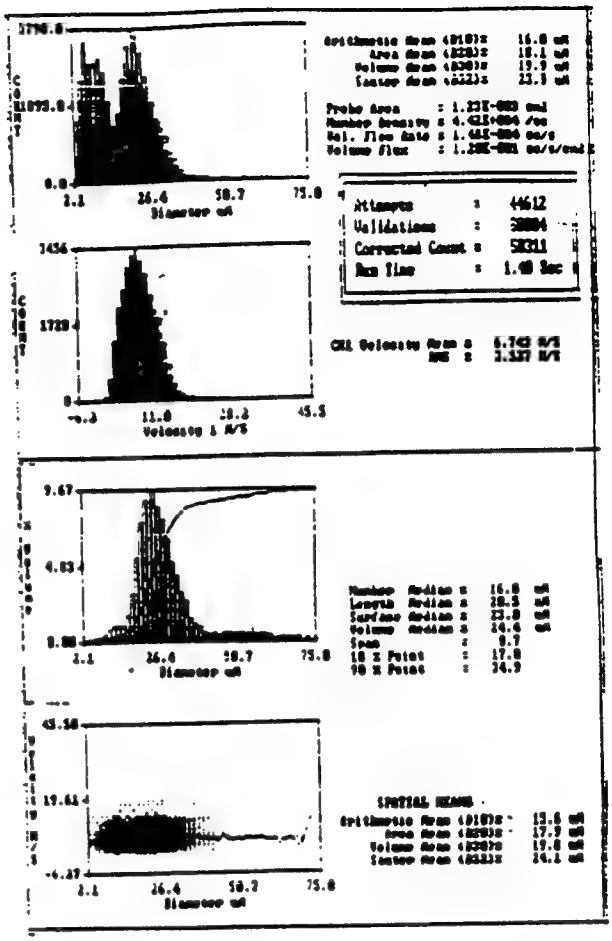

Fig. 6 Print-out from PDA's software for setting PDA.1 size (number and volume) and velocity histograms, and size-velocity correlations for a point about half-way from the axis of the spray.

The results of changing the shift frequency are shown in Fig. 9. The manufacturer of the PDPA does not encourage large values of the shift frequency in the operating manual. At the axis of the spray, the monotonic trends do not give any clue as to the appropriate setting, whereas in the dilute region, plateaus exist at least for the rms of the fluctuation of the velocity and for the SMD. Accepting the PM-tube voltage of 400 V with 10 m/s shift velocity, then 3.5 times the rms value subtracted from the mean axial velocity value at the axis of the spray gives about 0.8 m/s indicating that the probability of negative velocity at this location is close to zero. Higher shift velocities would give significant changes of unrealistic negative velocities at the axis of the spray. Calculations, indicate that with 30 m/s velocity vector (mean value, plus two standard deviations at the spray center) and 8 number of required fringes with 10 m/s shift velocity and 26 as total number of fringes available, all particles will be accepted in a total solid angle of approximately 3.13 π about the center of the measurement volume (note that the maximum value is 4 π). This solid angle is 1.63 π for PDA.9. This acceptance solid angle increases by increasing the number of available fringes and the shift velocity, and by decreasing the magnitude of the velocity vector (since the drop residence time increases). The acceptance angle for the LDV system used here was almost 4 π for the same set of conditions above. In addition, from radial velocity measurements on this spray one can show that at the center of the spray almost all the velocity vectors are within a cone with solid angle of 1.59 π stradient (almost the same acceptance angle as for the zero shift velocity case). These calculations indicate that the acceptance angle effect (fringe bias) is not important, particularly at the center of the spray. One possible explanation might be the improper filter settings. For example, for low and high pass filters of 6.144 and 0.512 MHz the PDPA software indicates that one can use velocity ranges (-16.2 → 45.5 m/s) and (-26.2 → 45.5 m/s) for shift velocities of 20 and 30 m/s respectively. However, the actual allowable maximum velocity (determined by pedestal removal and the low pass filter cutoff criteria) in each of the above ranges changes unless the low pass

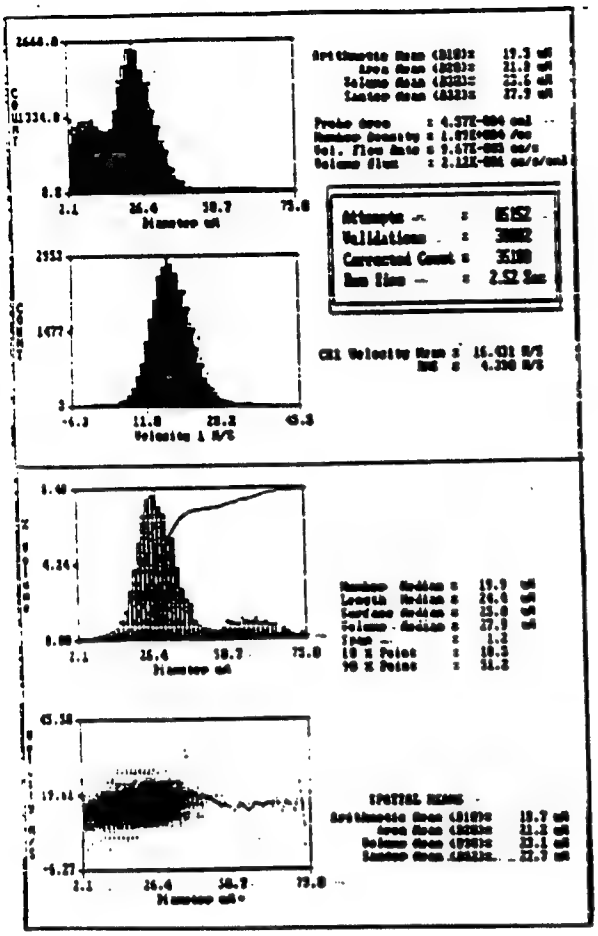

Fig. 7 Print-out from PDA's software showing size (number and volume) and velocity histograms, and size-velocity correlations for a point at the axis of the spray.

filter is either chosen or varied appropriately. Therefore the actual allowable maximum velocities should be 25.5 and 15.5 m/s for 20 and 30 m/s shift velocities respectively. Thus as one increases the shift velocity (keeping the low pass filter fixed) the maximum velocity that can actually be measured is decreased, explaining the trends of the shift velocity on the mean axial velocity. However this explanation is not complete and there are other factors that influence the observed effects of the shift velocity because of the following facts. First, it is known that the velocity probability distribution function (PDF) at the center of the spray is close to normal distribution (Felton et al (27)). Second, calculations of the acceptance cone angle at the center of the spray with zero shift velocity indicates that this angle is adequate and no fringe bias would occur. Third, the velocity PDF for the zero shift velocity with high and low pass filters of 0.512 and 3.072 MHz can be fitted with a guassian (normal) function with the average velocity of 18.62 m/s, about equal to the measured value of 18.96 m/s at the center of the spray. A print out of the measured results indicates that no drops exist with

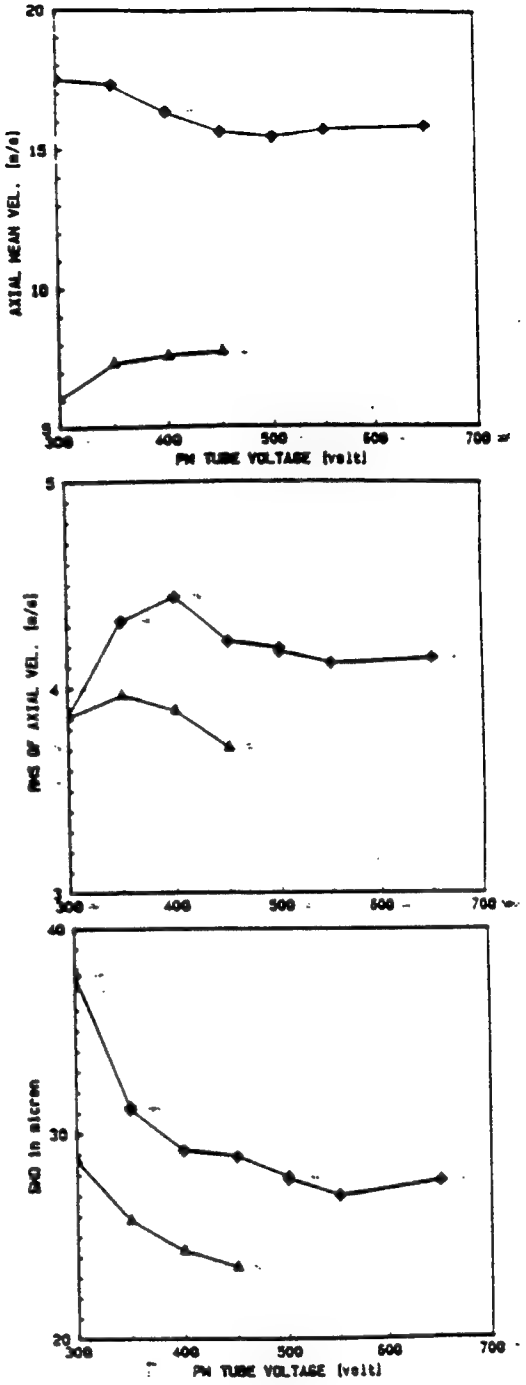

Fig. 8 Effects of PM-tube voltage on the mean and rms of the axial velocity, and on SMD at two radial positions. Diamond and triangle symbols are for center and half-way positions respectively.

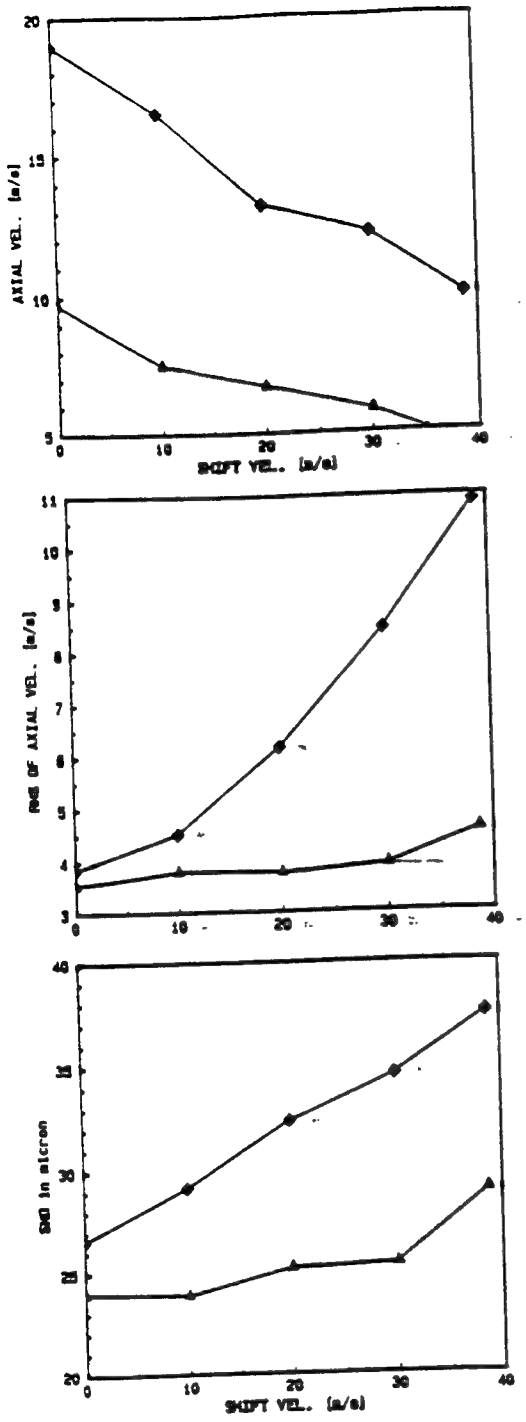

Fig. 9 Effects of shift velocity on the mean and rms of the axial velocities, and on SMD at the same two radial positions as Fig. 8.

velocities outside the [6.29, 36] m/s interval although as low as 3.3 m/s can be measured with the instrument settings. All of the above facts suggest that the average value obtained for the velocity with zero shift is reliable and can be trusted close to the center of the spray. Inspection of the velocity PDF for the case with 20 m/s (3.056 MHz) shift velocity with high and low pass filters of 0.512 and 6.144 MHz, which is almost equivalent to the zero-shift-velocity case (as far as the relative separation of the doppler spectrum and the low-pass filter cutoff in frequency domain representation is concerned) shows non-guassian skewed representation with negative velocities lower than -6.27 m/s (quite unrealistic) with average velocity of 13.142 m/s (quite low). In summary the effects of the filter settings for the above two cases are almost identical and, therefore, the observed differences between the results should originate from other sources, perhaps, noise and errors associated with the software. These other possible error sources can be examined by measurements using a spinning wire or Burglund Lui monosize drop generator where in one case velocity and (size) on the other, size are primarily kept constant. Note that the shape of the velocity probability distribution function at the center of the spray is close to normal distribution (see Felton et al. (27)). The situation in the dilute region is marginally better. At this location, the mean axial velocity decreases by about 22.6% when the shift velocity is increased from 10 m/s to 30 m/s, which is slightly less than 26% at the axis of the spray.

Fig. 10 shows comparisons of results obtained with settings PDA.1, PDA.2, PDA.3 obtained one after the other in the same day. Note that the diameter ranges for cases PDA.2 and PDA.3 were extended to include larger drops. Effects of shift velocity and PM-voltage combine to give mean velocity for PDA.3 which is about 20% smaller than that for PDA.1 and PDA.2 at most radial locations on the left side of the axis. With the exception of two locations, the rms values are about the same. In the SMD plots, while the PDA.2 and PDA.3 curves are asymmetric and very close to each other, the PDA.1 curve is lower due mainly to the change in the diameter measurement range. However, the conclusion is that there appear to be no reliable guidelines for the selection of the setting for all variables and that different settings appear to be better suited for different variables.

The PDPA's data acquisition logic provides on-off switching of the drop size measurement logic. Effect of this software switch at two different shift velocities are shown in Fig. 11 for the PM-voltage of 400 V. The mean velocity always decreased when the drop size switch was turned off, particularly in the central region of the spray. At each radial position, the experiments were performed by only turning the switch on or off without any other change in the entire system. It is possible that when the switch is off, drops smaller than 2.9 μm, which have smaller velocities, contribute to the velocity measurement and are responsible for the lowering of the mean value in the central region of the spray. The behavior of the rms of the drop velocity fluctuations is insensitive to the software drop size on-off switch at low shift velocities. The difference between the SMD values for PDA.4 and PDA.6 can be explained using the trends of Fig. 9 (c).

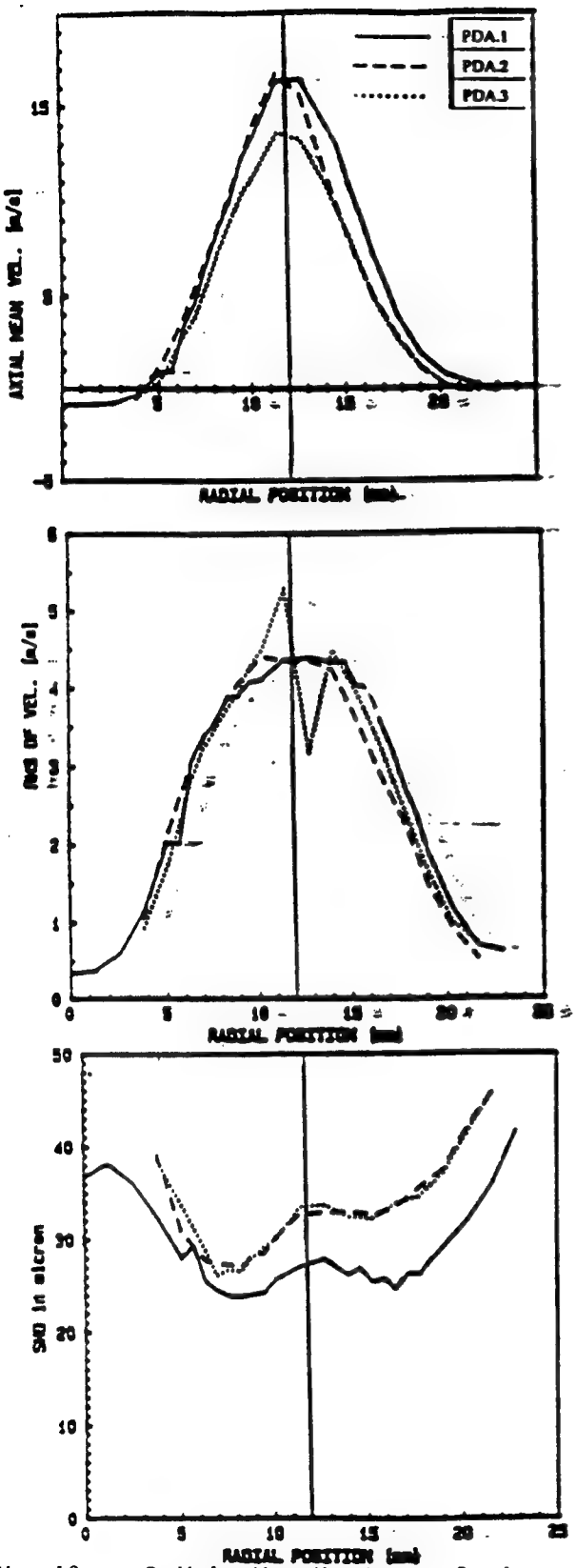

Fig. 10 Radial distributions of the mean axial drop velocity, the rms of the drop velocity fluctuations, and the SMD for settings PDA.1, and PDA.2, and PDA.3 of Table 1. The reference for the radial positions is arbitrary but fixed.

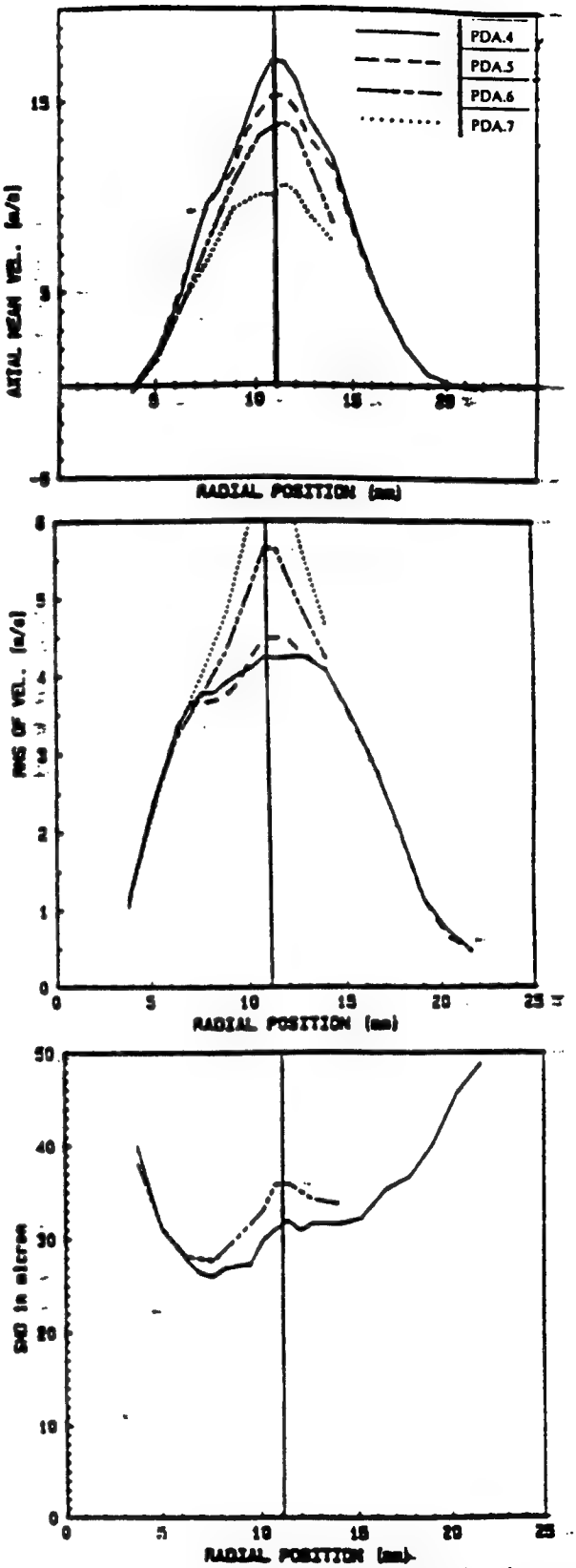

Fig. 11 Radial distributions of the mean axial drop velocity, the rms of the drop velocity fluctuation, and the SMD for settings PDA.4, PDA.5, PDA.6, and PDA.7 of Table 1. The reference for the radial positions is arbitrary but fixed.

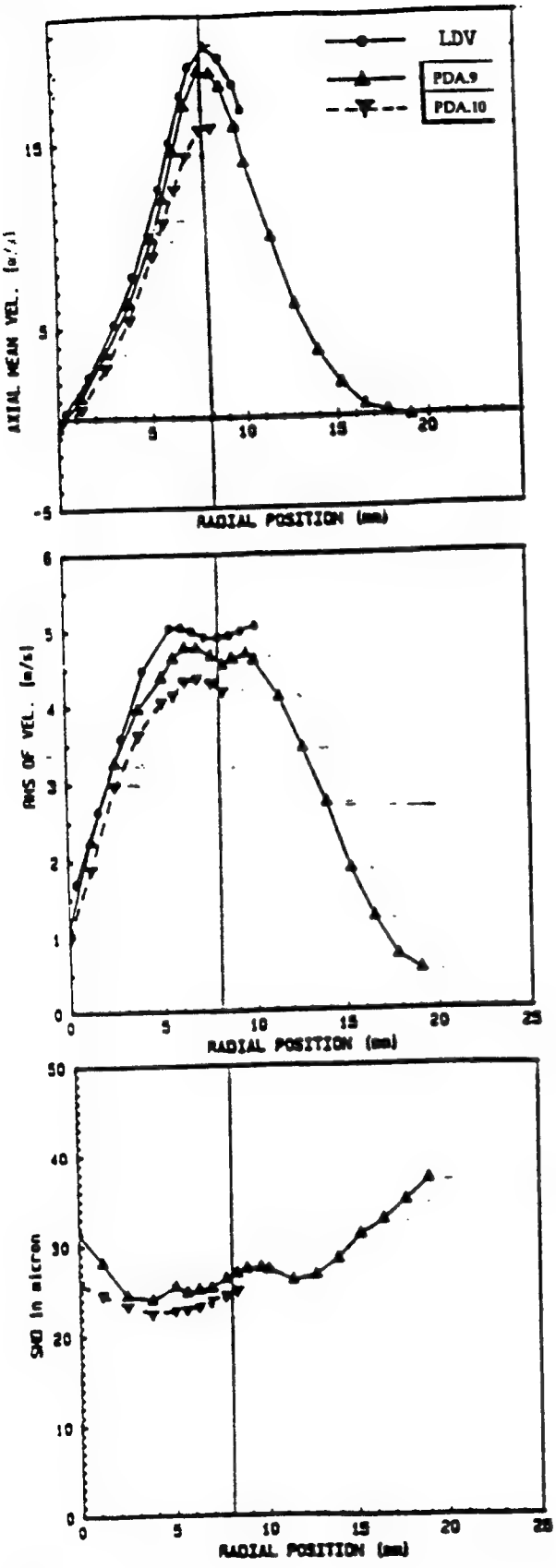

Fig. 12 Radial distributions of the mean axial drop velocity, the rms of the drop velocity fluctuation, and the SMD for settings PDA.9 and PDA.10 of Table 1 and velocities measured by LDV

The effects of PM-tube voltage and shift velocity were also investigated with 200 mm f.l. transmitting optics. The mean axial velocity changed without any special trend by at most 4.3% close to the axis of the spray for a change of PM voltage from 260 V to 450 V while it decreased monotonically by 4.9% from 260 V to 400 V about midway from the axis. The rms of the velocity fluctuations at the axis of the spray increased from 4.50 m/s at 260 V to a flat local maximum of 4.73 m/s at 325 V and decreased to 4.46 m/s at 450 V, while it increased from 4.23 m/s to 4.30 m/s for the same change in the PM-voltage values, and then decreased to 4.10 m/s at 400 V for the midway radial position, therefore both exhibiting similar shapes. The SMD at a point close to the axis decreased monotonically from 24 μm to 22.0 μm (25%) for PM-voltage of 260 V and 450 V respectively. At the midway position, it also decreased monotonically from 26.5 μm to 20.9 μm (21%) when PM-voltage was changed from 260 V to 400 V showing similar trends as in arrangement II. Change of the shift velocity from 0 m/s to 15 m/s decreased the mean axial velocity by about 9% monotonically at both the axis and the midway radial position in the spray. This shows less sensitivity compared with that of arrangement II. The rms of velocity fluctuations at both positions were flat to within at most ± 2% for the same change of the shift velocity (0 to 15 m/s) showing lower sensitivity compared to the 495 mm f.l. case particularly close to the axis of the spray. Finally, SMDs were insensitive to within 1.4% for both radial positions within the same range of shift velocity. Note that during the tests for the effects of PM-tube voltage the shift velocity was set at 10 m/s while the PM tube was at 360 V (Lower for arrangement II due to its smaller measurement volume and consequently higher light intensity) when effects of shift velocity were considered. Also, the maximum allowable shift frequency for 200 mm f.l. transmitting lens was 16.31 m/s. In summary, with the 200 mm f.l, the system was less sensitive to variations of shift velocity at PM voltage of 360 V, particularly around the axis of the spray, while being as sensitive as with the 500 mm f.l. case to the changes in the PM-tube voltage at 10 m/s shift velocity.

Results for conditions PDA.9 and PDA.10 of Table 1 are plotted in Fig. 12. Comparison between Figs. 10 and 12 shows that, except close to the axis of the spray, the mean velocity values for PDA.1, PDA.2, and PDA.9 are in excellent agreement. The maximum mean axial velocity for PDA.9 is about 2.5 m/s larger than the corresponding ones for the other two cases. The difference between PDA.9 and PDA.10 is the the size measurement range brought about by the change of the track on the rotating diffraction grating unit. The mean velocity is decreased due, perhaps, to elimination of the large high - velocity drops, although no strong size-velocity correlation is observed in the PDPA's size velocity plots.

Also shown in Fig. 12 are the results obtained with a one-component dual Bragg-cell LDV with effective shift frequency of 3 MHz, fringe spacing of 13.422 μm and measurement volume of about 125 μm at the same position and spray conditions as PDA.9 and PDA.10. The light was collected at 90° and a TSI counter processor was used for processing. The high and low pass filters were set at 1 MHz and 10 MHz respectively. 3,000 data points were collected for LDV and 60,000 for each of the PDPA settings except PDA.1, for which 30,000 data were collected. Effects of LDV system settings (laser power, and high and low pass filter values) were investigated and the parameters were set at values where the least sensitivity of the results occurred. For example, the amplitude limit was at the off position (meaning signals from all drop sizes were considered) and it was found that if large drops were eliminated by lowering the amplitude limit from its maximum to 60%, the mean and rms velocities decreased by 4.6% and 11.3% respectively at the axis of the spray. Change of the laser power from 1.5 W to 0.1 W decreased the mean velocity by only 1% and increased the rms by about 2.8%, and the value of 1.5 W was used at the axis of the spray (This in effect shows that there is no strong size-velocity correlation, indicated also by PDPA in Figs. 5 to 7, at the axial location selected, thus providing an appropriate environment for comparison between LDV and PDPA considering their unequal dynamic ranges). This latter result also implies that the PM-voltage and amplifier gain were set properly, although their effects were tested independently. Sensitivities of the LDV mean and rms velocity results to changes in PM-voltage and amplifier gain around the selected values were at the extreme ± 1.5% and ± 3.1% respectively, at the axis of the spray.

Note that the LDV-measured mean axial velocity is consistently higher than the PDPA's, in particular, by about 8% at the axis of the spray. However, the shapes of the two profiles are very similar and little differences would be obvious if plotted in normalized form. The determination of the location of the maximum velocity is crucial and must be done with care and high spatial resolution, as small shift in this position can produce large differences between the two results. However, this 8% difference cannot be entirely attributed to small errors in fuel differential pressure setting (possibly by 3.5% as explained later) and the spatial resolution in Fig. 12 seems to be quite adequate to determine the position of the maximum velocity. Closer to the nozzle, this consistently low value of the mean velocity for PDPA causes the estimates of low volume flow rates, as also reported by Dodge et al. (21) who used less dense sprays than ours. As far as the rms of the velocity fluctuations are concerned, both techniques give similar trends, although the maximum rms with LDV occurs farther from the axis of the spray than with PDPA. The PDPA shows lower fluctuations intensities by about 8% around the axis and closer agreement away from the axis. The rms curve for PDA.9 falls on the corresponding plots for cases PDA.1 and PDA.2 except in the central region where PDA.9 values are slightly larger but its shape conforms with present and past LDV results (e.g. (27)).

The SMD of PDA.9 agrees well with that of PDA.1, both in shape and magnitude on the left side of the spray axis. The agreement is reasonably explained due to closeness of the maximum cut-off diameters of 70 μm and 75 μm for PDA.9 and PDA.1 respectively, considering that the minimum diameter is defined as 1/35 of the maximum diameter. The difference between PDA.9 and PDA.10 is explained by the same reasoning. Note that the SMD at the radial position where the value of the axial velocity is 50% of its maximum, is about 9.5% lower than at the axis in Fig. 12, but about 17% and 22% lower in Figs. 10 and 11 respectively.

With a gas pressure of 200 psig, the fuel pressure was adjusted to give a gauge reading of 2200 psig for a differential pressure of 2000 psi (13.6 MPa). The effect of possible reading errors was tested with arrangement II by decreasing the fuel pressure from 2200 psig to 2000 psig at a fixed chamber pressure of 205 psig (1.49 MPa). This change decreased the mean velocity and the rms of the velocity fluctuations by about 3.5% at the center of the spray. The PM voltage was 360 V and the shift velocity 10 m/s.

CONCLUSIONS

Effects of the major instrument variables of a phase Doppler particle analyzer on the drop mean and rms axial velocity and SMD at a distance of 410 nozzle diameters were investigated in a fast and dense spray. For transmitting lens of 495 mm f.l., it was found that care must be exercised in order to choose the optimum PM-tube voltage, shift velocity, and drop size measurement range. In general, it is best to set the instrument parameters where the least sensitivity of the measured quantity occurs. All the measured quantities at the axis of the spray tended to level off at high values of the PM-tube voltage, but no such tendency was found for changes in the shift velocity. A seemingly good choice of instrument parameters, for example, based on the measured SMD trend, may not necessarily be appropriate for the measurement of other quantities, for example, the mean velocity. An arrangement which provided a smaller measurement volume showed lesser sensitivity to instrument parameters, and gave mean drop velocities and rms of the drop velocity fluctuations that were within 8% of those obtained by LDV.

It would appear that considerably more work is necessary with a variety of measuring techniques, e.g. LDV, PDPA, pulse-height and visibility, and Malvern, to establish the accuracy of drop size and velocity measurements in fast dense sprays.

ACKNOWLEDGEMENTS

This author would like to thank Professor F.V. Bracco for providing facilities from Princeton University to perform the measurements.

REFERENCES

1. Farmer, W.J., "Measurement of Particle Size Number Density and Velocity Using a Laser Interferometer," Applied Optics, Vol 11, p. 2603, 1972.

2. Robinson, D.H. and Chu, W.P., "Diffraction Analysis of Doppler Signal Characteristics for a Cross-Beam Laser Doppler Velocimeter," Applied Optics, Vol. 9. pp. 2177-2183, 1975.

3. Adrian, R.J. and Orloff, K.L., "Visibility Characteristics and Application to Particle Sizing," Applied Optics, Vol. 3 pp. 677-684, 1977.

4. Roberds, D.W., "Particle Sizing Using Laser Interferometry," Applied Optics, Vol. 7, pp. 1861-1866, 1977.

5. Bachalo, W. D., "Method for Measuring the Size and Velocity of Spheres by Dual-beam-light - scatter interferometry," Applied Optics, Vol. 3, pp. 363-370, 1980.

6. Negus, C.R. and Drain, L.E., "The Calculation of the Scattered Light from a Spherical Particle Traversing a Fringe Pattern Produced by Two Intersecting Beams," J. Phys D.: Appl. Phys., Vol. 15, pp. 375-402, 1982.

7. Roberds, D.W., Brasier, C.W., and Bomar, B.W., and Bomar, B.W., "Use of a Particle Sizing Interferometer to Study Water Droplet Size Distribution," Optical Engineering, Vol. 3, pp. 236-242, 1979.

8. Bachalo, W.D., Hess, C.F., and Hartwell, C.A., "An Instrument for Spray Droplet Size and Velocity Measurements," ASME Paper No. 79-WA.GT-13, 1979.

9. Durst, F., "Review - Combined Measurements of Particle Velocities, Size Distribution, and Concentrations," Trans. of ASME, J. of Fluids Engineering, Vol. 104, pp. 284-296, 1982.

10. Negus, C.R., "Extension of the LDA Technique to the Simultaneous Measurement of Fuel Droplet size and Velocity in a Kerosene-Fired Furnace," Intl. Symp. on applications of LDA to Fluid Mechanics, July 5-6, Lisbon Portugal, 1982.

11. Yoeman, M.L., Lightfoot, N.S., and Morse, A.P., "The Simultaneous Measurement of Particle Size, Velocity and Mass Transfer in a Pulsed Two Phase Flow Field," Intl. Symp. on Applications of LDA to Fluid Mechanics, July 5-6, Lisbon, Portugal, 1982.

12. Yule, A.J., Chigier, N.A., Atakans, and Ungut, "Particle Size and Velocity Measurement by Laser Anemometry," J. Energy, Vol. 1, pp. 220-228, 1977.

13. Allano, D., Gouesbet, G., Grehan, G., and Lisiecki, D., "Droplet Sizing Using a Top-Hat Laser Beam Technique," J. Phys. D.: Appl. Phys., Vol. 17, pp. 43-58, 1984.

14. Lee, W.H., "Method for Converting a Gaussian Laser Beam into a Uniform Beam," Optics Commun., Vol. 6, pp. 469-471, 1981.

15. Holve, D. and Self, S., "Optical Particle Sizing for in Situ Measurements - Part I and Part II," Applied Optics, Vol. 18, pp. 1632-1652, 1982.

16. Hess, C.F., "A Technique Combining the Visibility of a Doppler Signal with the Peak Intensity of the Pedestal to Measure the Size and Velocity of Drops in a Spray," AIAA-84-0203, AIAA 22nd Aerospace Science Meeting, Reno, Nevada, 1984.

17. Jackson, T.A. and Samuelson G.S. "Droplet Sizing Interferometry: A Comparison of the Visibility and Phase/Doppler Techniques," Applied Optics, Vol. 26, No. 11, pp. 137-2143, 1987.

18. Jackson, T.A. and Samuelson, G.S., "Spatially REsolved Droplet Size Measurements," ASME Paper No. 85-GT-38, 1985.

19. Bachalo, W.D. and Houser, M.J., "The Phase Doppler Spray Analyzer for Simultaneous Measurements of Drop Size and Velocity Distributions," Optical Engineering, Vol 23, pp. 583-591, 1984.

20. Bachalo, W.D. and Houser, M.J., "Spray Drop Size and Velocity Measurements Using Phase Doppler Analyzer," ICLASS-85, Paper VC/2, 1985.

21. Dodge, L.G., Rhodes, D.J., and Reitz, R.D., "Drop Size Measurement TEchniques for Sprays: Comparison of Malvern Laser -Diffraction and Aerometerics Phase/Doppler," Applied Optics, Vol. 26, No. 11, pp. 2144-2154, 1987.

22. Dodge, L.G. and Schwalb, J.A., "Fuel Spray Evaluation: Comparison of Experiment and CFD Simulation of Non-evaporating Spray," ASME Gas Turbine and Aeroengine Congress and Exposition, Amsterdam, Netherlands, 1988.

23. Cheroudi, B. and Bracco, F. V., "Drop Size and Velocity Measurements in Dense Fast Sprays," 7th Army Research Office Engine/Fuel Workshop, Dearborn, Michigan, 1987.

24. Felton, P. G., Hamidi, A.A., and Aigal, A.K., "Measurement of Drop Size Distribution in Dense Sprays by Laser Diffraction," ICLASS Proceedings, Vol. 2, Pp. IVA/4/1-11, July 1985.

25. Dodge, L.G. and Bigalow, J.W., "Effect of Elevated Temperature and Pressure on Sprays from Simplex Swirl Atomizers," J. of Eng. for Gas Turbine and Power, Paper No. 85-GT-58, 1985.

26. Wu, K.J., Coghe, A., Santavicca, P.A., and Bracco, F.V., "LDV Measurements of Drop Velocity in Diesel-Type Sprays," AIAA Journal, Vol. 22, pp. 1263-1270, 1984.

27. Felton, P.G., Chehroudi, B., Bracco, F.V., and Onuma, Y., "LVD Measurements of Axial Drop Velocity in Evaporating, Dense Sprays," ASME J. of Propulsion and Power, Vol. 4, 399-405, 1988.

APPENDIX H

Numerical Approaches to Combustion Modeling

Edited by
Elaine S. Oran and Jay P. Boris
Naval Research Laboratory
Washington, DC

Volume 135 1990
PROGRESS IN
ASTRONAUTICS AND AERONAUTICS

A. Richard Seebass, Editor-in-Chief
University of Colorado at Boulder
Boulder, Colorado

Published by the American Institute of Aeronautics and Astronautics, Inc.
370 L'Enfant Promenade, SW, Washington, DC, 20024-2518

Chapter 20

Comparisons of Deterministic and Stochastic Computations of Drop Collisions in Dense Sprays

J. M. MacInnes and F. V. Bracco

I. Introduction

COMBUSTION in direct-injection engines is influenced by the dynamics of the sprays that are formed when the jets of liquid fuel encounter the combustion-chamber gas. The evolution of such sprays, which typically consist of millions of individual drops, is computed primarily by the stochastic method of Dukowicz[1] that was extended by O'Rourke and Bracco[2] to account, again stochastically, for drop collisions and coalescences.

There are two main elements of the stochastic collision model: the estimate of the mean collision rate within a fixed volume and that of the actual number of collisions a drop experiences in a given time interval. The equations for the estimates are derived from the kinetic theory of gases and are precise only when the drops are distributed uniformly within the volume, undergo elastic collisions, experience no significant forces between collisions, and have a volume that is small compared with the volume containing them. In a spray, such conditions are not always met, and it is difficult to evaluate accurately the corresponding errors because of the complexity of the flow. In fact, the model has been evaluated primarily by comparison of its predictions with measurements in the far field, i.e., beyond the region of the spray that is influenced directly and strongly by drop collisions and coalescences.

In this chapter, the accuracy of the stochastic method of computing collisions is examined by comparing its results with those obtained with direct, deterministic calculations of drop trajectories and collisions. The comparison is made for a practical spray of the sort used in diesel engines with fine, but still practical, space and time resolutions. However, other restrictions have been accepted that limit the full extension of our conclusions to practical sprays. These include disregard of drop breakup (see, for example, Refs. 3–5) and drop vaporization. For the present study, the

neglected effects are not essential but may be contributing. They will have to be considered in future work aimed at evaluating the overall accuracy of the spray model in practical applications.

It is shown that the stochastic method underestimates drop collision and coalescence rates by about a factor of 2 with respect to those computed deterministically for selected numerical cells in the stochastic calculation. Most of the difference is due to the stochastic parcel treatment of the spray, rather than to the stochastic algorithm used to compute drop collisions. When the stochastic calculation of drop collisions and coalescence is carried out using exactly the same sequence of drops as for the deterministic calculation, rather than with the stochastic parcels of drops, the difference between the two is much smaller. It is also found that near the injector the stochastic drop parcel technique results in undesirable fluctuations of the steady mean gas velocity. Far from the injector, insensitivity of the mean gas and drop velocities (but not necessarily of the drop size) to the physics and numerics of the region near the injector is confirmed. It is suggested that future spray computations be made with an orthogonal mesh that approaches spherical coordinates far from the injector.

In the following sections, the stochastic model is reviewed, and the stochastic and deterministic methods of computing drop collisions are stated. Then a specific steady spray and sample numerical cells within it are selected, and the two methods of computing collisions are applied to those cells. The results of some computations with greater numerical resolution are then considered, and the main conclusions are summarized.

II. Calculation Approaches

A description of the two calculation methods is now given. First, the stochastic method is reviewed, including details that pertain both to the momemtum exchange between the drops and the gas and to drop collision. The deterministic calculation approach is then described, followed by a discussion of the method of comparing the stochastic and deterministic results.

A. Stochastic Method

The stochastic approach to representing spray dynamics originates in the work of Dukowicz,[1] who used a Lagrangian calculation of sample parcels of drops. The parcels are assigned properties at the inlet according to a statistical distribution and are allowed to interact through an assumed drag law with a continuum gas field, which is determined by solution of Eulerian finite-difference equations. The effect of turbulent dispersion is included by associating with each parcel a turbulent gas velocity, sampled from a Gaussian distribution with a selected standard deviation, and allowing the parcel to be affected by that velocity for a specified length of time. O'Rourke and Bracco[2] and O'Rourke[6] extended that work by placing the method on a firm theoretical basis and by developing models for drop collisions producing coalescence of smaller drops into larger ones.

Gosman and Ioannides[7] used the two-equation k-ϵ model to evaluate scales of the gas turbulence and also improved the method of O'Rourke

and Bracco[7] for computing the residence time of a drop in a turbulent eddy. Finally, the introduction of drops into the domain, corresponding to the physical process of drops being stripped from the surface of the injected liquid jet, is accomplished with a version of the line-source method of Chatwani and Bracco.[8] Parcels of drops with properties determined from aerodynamic instability theory are injected along the jet axis from the nozzle exit to the end of the intact liquid core. The implementation used here differs from that reported in Ref. 8 in two ways. First, the size of the drops in injected parcels is assigned by sampling the empirical size distribution function of Hiroyasu and Kadota[9] instead of injecting each parcel with the same drop size. Second, rather than introduce all parcels on the axis, they are distributed uniformly in the radial direction from the axis out to one nozzle radius.

Since the aim of the present study is the evaluation of the purely dynamic aspects of sprays associated with collisions, mass and thermal energy exchanges between the drops and the gas are not considered and the corresponding terms are dropped from the equations. Those interested in the complete model may consult the references given earlier. The equations expressing the behavior of the gas field are

Mass continuity:

$$\frac{\partial \hat{\rho}_g}{\partial t} + \nabla \cdot (\hat{\rho}_g \boldsymbol{u}) = 0 \tag{1}$$

Momentum conservation:

$$\frac{\partial \hat{\rho}_g \boldsymbol{u}}{\partial t} + \nabla \cdot (\hat{\rho}_g \boldsymbol{u}\boldsymbol{u}) = -\nabla p + \nabla \cdot \underline{\tau}_t - \iint \rho_l \frac{4}{3} \pi r^3 \dot{\boldsymbol{v}} f \, dr \, d\boldsymbol{v} \tag{2}$$

Enthalpy balance:

$$\frac{\partial \hat{\rho}_g h_g}{\partial t} + \nabla \cdot (\hat{\rho}_g h_g \boldsymbol{u}) = \theta \left(\frac{\partial p}{\partial t} + \boldsymbol{u} \cdot \nabla p \right) + \underline{\tau}_t : \nabla \boldsymbol{u}$$

$$+ \nabla \cdot \left[\hat{\rho}_g C_{p_g} D_t \nabla \left(\frac{h_g}{C_{p_g}} \right) \right] - \iint \rho_l \frac{4}{3} \pi r^3 \dot{\boldsymbol{v}}_a \cdot (\boldsymbol{u} + \boldsymbol{u}' - \boldsymbol{v}) f \, dr \, d\boldsymbol{v} \tag{3}$$

Turbulence kinetic energy and dissipation rate:

$$\frac{\partial \hat{\rho}_g k}{\partial t} + \nabla \cdot (\hat{\rho}_g \boldsymbol{u} k) = \nabla \cdot \left(\frac{\hat{\rho}_g D_t}{\sigma_k} \nabla k \right) + G - \hat{\rho}_g \epsilon \tag{4}$$

$$\frac{\partial \hat{\rho}_g \epsilon}{\partial t} + \nabla \cdot (\hat{\rho}_g \boldsymbol{u} \epsilon) = \nabla \cdot \left(\frac{\hat{\rho}_g D_t}{\sigma_\epsilon} \nabla \epsilon \right)$$

$$+ \frac{\epsilon}{k} (C_1 G - C_2 \hat{\rho}_g \epsilon) + C_3 \hat{\rho}_g \epsilon \nabla \cdot \boldsymbol{u} \tag{5}$$

Here

$$G = \underline{\tau}_t : \nabla \boldsymbol{u} - (2/3) \hat{\rho}_g k \nabla \cdot \boldsymbol{u} \tag{6}$$

and

$$\underline{\tau}_t = \hat{\rho}_g D_t \left[\nabla \boldsymbol{u} + \nabla \boldsymbol{u}^{\mathsf{T}} - (2/3)\nabla \cdot \boldsymbol{u}\underline{I} \right] \tag{7}$$

The model relation for the diffusivity due to molecular effects and to turbulent motions is $D_t = D + C_\mu k^2/\epsilon$. The model coefficients are $C_1 = 1.5$, $C_2 = 1.9$, $C_3 = -1.0$, $\sigma_k = 1.0$, $\sigma_\epsilon = 1.3$, and $C_\mu = 0.09$.

In these equations, the mean gas velocity is designated by $\boldsymbol{u}$ and the drop velocity by $\boldsymbol{v}$; $\hat{\rho}_g$ is the mass of gas per volume of space (which when divided by the fraction of volume occupied by the gas—the "void" fraction, θ—gives the gas density ρ_g); $f(r,\boldsymbol{v},\boldsymbol{x},t)$ is the number distribution function of the drops, i.e., the number of drops per unit volume in physical space and drop property space; and the usual meanings are attached to the other variables. In the gas momentum and energy equations, the integral terms on the right-hand side represent the rates of momentum and energy exchange between drops and gas.

The equation governing f is the spray equation of Williams[10] with terms added by O'Rourke and Bracco to account for distribution changes due to drop collisions:

$$\frac{\partial f}{\partial t} + \nabla \cdot (f\boldsymbol{v}) + \nabla_v \cdot (f\dot{\boldsymbol{v}}) = \frac{1}{2}\int_a \int_b \nu_{ab}[\sigma_{ab} - \delta(r - r_a)\delta(\boldsymbol{v} - \boldsymbol{v}_a) - \delta(r - r_b)\delta(\boldsymbol{v} - \boldsymbol{v}_b)]\, dr_a\, d\boldsymbol{v}_a\, dr_b\, d\boldsymbol{v}_b \tag{8}$$

The terms on the left-hand side describe changes in f resulting from unsteadiness and convective effects in physical and velocity space. The integral on the right-hand side represents the rate of change of f resulting from collisions. The integral accounts for binary collisions between all possible drop pairs. The quantity ν_{ab} is the collision rate per volume in physical and phase space for drops with properties $(\boldsymbol{v}_a, r_a)$ colliding with drops with properties $(\boldsymbol{v}_b, r_b)$. The first term in the brackets represents the source term due to collisions, being the probability that a collision between a drop with properties a and one with properties b will produce a drop with $(\boldsymbol{v}, r)$. The other two terms in the brackets describe the loss of drops with properties $(\boldsymbol{v}, r)$ due to collisions.

Relations must be given for ν_{ab} and σ_{ab} to complete the spray equation. These relations are central to the present investigation and will be presented in the next section. Also needed are the equations governing the motion of a drop having density ρ_l,

$$\dot{\boldsymbol{v}} = \dot{\boldsymbol{v}}_a - \nabla p/\rho_l \tag{9}$$

with

$$\dot{\boldsymbol{v}}_a \equiv \frac{3}{8}\frac{\rho_g}{\rho_l}\frac{|\boldsymbol{u} + \boldsymbol{u}' - \boldsymbol{v}|}{r}(\boldsymbol{u} + \boldsymbol{u}' - \boldsymbol{v})C_d$$

and the equation of state

$$p = \rho_g R h_g / c_{p_g} \tag{10}$$

In the drop equation of motion, the empirical relation used for the drag coefficient is

$$C_d(\theta, Re) = \frac{24}{Re}\left(\theta^{-2.65} + \frac{Re^{2/3}\theta^{-1.78}}{6}\right) \tag{11}$$

where

$$Re = (2\rho_g|u + u' - v|r)/\mu_g$$

As previously stated, the influence of turbulent gas motion is felt through the drag term. The drop responds to the difference between the gas velocity $(u + u')$ and the drop velocity v. The turbulent velocity, u', that is assigned to a given drop is determined by randomly sampling a Gaussian distribution having zero mean and a standard deviation equal to the local value of the turbulence velocity scale $\sqrt{\frac{2}{3}k}$. The sampled turbulent velocity remains in effect for a time corresponding to the lesser of the eddy lifetime, τ_e, and the time taken for the drop to cross the turbulent eddy, τ_l. The characteristic times are those proposed by Gosman and Ioannides[7]:

$$\tau_e = \min [\tau_t, \tau_l] \tag{12}$$

where

$$\tau_t = C_\mu^{3/4} \sqrt{3/2}(k/\epsilon)$$

and τ_l is determined from the implicit equation

$$\int_t^{t+\tau_l} |u + u' - v| \mathrm{d}t = l_t$$

where

$$l_t = C_\mu^{3/4} k^{3/2}/\epsilon$$

Collision Model

The collision characteristics that remain to be described are the collision rate, ν_{ab}, and the transition probability function, σ_{ab}, for a binary collision between drops of class a and drops of class b. The collision frequency relation used in the model is derived from the kinetic theory of gases and is accurate for elastic particles occupying uniformly a negligible volume in space and traveling in a vacuum. The collision frequency per unit volume in physical space is

$$\nu_{ab}\, \mathrm{d}v_a\, \mathrm{d}r_a\, \mathrm{d}v_b\, \mathrm{d}r_b \tag{13}$$

where

$$\nu_{ab} = f_a f_b \pi (r_a + r_b)^2 |v_a - v_b|$$

The transition probability function σ_{ab} is constructed with the view that the outcome of collisions is either coalescence of the two drops or a collision in which the two drops do not combine but do exert an influence on each other. When the drops coalesce, the outcome of the collision is a single drop having the velocity which preserves the total translational momentum of the original two drops. The translational energy and angular momentum with respect to the center of mass of the two drops is assumed to be transformed into rotation and internal energy of the coalesced drop. When the rotation energy of the colliding drops exceeds the drop breakup energy, the model prescribes a "grazing" collision in which the two drops do not combine, but in which the kinetic energy and angular momentum (in the mass center coordinate system) are partially dissipated to internal forms of motion. The degree of dissipation is required to conform to the limits of complete dissipation when coalescence occurs and to zero dissipation when the two drops just barely touch one another as they pass. Between these two limits, a dissipation of angular momentum varying linearly with the collision separation distance is prescribed. The fraction of dissipated energy is selected so that the direction of motion of the two grazing drops is not altered when viewed from the center-of-mass coordinate system. The σ_{ab} function that follows from these considerations is rather complicated and is not given here (see Ref. 6), since in the numerical scheme the function is not used directly.

Numerical Implementation

The gas field equations are solved using a first-order pressure-implicit scheme (the Implicit Continuous-Fluid Eulerian (ICE) method of Harlow and Amsden[11]). These equations are coupled through the drag terms to the drop equations and that coupling is included in the implicit pressure solution using the scheme proposed by Dukowicz.[1] The spray equation is solved indirectly using a Monte Carlo technique in which the paths of stochastic parcels of drops are followed in physical, velocity, and radius space. Each parcel contains a specific number of drops and is associated with particular values of velocity, radius, and turbulent eddy parameters. The parcels in the calculation domain at any moment represent the drop number distribution. As the number of parcels is increased, the representation of the number distribution should become more accurate. In the calculations, the numerical cell volume is used to compute collisions and momentum exchange terms. In each time step, the drops in the parcels in each cell are allowed to collide according to a scheme that stochastically selects which parcel pairs collide and what the outcome of the collision is. The properties and the number of drops in the colliding pairs of parcels are adjusted as described in the previous section. The parcels replace the drops of classes a and b. The mean collision rate between each pair of parcels coexisting in a given numerical cell is given by

$$v_{ab}\Delta r_a \Delta v_a \Delta r_b \Delta v_b \mathrm{Vol}_{\mathrm{cell}} = n_a \pi (r_a + r_b)^2 |v_a - v_b| / (\mathrm{Vol}_{\mathrm{cell}}/n_b) \qquad (14)$$

The ratio on the right-hand side is the rate at which the drops in parcel a sweep the volume in which a collision with parcel b drops may occur,

divided by the volume in which the center of one drop from b will, on average, be found. In the numerical scheme, the number of collisions occurring between drops in parcels a and b in time Δt is assumed to have a Poisson distribution about the mean number of collisions given by Eq. (14). The number of collisions occurring is determined by the selection of a random number uniformly distributed in the interval [0, 1] and allowing the number of collisions to occur that corresponds to the cumulative Poisson-distribution probability equal to the random number.

Once it is determined that a pair of parcels collide, the outcome of the collision is determined by selecting a second random number that, in effect, specifies the impact parameter of the collision and, thus, determines whether the collision results in coalescence of the drops or a grazing collision. The decision is based on the coalescence parameter

$$b/b_{crit} = \sqrt{\min[1.0, 2.4F(\gamma)/We_{ab}]} \tag{15}$$

where

$$We_{ab} = \rho_l(\boldsymbol{v}_a - \boldsymbol{v}_b)^2 \min[r_a, r_b]/\sigma$$

and

$$F(\gamma) = \gamma^3 - 2.4\gamma^2 + 2.7\gamma \tag{16}$$

When the second random number is greater than $(b/b_{crit})^2$, the energy of angular motion of the two drops exceeds the surface energy decrease in forming a single drop, and a grazing collision occurs. Below this value, the parcel drops coalesce. The function F expresses the effect that the relative size of the colliding parcel drops has on the collision outcome. The parameter γ is the ratio of the radii of the larger to the smaller size drops of the parcel pair and is always greater than unity. From the form of $F(\gamma)$, drops of greatly unequal size will be more apt to coalesce than drops of nearly equal size. The collision outcome is also influenced by the collision Weber number, We_{ab}, which brings in a dependence on relative drop velocity and absolute drop size. Larger We_{ab} corresponds to reduced likelihood of coalescence.

B. Deterministic Model

The results obtained with the stochastic method will be compared with those obtained with a deterministic approach that uses the same algorithm to determine the outcome of collisions, but where the decision of which drops collide and when they collide is made deterministically. The computational work is devoted almost entirely to determining the time to the next collision. This requires calculating the future time of closest proximity for each of the $N(N - 1)/2$ possible pairs of N drops in the computational cell and determining whether the closest approach allows contact. Thus, the computational time increases as N^2. Reduction of this time is possible when the trajectories of the drops between collisions are straight, but not when they are curved. For the conditions of interest, the integration time

step was set equal to the time between successive collisions, and it was typically less than the integration time used in the stochastic calculations.

The deterministic code has undergone thorough tests, including ones to ensure that individual collisions are worked out correctly (so that momentum and energy are conserved, and so that none that should occur is overlooked). In addition, the code has been applied to calculating the distribution of velocities in an elastic-sphere gas as well as the diffusion coefficients of momentum and mass transfer. The equilibrium results showed excellent agreement with the Maxwell-Boltzmann velocity distribution, and the diffusion coefficients were in good agreement with those determined from Enskog gas theory.

Correspondence of Deterministic and Stochastic Conditions

The strength of the comparison between the stochastic and deterministic results depends greatly on how closely the conditions of the deterministic calculation approach those of the corresponding stochastic calculation. What is desired in the deterministic computation is a schedule with which drops of various sizes, velocities, and associated gas turbulence properties are introduced at the cell boundary. This schedule should reproduce the same statistical distribution of the parcels entering the cell in the stochastic computation. The method used in this work is based on treating the stochastic results as statistically steady with the parcels entering a given mesh cell treated as independent samples from the same, steady drop distribution function. This view is consistent with the stochastic calculation method, which solves the distribution function equation using a finite number of sample parcels.

The task of devising a schedule for introducing drops at the cell boundary in the deterministic calculation involves deducing the drop distribution function from the parcels entering that cell in the stochastic calculation. That is, a representation of

$$f(\boldsymbol{x},\boldsymbol{s}) \equiv f(\boldsymbol{x},\boldsymbol{v},r,l_t,\tau_t) \tag{17}$$

must be made, where $\boldsymbol{s}$ is used to abbreviate the list of properties, excluding position, that characterize a drop entering the cell. Once $f(\boldsymbol{x},\boldsymbol{s})$ is available, the number of drops that enter the cell through area ΔA and have properties in $(\boldsymbol{s},\boldsymbol{s}+\Delta\boldsymbol{s})$ is given by the convection formula

$$n(\boldsymbol{x},\boldsymbol{s},\Delta\boldsymbol{s},\Delta t) = f(\boldsymbol{x},\boldsymbol{s})\Delta\boldsymbol{s}\boldsymbol{v}\cdot\Delta\boldsymbol{A}\Delta t \tag{18}$$

In this relation, $f\Delta\boldsymbol{s}$ is simply the number of drops per unit volume at $\boldsymbol{x}$ with properties in the interval $[\boldsymbol{s},\boldsymbol{s}+\Delta\boldsymbol{s}]$, and $\boldsymbol{v}\cdot\Delta\boldsymbol{A}$ is the rate at which volume is passing across the area element at the velocity of the drops.

The stochastic computation results in some number of sample parcels n_p that entered a cell over a collection period T. There are two approaches to representing $f(\boldsymbol{x},\boldsymbol{s})$ using the collected parcels. A smooth distribution function could be fitted through the collected samples, perhaps requiring the function to satisfy certain moments of the actual samples, or one could make use of the sample parcels directly, which is equivalent to using a

discrete representation of the distribution function. The first method requires constructing the distribution function and then sampling that function to arrive at the number of drops and their properties that should be introduced in each time step in the deterministic calculation. However, fitting a distribution introduces errors, and so the direct use of the collected samples was selected.

The n_{d_j} drops in each of the n_p parcels collected over a total time T in the stochastic calculation are introduced according to the following relation:

$$n_j(\boldsymbol{x},\Delta t) = n_{d_j}\Delta t/T, \qquad j = 1, n_p \tag{19}$$

where n_{d_j} is the number of drops in the jth parcel, and n_j is the number of drops with the properties of parcel j introduced at the cell surface in the numerical time step Δt. This formula may be derived by first constructing the discrete distribution function having one parcel in each discrete volume of physical space and phase space and substituting into the number flux relation, Eq. (18). To demonstrate the relationship, one may substitute the preceding formula into the number flux relation to arrive at the implied discrete distribution function:

$$f_j(\boldsymbol{x},\boldsymbol{s}_j,\Delta s_j) = n_{d_j}(\Delta s_j \boldsymbol{v}_j \cdot \Delta \boldsymbol{A} T), \qquad j = 1, n_p \tag{20}$$

which is clearly the correct form of the discrete distribution function, being the number of drops with certain properties $\boldsymbol{s}_j$ per property space volume Δs_j and per physical space volume $\boldsymbol{v}_j \cdot \Delta \boldsymbol{A} T$. The point at which the drops are introduced is chosen randomly over the surface according to a uniform distribution over the projected cell surface area in the direction of the entering drop velocity. All drops introduced in a given time step are started at the same time from the cell boundary. The time step is always much smaller than the time for a drop to cross the numerical cell in order to resolve the collision and turbulent dispersion processes.

In practice, when the number of parcels in the field is large enough to provide reasonable statistical resolution, the number of drops from a given parcel to be introduced in one time step may be much less than one. Thus, it is necessary to accumulate fractions of drops over consecutive time steps until a complete drop is accumulated and may be introduced. There is a further difficulty that must be overcome. If many of the parcels in the ensemble require a long time for a single drop to be accumulated, very few drops will be introduced into the cell until sometime after the beginning of the calculation. Then the introduction rate will rise suddenly. This problem is avoided in the calculation by randomly assigning to each sample parcel an initial accumulated drop fraction in the range [0, 1].

The correct operation of the drop introduction scheme of Eq. (19) was checked by comparing the average properties of the entering drops in the deterministic calculation with those of the stochastic calculation. The average rates of entry for the number, mass, and momentum of drops agreed to within 1% of the stochastic values. Similarly, the average drop velocity, radius, and turbulence scales associated with incoming drops were the same.

III. Stochastic Results

Since the investigation takes as its starting point the spray field and gas field conditions obtained with the stochastic result, it is useful to examine those results in some detail before considering the deterministic computations and comparing the two results. Thus, the results of previous stochastic calculations of the spray examined in this chapter are presented, compared with measurements, and used to select the numerical parameters for our study. Then two sets of stochastic results are discussed that were obtained with different treatments of the gas field.

A. Selected Spray and Earlier Comparisons with Experiments

The particular spray considered is that formed by a round jet of liquid hexane at 300 K issuing at 19.4 cm/ms from a tubular nozzle with diameter $d_n = 127$ μm into gaseous nitrogen at 293 K and 4.24 MPa absolute pressure. This is case C studied by Wu et al.,[12] who measured the steady-state axial and radial drop velocity components at various locations for $x/d_n \geq 300$. The high gas density and low temperature make this case attractive for the purposes of the present study since the dynamic effect of drop momentum exchange is significant but the complicating process of drop vaporization is practically eliminated. In addition, since drop densities will be high in the developing near-field region of the spray, coalescence of drops will be a strong effect. The intact core length is estimated to be 26 nozzle diameters from $d_c = 7d_n\sqrt{\rho_l/\rho_g}$.[13]

The stochastic computation method has been demonstrated to give an adequate account of the drop velocity measurements for $x/d_n \geq 400$. Calculations of this spray are reported in Refs. 8, 14, and 15. The results given in Ref. 15 are used here to demonstrate the agreement achieved with the measured drop velocities. This same calculation using an identical computational grid and identical conditions has been repeated as a check in this chapter.

Various statistical properties of the measured and calculated drop velocities are plotted as functions of radial position in Fig. 1 at axial locations of $x/d_n = 400$, which is the measurement location nearest the spray origin, and at $x/d_n = 500$ and 600. The radial profiles of the mean, skewness, and flatness of the axial component of drop velocity produced in the calculation (Figs. 1a, 1d, and 1e) show good agreement with the measurements. The statistical uncertainty of properties at the edge of the layer is high because few samples are collected there, both experimentally and computationally. The calculated skewness and flatness of the radial component of drop velocity show a similar level of agreement with experiment as for the axial skewness and flatness shown. The root-mean-squared fluctuation of the axial drop velocity (Fig. 1b) is somewhat underestimated and that of the radial drop velocity (Fig. 1c) is somewhat overestimated. There are no measurements of the drop size for which usefully small uncertainties have been demonstrated. The quoted works had also shown that the computed drop velocity field beyond $x/d_n = 400$ did not change significantly when the numerical resolution was doubled.

Thus, at the beginning of the present study, indications were that the model reproduces the far-field mean drop velocities of the sprays with

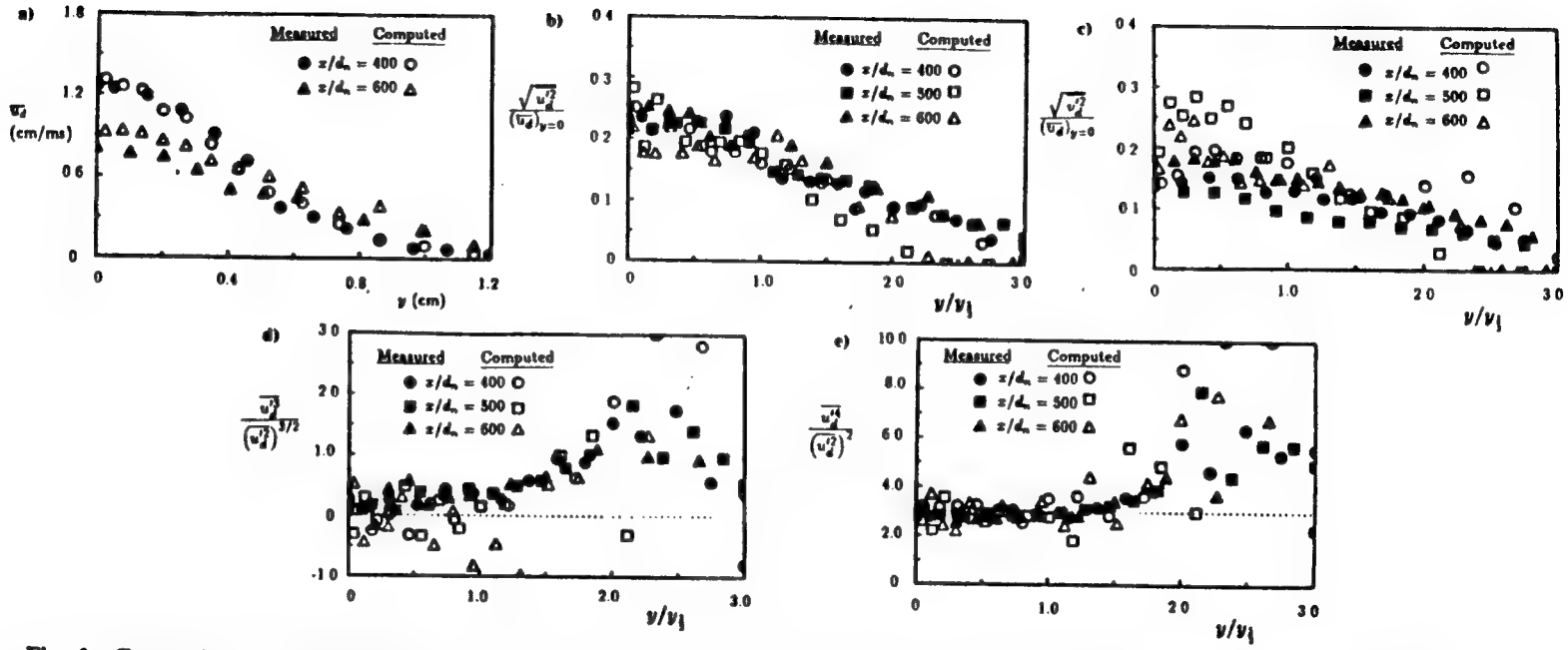

Fig. 1 Comparison of stochastic calculation and measurements of Ref. 12 in a full-cone spray: a) average axial drop velocity, rms fluctuation of b) axial and c) radial drop velocity fluctuation, and d) skewness and e) flatness factors of axial drop velocity fluctuation. $y_{1/2}(x)$ is the position at which u_d is one-half of its centerline value. (Figures from Ref. 15.)

about the same accuracy with which such velocities can, at present, be measured but that there are uncertainties about the drop size.

The cylindrical grid used in all of the computations quoted earlier has 44 cells in the axial direction, 26 cells in the radial, a cell-to-cell axial expansion factor of 4% and a radial factor of 7%, and minimum cell size nearest to the injector nozzle of $\Delta y = 0.5$ mm and $\Delta x = 1.0$ mm. This grid is referred to here as the X1 grid. To reduce the number of drops in each numerical cell and improve numerical accuracy, the present study employs the same number of cells and expansion factors but a minimum cell size of $\Delta y = 0.17$ mm and $\Delta x = 0.33$ mm. This grid, shown in Fig. 2, is referred to as X3 since its resolution is three times greater than that of the earlier studies. Note that the X1 grid extends to $x/d_n = 850$, whereas the X3 grid extends to $x/d_n = 130$ with a corresponding reduction in the radial direction. Because the drop velocities remain high in the shortened X3 grid domain, the time required in the calculation to reach a steady state and to collect an adequate number of samples thereafter is reduced considerably. This partially offsets the decrease in computation time step size and the greater computation time per step due to the finer grid and the increased number of parcels needed to maintain resolution of the distribution function in each grid cell. A total of about 1000 parcels was used in the X1 calculation, and around 10,000 in the X3 calculation.

Results of preliminary calculations were used to identify the cells for comparisons of the stochastic and deterministic models. A region of the grid was found that had cells with a high collision rate and an average number of drops below a few thousand per radian of azimuthal angle. This region extended from about 30 to 60 nozzle diameters downstream and radially for about $5d_n$. Upstream of this region, drop numbers become too high to allow use of the deterministic calculation. Downstream and further away from the axis, the collision rates become small. From this region, six specimen cells were selected. The cells are at three radial positions—$r/d_n = 0.7$ (the cell that adjoins the domain centerline), 2.0, and 4.6—and at the two axial locations—$x/d_n = 38$ and 49. The relation of the cells

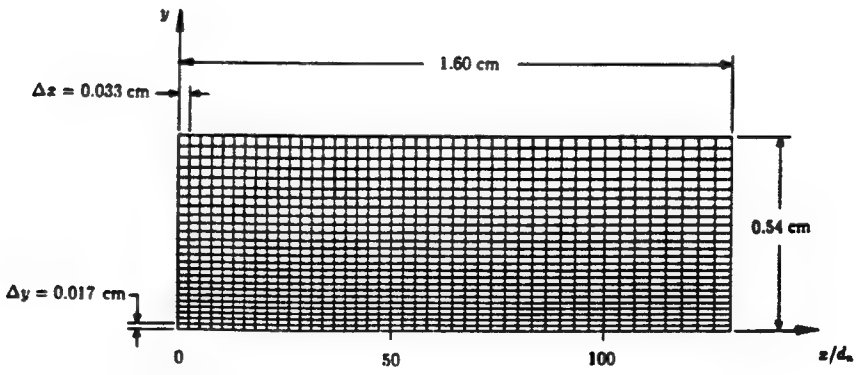

Fig. 2 X3 grid used for stochastic calculations herein.

to the spray and to the initial, continuous liquid core of the hexane jet is illustrated in Fig. 3. The dots mark the locations of parcels at a particular time under steady-state conditions in the stochastic calculation.

B. Stochastic Results with Calculated Gas Field

The average conditions found in the stochastic calculations are summarized for each specimen cell in Table 1. In the first portion of the table, the velocities, pressure gradients, and other cell gas properties needed to make deterministic calculations are given. Because of the staggered grid used in the numerical scheme, different values of velocity and static pressure gradient apply to parcels in the same cell depending on which of the staggered momentum cells (two for u_g and two for v_g) the parcel is in. The staggered locations of the velocities and pressure gradients indicated in Table 1 are shown for a typical cell in Fig. 4. Values given in the table are cell averages corresponding to the time interval from 0.32 to 0.66 ms following the start of the calculation when gas is at rest and no drops are in the domain. The uncertainty of the average gas velocities is about $\pm 1\%$ of their local values. The average pressures have an uncertainty of about $\pm 1\%$ of the local dynamic pressure ($\rho_g \boldsymbol{u} \cdot \boldsymbol{u}$). Other gas properties are uncertain by about $\pm 1\%$ of their local values. All of these uncertainties are based on the root-mean-squares of the values accumulated within the time window from 0.32 to 0.66 ms. The second part of the table gives (volume) average properties of the parcels that entered and exited each specimen cell during the calculation, together with the rates at which parcels, drops, and drop mass entered the cell on average. The number of

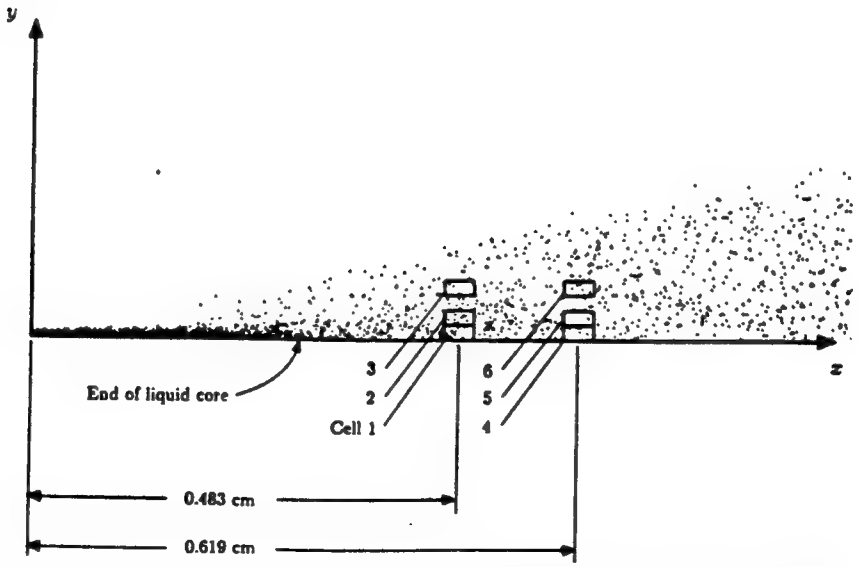

Fig. 3 Positions of specimen cells in relation to the spray. Spray represented by positions of all parcels at a particular instant of time at stochastic steady state.

Table 1 Average stochastic results with computed gas field

	Specimen cell					
	1	2	3	4	5	6
	Average gas properties in specimen cells					
u_g^-, cm/ms	12.3	9.01	2.76	10.6	8.75	3.82
u_g^+, ...	11.9	9.00	3.07	10.1	8.61	4.04
v_g^-, ...	0.0	0.08	−0.09	0.0	0.09	0.02
v_g^+, ...	0.08	0.04	−0.21	0.09	0.09	−0.07
w_g, ...	−0.04	0.03	0.01	−0.03	−0.01	0.0
$(\partial p/\partial x)^-$, g/(cm²-ms²)	−0.4	0.5	−0.3	1.6	1.0	0.1
$(\partial p/\partial x)^+$, ...	0.8	0.6	−0.3	−0.2	0.8	0.0
$(\partial p/\partial r)^-$, ...	0.0	−0.1	6.3	0.0	−1.9	3.6
$(\partial p/\partial r)^+$, ...	−0.1	4.8	4.4	−1.9	1.9	3.5
ρ_g, g/cm³	0.0449	0.0451	0.0464	0.0453	0.0454	0.0463
θ	0.938	0.957	0.999	0.962	0.960	0.996
$\sqrt{2k/3}$, cm/ms	2.71	2.65	1.67	2.36	2.30	1.79
τ_t, μs	2.9	3.2	5.3	3.8	4.2	5.9
l_t, μm	77	84	88	90	97	106
	Average properties of entering droplets					
$\dot{n}_p$, parcels/μs	5.89	4.46	0.96	2.93	3.48	1.33
$\dot{n}_d$, droplets/μs	1200	831	162	290	463	172
$\dot{m}_d$, g/s	0.0975	0.1741	0.0067	0.0543	0.1331	0.0223
$\overline{u_d}$, cm/ms	12.52	10.80	3.60	11.37	9.90	4.58
$\overline{v_d}$, ...	1.18	1.12	0.55	0.46	0.58	0.35
$\overline{w_d}$, ...	−0.07	−0.06	0.16	−0.03	0.15	−0.14
SMR, μm	5.15	5.76	3.54	5.53	5.87	4.71
$\overline{r_d}$, μm	1.35	2.69	1.22	2.62	3.46	2.19
	Average properties of exiting droplets					
$\dot{n}_p$, parcels/μs	5.32	4.16	0.94	2.78	3.33	1.30
$\dot{n}_d$, droplets/μs	892	670	158	262	432	157
$\dot{m}_d$, g/s	0.1005	0.1727	0.0066	0.0540	0.1337	0.0223
$\overline{u_d}$, cm/ms	12.02	10.34	3.55	10.97	9.66	4.83
$\overline{v_d}$, ...	1.55	0.60	0.24	0.93	0.55	0.27
$\overline{w_d}$, ...	−0.13	−0.01	−0.05	0.0	0.0	−0.14
SMR, μm	5.30	5.84	3.68	5.68	5.98	4.78
$\overline{r_d}$, μm	1.65	3.03	1.31	2.74	3.65	2.57

parcels collected is the sample population size; this is over 1000 for each of the four cells nearest the axis and around 500 in the two outer cells.

The pattern observed in the results is that which is expected. The gas and the drop velocities decrease with both radial and axial distances. The gas volume fraction, θ, is lowest upstream and near the centerline, where there is a greater drop density. The Sauter mean radius (SMR, the ratio

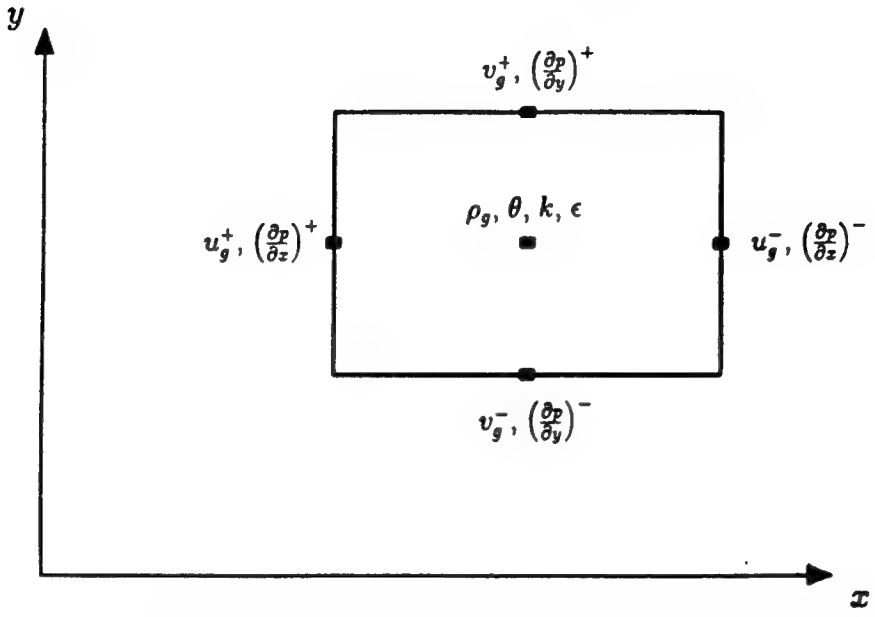

Fig. 4 Typical specimen cell showing storage locations of gas field variables.

of the average of the drop radius cubed divided by the average of the drop radius squared) and the number average radius increase in the axial direction because of coalescences. In general, they decrease radially because small drops tend to be diffused by turbulence more effectively than large ones.

Some results indicating the relative importance of various processes in the specimen cells are listed in Table 2. The number of drops per unit volume decreases both axially and radially. The proportion of collisions resulting in coalescence—the coalescence fraction—is about 70–80% in the upstream cells and about 40% in the downstream cells. The cause of the change appears to be related to the tendency for colliding drops of similar size to favor grazing over coalescence [which is represented by the function $F(\gamma)$ in the transition probability model]. Indeed, the standard deviation in size of drops entering cells 4 and 5 is noticeably lower than for the other cells. The final quantity in the table is the rate at which drops change to a new eddy in the calculation. The eddy exchange rate per unit volume is nearly a constant proportion of the number of drops per unit volume at each of the two streamwise positions. The exchange rate is, however, a slightly greater proportion of the number density at the upstream position compared with the downstream position. This reflects the fact that the turbulent time and length scales are larger downstream (Table 1).

It is observed that, within the steady jet, the computed steady (mean) velocity of the gas is, in fact, fluctuating in time and with an amplitude that is comparable to the turbulence intensity. One can see from Table 3 that the root-mean-squared fluctuations of the "steady" axial and radial gas velocity components are about 10% of the average axial velocity com-

Table 2 Cell conditions of the stochastic results with computed gas field

	Specimen cell					
	1	2	3	4	5	6
$\bar{n}_p$	13.2	11.2	5.5	7.3	9.4	6.9
$\bar{n}_d/\mathrm{Vol}_{\mathrm{cell}}$, millions/cm^3	493	136	27	146	81	25
$\bar{m}_d/\mathrm{Vol}_{\mathrm{cell}}$, g/cm^3	0.0358	0.0279	0.0008	0.0293	0.0278	0.0027
$\mathrm{Vol}_{\mathrm{cell}}$, 10^{-5} cm^3	0.463	1.389	3.241	0.4847	1.454	3.393
SMR, μm	4.76	5.88	3.46	5.63	6.39	4.69
Collision rate, millions/cm^3-μs	108	20.1	0.2	9.7	9.1	1.3
Coalescence rate, millions/cm^3-μs	88	12.3	0.2	3.7	3.6	1.1
Grazing rate, millions/cm^3-μs	20	7.8	0.0	6.0	5.5	0.2
Eddy exchange rate, millions/cm^3-μs	205	57.1	6.4	47.4	31.8	5.1

ponent taken over a time window of 0.34 ms in the steady spray. The steady void fraction and the turbulence kinetic energy also fluctuate by similar magnitudes.

The cause of the gas field fluctuations is a variation in time of the number of drop parcels that are within each numerical cell coupled with the significant momentum exchange between drops and the gas. That is, the roughness of the representation of the drop distribution function and the strong coupling between gas and drops in the sample cells produces the gas field fluctuations. The number of parcels in the sample cells is shown at 0.005-ms intervals in Fig. 5. The large variations are a result of statistical

Table 3 Normalized rms fluctuations of the steady gas properties of the stochastic results with computed gas field

	Specimen cell					
	1	2	3	4	5	6
$\sqrt{(u_g^*)^2}/\bar{u}_g^*$, %	10.2	8.1	9.3	10.5	8.3	8.1
$\sqrt{(v_g^*)^2}/\bar{u}_g^*$, %	10.2	8.1	9.8	11.8	8.6	8.5
$\sqrt{(w_g^*)^2}/\bar{u}_g^*$, %	3.1	1.8	1.1	3.0	1.9	0.6
$\sqrt{k^*}/\bar{k}$, %	12.8	5.8	3.7	14.5	6.9	3.2
$\sqrt{\theta^*}/\bar{\theta}$, %	7.9	4.3	0.5	6.7	4.5	0.7
$\sqrt{p^*}/\frac{1}{2}\rho_g\bar{u}_g^*$, %	109	100	316	140	111	207
$\sqrt{p^*}/\bar{v}_a\mathrm{SMR}\rho_l$, %	2.1	0.8	1.6	5.5	1.8	1.5

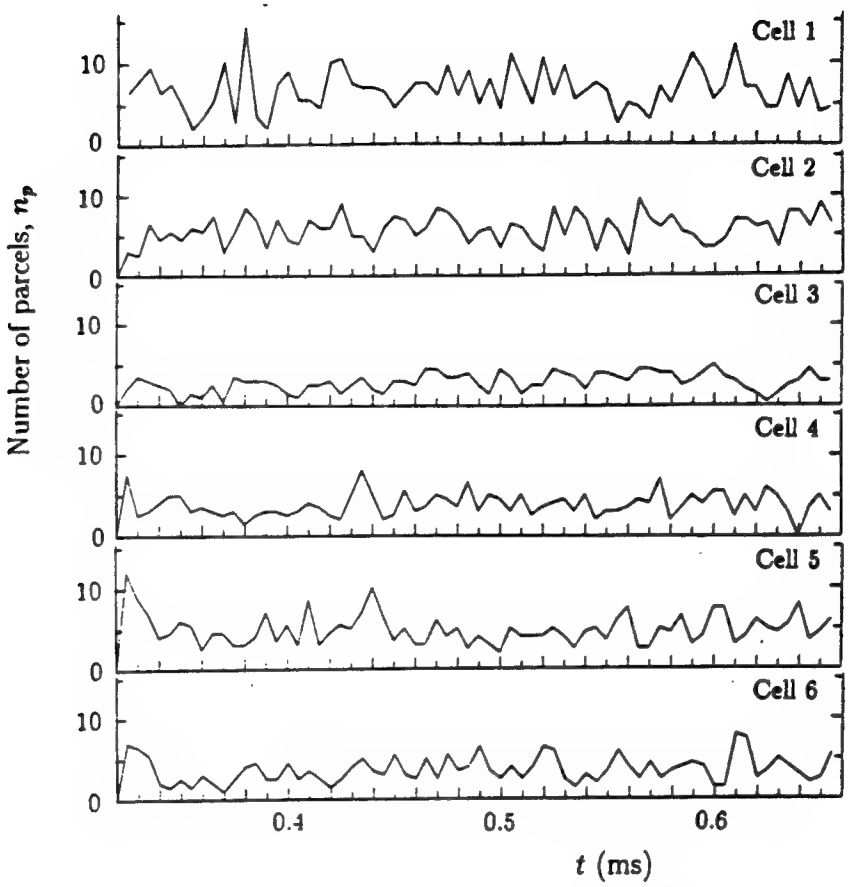

Fig. 5 Time history of the number of drop parcels in the X3 specimen cells for the computed gas field stochastic calculation, shown at intervals of 0.005 ms.

scatter associated with a relatively small average number of parcels in each cell, $\bar{n}_p$, between 5 and 14 in the sample cells (Table 2).

That the fluctuation of the steady mean gas velocity is as strong away from the axis as on the axis reflects the elliptic character of gas motions in which a strong disturbance in one cell can propagate through adjustments in the static pressure field to other locations. The time history of the axial velocity at the upstream face of cell 2 is plotted in Fig. 6. Indicated on the figure is the transit time of drops, $\tau_{trans} = \Delta x/u_d$. The higher frequency components of the fluctuations appear to scale with the transit time. The shear-layer time scale $y_{\frac{1}{2}}/(u_g)_{CL}$ at the position of cell 2 is about equal to τ_{trans}. The low-frequency fluctuation is related to acoustic propagation of disturbances reflected by the boundaries of the computational domain. It is found[16] that the amplitude of the high-frequency fluctuation decreases to less than 4% of the average axial velocity for $x/d_n > 200$. Thus, these fluctuations do not constitute a significant problem in the far field.

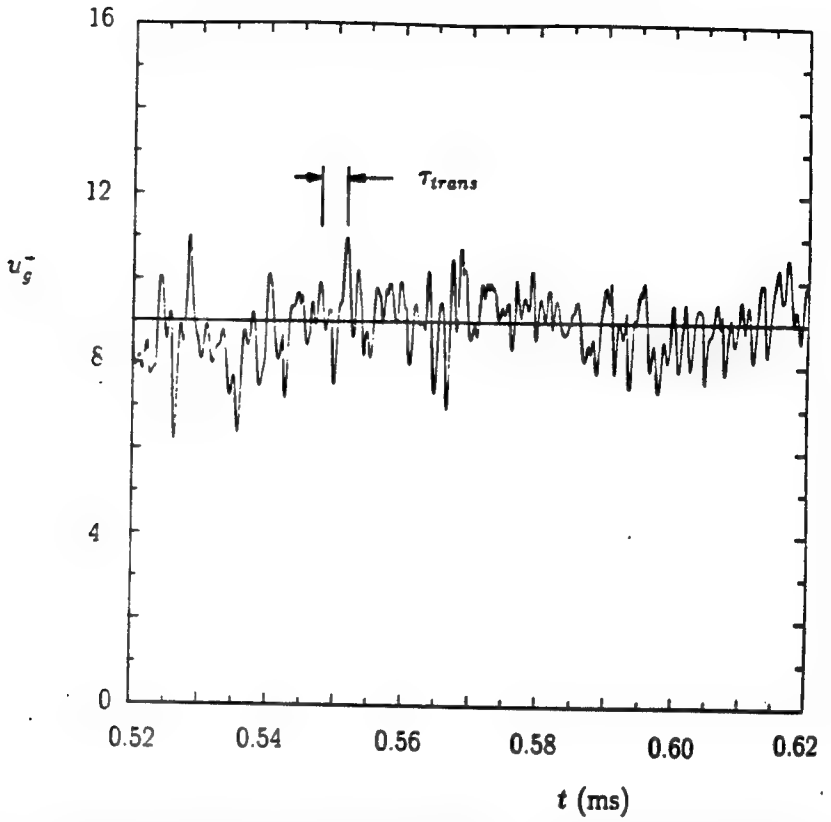

Fig. 6 Time history of u_g^* gas velocity in specimen cell 2 for the stochastic calculation with computed gas field. The average over the entire duration is indicated with the horizontal line at $u_g^* = 9.0$ cm/ms.

C. Stochastic Results with Fixed Gas Field

A large fluctuation of the steady mean gas velocity is highly undesirable because, according to Eq. (9), it acts as an artificial turbulence. In particular, such fluctuations complicate the comparison between stochastic and deterministic methods of evaluating drop collision frequencies because the drop and gas properties needed in the deterministic computation are averages obtained from the stochastic computation, as explained in Sec. II. For this reason, we decided to perform a second stochastic computation of the same drops injected into a fixed gas field. The fixed gas field was obtained by averaging the gas properties over a time that is long compared with the transit time from injection to the location of the furthest downstream specimen cell. It is realized that the flowfield obtained in this way is somewhat inaccurate since the gas and drop fields are not from the same solution of the governing equations. However, the point is irrelevant to the comparison of drop collisions within numerical cells with given gas properties. In fact, one can get a qualitative appreciation of the effect of the fluctuations of the steady gas velocity on the computed near field of

the spray by comparing the results obtained with the fixed gas field with those of the calculated gas field.

Tables 4 and 5 show the results for the fixed gas field, the entering and exiting drop properties, and the processes of collision and eddy exchange for the same specimen cells as before. Included in the table, as for the calculated gas field results, are the rates of drop mass inflow and outflow for each cell. It is clear from these mass fluxes that diffusion of drops in

Table 4 Average stochastic results with fixed gas field

	Specimen cell					
	1	2	3	4	5	6
	Average gas properties in specimen cells					
u_g^-, cm/ms	12.3	9.04	2.84	10.5	8.75	3.84
u_g^+, . . .	11.9	9.01	3.15	10.3	8.56	4.02
v_g^-, . . .	0.0	0.07	−0.07	0.0	0.08	0.03
v_g^+, . . .	0.07	0.05	−0.18	0.08	0.09	−0.05
w_g, . . .	0.04	0.0	0.0	−0.02	−0.06	−0.02
$(\partial p/\partial x)^-$, g/(cm²-ms²)	0.4	0.7	−0.4	−0.8	−0.3	−0.1
$(\partial p/\partial x)^+$, . . .	0.2	0.0	−0.4	1.5	0.3	−0.1
$(\partial p/\partial r)^-$, . . .	0.0	−1.8	6.4	0.0	0.9	3.3
$(\partial p/\partial r)^+$, . . .	−1.8	4.0	4.5	0.9	3.2	3.6
ρ_g, g/cm³	0.0487	0.0440	0.0464	0.0506	0.0444	0.0462
θ	0.858	0.979	1.0	0.850	0.974	1.0
$\sqrt{2k/3}$, cm/ms	2.69	2.65	1.69	2.39	2.35	1.80
τ_t, μs	3.0	3.2	5.3	3.9	4.2	5.9
l_t, μm	80	86	89	92	98	107
	Average properties of entering droplets					
$\dot{n}_p$, parcels/μs	5.30	3.09	0.72	2.77	2.11	0.72
$\dot{n}_d$, droplets/μs	676	492	106	373	350	87
$\dot{m}_d$, g/s	0.1908	0.0830	0.0001	0.1808	0.0964	0.0028
$\overline{u_d}$, cm/ms	13.67	9.77	3.25	11.85	9.69	3.99
$\overline{v_d}$, . . .	0.03	0.02	0.52	−0.23	−0.07	0.05
$\overline{w_d}$, . . .	0.04	0.05	−0.13	−0.17	0.01	0.48
SMR, μm	5.71	5.28	1.28	6.59	5.69	3.19
$\bar{r}_d$, μm	3.53	2.27	5.38	4.57	3.31	1.03
	Average properties of exiting droplets					
$\dot{n}_p$, parcels/μs	4.59	2.97	0.67	2.47	2.05	0.70
$\dot{n}_d$, droplets/μs	578	446	98	310	314	79
$\dot{m}_d$, g/s	0.1894	0.0830	0.0001	0.1783	0.0964	0.0028
$\overline{u_d}$, cm/ms	13.48	10.40	3.24	11.45	9.95	4.48
$\overline{v_d}$, . . .	0.25	0.35	0.12	0.10	0.17	0.79
$\overline{w_d}$, . . .	0.05	0.05	0.03	−0.29	−0.08	0.07
SMR, μm	5.83	5.33	1.23	6.90	5.79	3.24
$\bar{r}_d$, μm	3.88	2.61	4.65	4.86	3.65	1.19

Table 5 Cell conditions of the stochastic results with fixed gas field

	Specimen cell					
	1	2	3	4	5	6
$\bar{n}_p$	9.9	7.4	2.8	7.0	6.5	3.1
$\bar{n}_d/\mathrm{Vol}_{\mathrm{cell}}$, millions/cm^3	289	85.7	14.4	166	69.1	9.5
$\bar{m}_d/\mathrm{Vol}_{\mathrm{cell}}$, g/cm^3	0.0993	0.0149	0.0000	0.0914	0.0230	0.0000
SMR, μm	5.98	5.66	1.49	6.84	6.09	1.75
Collision rate, millions/cm^3-μs	74.2	5.6	0.0	54.7	6.2	0.0
Coalescence rate, millions/cm^3-μs	34.3	3.5	0.0	12.1	2.8	0.0
Grazing rate, millions/cm^3-μs	39.9	2.1	0.0	42.6	3.4	0.0
Eddy exchange rate, millions/cm^3-μs	136	35.3	3.1	73.5	22.9	1.8

the fixed gas field case is reduced significantly from that in the calculated gas field case. The axial cells show a strong increase in drop mass-flow rate while the mass flow rate into the outer cells is reduced—and nearly zero in the two cells furthest from the axis. Although drop mass-flow rates into the cells on the axis increase, the number of drops in the cells decreases. The increased average drop size reveals that the decreased drop numbers in the cells on the axis must be largely the result of an increased coalescence rate upstream of each cell, whereas away from the axis the decrease in drop size indicates that reduced diffusion is the cause. Again, large fluctuations in the number of parcels in a cell occur even though the gas field is fixed. This confirms that the fluctuations are due primarily to the poor resolution of the drop distribution function.

Thus, it has been established that gas fluctuations, which are set up by the rough discretization of the distribution of drop properties—in particular, the drop number density—as represented by the parcels, cause considerable augmentation of drop diffusion in the near field of the computed spray. The drop number distribution is too crudely resolved with the number of parcels used in the calculations, even though the number of parcels is greater than is practical in current spray applications.

IV. Deterministic Results

The deterministic calculations were performed using the spray and gas properties obtained with both the calculated gas and the fixed gas fields. In examining the deterministic results, the focus is on differences in what occurs within the cells.

Most of the details of the procedure used to make the deterministic calculations have been provided in Sec. II.B. Some additional aspects of the calculation remain to be discussed. The calculation domain used in the stochastic computation extends for 1 rad in the azimuthal direction. This

has been reduced to 0.2 rad since the larger domain increases computation time considerably as a result of the proportionally larger number of drops involved and is judged to be unnecessary. For each cell, the calculation is made for a length of time equal to 40 τ_{trans}, which has been found to allow for transient adjustment from the initial conditions and a suitably long averaging time to form accurate statistical quantities. The transient time was typically only a few transit times. Still, averages were performed only over the final 20 τ_{trans} of the calculations. The number of drops entering the cell and the number of collisions occurring during this time are, typically, of the order of thousands.

A. Comparison of Deterministic and Stochastic Results

Summaries of the main results of the deterministic and stochastic calculations are provided in Tables 6 and 7 for the calculated gas field and the fixed gas field, respectively. Starting with the calculated gas field results in Table 6, the main difference between the stochastic and deterministic calculations is in the collision rate. The deterministic calculation produces a collision rate roughly 50% greater than the stochastic calculation.

A secondary effect is a reduction in the number density in the deterministic calculation. The increase in the collision rate and, hence, in the coalescence rate results in fewer drops of larger size. The larger drops experience a smaller drag force in relation to their inertia and, therefore, move more rapidly through the cell, which further reduces the number density. In addition, as a result of the greater coalescence rate in the deterministic calculation, the drop size is more uniform, which produces a tendency toward lower coalescence fractions in the deterministic results.

The cause of the larger collision rate in the deterministic calculation was thought perhaps to be the fluctuation of the steady gas velocity. In the stochastic calculation, all parcels in a cell at any one moment are influenced by a common mean gas field fluctuation, and, therefore, the fluctuation does not contribute significantly to the relative velocity between drops, which influences the collision rate. The drops that are collected from the stochastic calculation to be injected into the cell in the deterministic calculation, though, come from different parcels from different times and thus exhibit a broader drop velocity distribution function as a result of the gas velocity fluctuation. Larger drop relative velocity and, consequently, greater drop collision rates would result from the broader distribution. In the end, however, the deterministic collision rate is about 50% greater than the stochastic one with both computed and fixed gas fields. Thus, the gas fluctuation itself is not the dominant cause of the increased collision rates.

One reason for the underestimate of the collision rate in the stochastic method follows. In the stochastic calculation, drops are assumed to be distributed evenly throughout the numerical cell. In the deterministic calculation, the drop-number density is found to be significantly larger in the upstream portion of a cell and then to decrease due to collisions and coalescences. Since the collision frequency is proportional to the square of the number density [Eq. (14)], the deterministic computations will give greater collision frequencies when the number density changes significantly

Table 6 Comparison of deterministic and stochastic results with calculated gas field

	Specimen cell					
	1	2	3	4	5	6
$\overline{n_d}/\mathrm{Vol}_{\mathrm{cell}}$, millions/cm^3						
Deterministic	388	118	28	127	80	24
Stochastic	493	136	27	145	81	25
Collision rate, millions/cm^3-μs						
Deterministic	156	34.3	0.4	28.6	17.2	0.8
Stochastic	108	20.1	0.2	9.7	9.1	1.3
Coalescence fraction, coalescences/collision						
Deterministic	0.72	0.51	0.75	0.52	0.41	0.50
Stochastic	0.81	0.61	1.00	0.38	0.39	0.85
Eddy exchange rate, millions/(cm^3-μs)						
Deterministic	174	53.4	6.0	42.8	27.0	5.0
Stochastic	205	57.1	6.4	47.4	31.8	5.1

Table 7 Comparison of deterministic and stochastic results with fixed gas field

	Specimen cell					
	1	2	3	4	5	6
$\overline{n_d}/\mathrm{Vol}_{\mathrm{cell}}$, millions/cm^3						
Deterministic	227	81.0	17.7	158	63.3	12.7
Stochastic	289	85.7	14.4	166	69.1	9.5
Collision rate, millions/(cm^3-μs)						
Deterministic	148	14.1	0.0	89.8	9.6	0.0
Stochastic	74.3	5.6	0.0	54.7	6.2	0.0
Coalescence fraction, coalescences/collision						
Deterministic	0.38	0.47	—	0.27	0.39	—
Stochastic	0.46	0.62	—	0.22	0.45	—
Eddy exchange rate, millions/(cm^3-μs)						
Deterministic	100	30.6	3.2	62.1	23.0	2.6
Stochastic	136	35.3	3.1	73.5	22.9	1.8

within a numerical cell. As an alternative way of expressing the same concept, it could be argued that the distance for significant change of the drop distribution function is the drop mean free path relative to the grid, since approximately every other collision yields a coalescence. Therefore, the spatial discretization should be no greater than the drop mean free path.

A further difference is associated with the resolution of the drop property space by the stochastic parcels. In the limit in which only a single parcel of drops is present in a cell, no collisions are computed even though in reality the drops of the parcel would undergo some collisions. Typically, spray calculations use a number of parcels that result in around 10 parcels in cells where collisions are significant. The present stochastic calculations result in an average of 3–13 parcels in the specimen cells (Tables 2 and 5). It is likely for this low number of parcels to result in underprediction of the collision rate. Resolving this issue by increasing the number of parcels in the calculation does not appear to be a viable approach. Already, the number of parcels used in the fine grid calculations stretches available computer resources—there are over 10,000 parcels in the domain with the X3 grid. Notice that it is not possible to allow for collisions of the drops within a parcel because such drops have the same velocity and, therefore, their relative velocity and collision frequency are zero. It is possible to alter the number of collisions (and to improve the resolution of the drop distribution function) by splitting parcels, but the total number of parcels within the domain is restricted by practical considerations.

B. Higher Resolution Computations

Since the reason for the difference between the stochastic and deterministic results is mainly inadequate numerical resolution of the stochastic computations, higher resolution calculations were made. As explained in this section, they provided some additional insight, but also presented some new difficulties.

Table 8 shows the resolution of two additional computations, the X6 and X12 cases. Again, the total number of cells was kept constant so that the higher resolution cases cover smaller axial and radial domains. For the X1 resolution, the radial extent of the cell was 7.94 times larger than the liquid core radius and use of a line-source technique was justified. For the X12 computation, the ratio is 0.65; i.e., the first row of cells is within the liquid core. Moreover, the spray model, constructed for dense sprays, still requires the liquid volume fraction to be no more than 10% ($\theta > 0.90$) so that the average surface-to-surface interdrop distance could be at least equal to the drop diameter; otherwise, the assumption of isolated spherical drops is most likely incorrect. It is seen that conditions in the X6 and X12 computations violate the limit on θ. Thus, the X6 and X12 computations push the model beyond its limits. Even when $\theta > 0.9$, breakup of drops has been disregarded, and yet, according to the criterion $We > 6$, where $We \equiv \rho_g(u + u' - v)^2 r/\sigma$,[5] a significant fraction of the drops in the domain would undergo secondary breakup.

An additional problem is due to the cylindrical grid that seems to be used routinely for spray computations and yet is not the natural grid for the flowfield of a jet. In the far field, the angle of the jet becomes constant and a spherical grid would maintain the same number of grid cells within the jet boundary layer at all axial locations. A cylindrical grid gives the optimal number of grid points at one axial location, but too few points upstream of that location and too many downstream. Conversely, very near the nozzle, the jet broadens slowly, and nearly cylindrical coordinates

Table 8 Features of the stochastic computations with calculated gas field and for four grid sizes

Grid	$\frac{\Delta x_{min}}{d_n/2}$	$\frac{\Delta y_{min}}{d_n/2}$	θ_{min} (x/d_n)	Drop mass with $We > 6$, %	Number of drops with $We > 6$, %
X1	15.9	7.94	0.96 (50)	97	12
X3	5.29	2.64	0.86 (20)	98	17
X6	2.64	1.32	0.72 (12)	96	3
X12	1.32	0.66	0.64 (7)	92	11

may be best. The optimal grid would maintain about the same number of points within the boundary layer at all distances from the injector and would tend to a spherical grid whose center is the virtual origin far from the injector. Such a grid can be achieved with arbitrary orthogonal coordinates. The present cylindrical grid brings about several interesting anomalies. As the resolution is increased, the computed near field changes drastically, whereas the computed far-field velocity is scarcely altered. In the near field, where the boundary layer is not resolved by the X1 grid, the increased resolution reduces various forms of numerical diffusion and results in a narrower, faster, more penetrating spray. In the far field, where the resolution of the velocity boundary layer was already adequate, the higher resolution simply pushes downstream the virtual origin of the fully developed jet, but the position of the virtual origin is irrelevant at a sufficient distance from the nozzle. Thus, we can explain both the reported insensitivity to numerical resolution of the computed far-field velocity that was mentioned at the beginning of this chapter and the strong sensitivity of the near-field results.

For all of the preceding reasons, the results of the X6 and X12 calculations are considered just computational experiments as far as the structure of the near field is concerned. However, they do provide progressively smaller numerical cells within which the gas and spray properties are known. The local comparison between the stochastic and deterministic approaches to computing drop collisions and coalescence within selected numerical cells is still valid for cells with $\theta > 0.9$.

Thus, deterministic calculations for six specimen cells in the X12 grid, taken here from the same region of the domain as the X3 specimen cells (see Fig. 7), were made. For the cells of the X12 grid, $\Delta x \approx 80$ μm, $\Delta y \approx 40$ μm, $2.1 < \overline{r_d}$ (μm) < 3.8, and $\theta \geq 0.93$. Comparison of the deterministic and stochastic results in these cells is shown in Table 9. Again, the collision rate is lower in the stochastic computation than in the deterministic one.

At this point, we must remind the reader that we have considered a very severe test of the stochastic method of computing drop collisions and coalescences. Let us reconsider how the comparison between stochastic and deterministic computations was set up. The stochastic computation is performed. Stochastic cell drop collisions and coalescences are counted, and contributions to f are accumulated over a time that is much longer than

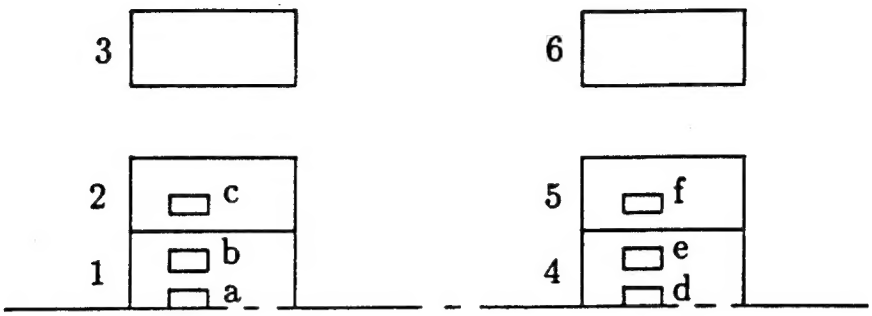

Fig. 7 Relation of X12 grid specimen cells, a, b, c, d, e, and f to the X3 grid specimen cells.

the drop cell transit time. By sampling the accumulated distribution function data, individual drops are introduced into the cell, and the deterministic computation of cell drop collisions and coalescences is performed. Notice that the stochastic and deterministic computations of the collisions and coalescences within the cell do not start from exactly the same drops entering the cell; the stochastic collision computations use the *parcels* of drops that enter the cell, whereas the deterministic collision computations use *individual* drops sampled from the entering drop parcels. When the same sequence of individual drops is introduced into the cell for both the stochastic and the deterministic evaluation of the cell drop collision rate, the difference in the two rates is greatly reduced, as can be seen from Table 10. In the case of the X3 grid, the stochastic collision rates are no longer systematically lower than deterministic ones and differ by 10% at most. The stochastic collision rates do remain consistently lower for the X12 grid but now by only about 20%. This second method of comparison is fairer to the stochastic collision algorithm itself, but less representative

Table 9 Comparison of deterministic and stochastic results; X12 grid for calculated gas field

	X12 grid cell					
	a	b	c	d	e	f
$\overline{n_d}/\mathrm{Vol}_{\mathrm{cell}}$, millions/cm^3						
Deterministic	74	117	90.4	55.7	78.7	60.4
Stochastic	170	152	95.0	104	104	73.0
Collision rate, millions/(cm^3-μs)						
Deterministic	256	90.7	15.7	63.5	17.4	7.8
Stochastic	52.0	35.3	11.8	18.0	11.9	6.1
Coalescence fraction, coalescences/collision						
Deterministic	0.39	0.42	0.55	0.51	0.61	0.71
Stochastic	0.23	0.29	0.61	0.30	0.60	0.67

Table 10 Comparison of deterministic and stochastic results when sequence of entering drops is identical

	X3 grid cell					
	1	2	3	4	5	6
Collision rate, millions/cm^3-μs						
Deterministic	157	36.3	0.400	33.2	15.8	0.630
Stochastic	174	36.2	0.396	36.0	15.6	0.612
Coalescence fraction, coalescences/collision						
Deterministic	0.713	0.525	0.640	0.496	0.431	0.509
Stochastic	0.708	0.503	0.639	0.480	0.418	0.503
	X12 grid cell					
	a	b	c	d	e	f
Collision rate, millions/(cm^3-μs)						
Deterministic	98.6	71.3	14.3	24.8	13.8	7.70
Stochastic	73.1	50.0	11.4	17.1	10.8	6.3
Coalescence fraction, coalescences/collision						
Deterministic	0.328	0.403	0.495	0.467	0.549	0.653
Stochastic	0.235	0.342	0.499	0.381	0.572	0.685

of the accuracy of the stochastic computation of collisions within a stochastic spray computation.

Other factors expected to influence the difference between the stochastic and deterministic collision rates are drop breakup and drop vaporization, but they have not been evaluated in this study.

V. Conclusions

Comparisons of stochastic and deterministic computations of drop collision and coalescence within selected numerical cells of a self-consistent multiphase spray-flow computation were presented. The numerical resolution was greater than that currently used in practical spray computations. The selected spray is narrow, fast, dense, and of the type found in diesel and stratified-charge engines. However, the spray computed was steady, and drop vaporization and breakup were not considered.

The stochastic method was found to underestimate drop collision and coalescence rates by about a factor of 2 with respect to those computed deterministically. A significant fraction of the difference is not due specifically to the stochastic technique of computing drop collision frequencies but originates in the stochastic parcel treatment of the spray. In addition, it is expected that the difference will decrease when drop breakup and vaporization are considered, because both effects tend to narrow the drop size and velocity distribution function, which, in turn, reduces both collision and coalescence frequencies. Indeed, one origin of the difference is that a large fraction of the drops that enter a numerical cell undergo collisions

and coalescences within the cell, thus causing significnt changes in the drop number density. The stochastic technique assumes a uniform distribution of drops within a cell, whereas the deterministic technique computes the spatial variation of that distribution. The obvious remedy is to increase the numerical resolution, but since the drop distribution function changes significantly within distances of the order of the drop mean free path, impractically small grids may be necessary for all numerical techniques. Actually, the reported work has progressed only to the point of identifying some inaccuracies of the stochastic method of computing drop collisions and coalescences. Further work is needed to determine the specific sources of the inaccuracies and the conditions necessary to avoid them.

The present work has focused on the near field, where drop collisions and coalescence are among the controlling processes. Several significant difficulties were encountered. The cylindrical grid that was used, and that is common for spray computations, is not the natural one; future work should adopt a general orthogonal grid that tends to spherical coordinates in the far field. Fluctuations, found in the steady gas velocity, are due to the stochastic drop parcel technique. These fluctuations are comparable in magnitude to the gas turbulence and act as artificial gas turbulence. When progressively higher resolution was used, the physical accuracy of the results became determined by physical processes that are not included in the model.

For the far field, i.e., for $x/d_n > 300$ to 400,[12,14,17] certain more favorable conclusions have been confirmed. The computed far-field mean drop and gas velocities are largely independent of the near-field model and resolution. The model and resolution affect the computed location of the virtual origin of the fully developed jet, but this location is immaterial at a sufficient distance from the nozzle. The artificial fluctuations of the computed steady mean gas velocity become of the order of 10% of the gas turbulence and, therefore, are not of dominant importance. However, there remain questions as to the sensitivity of the computed far-field drop size to the near-field physical and numerical inaccuracies.

Even though the accuracy of far-field computations approaches acceptability, those interested in diesel and stratified-charge engines can derive little comfort from it because in such applications it is the near field that counts.

References

[1]Dukowicz, J. K., "A Particle-Fluid Numerical Model for Liquid Sprays," *Journal of Computational Physics*, Vol. 35, 1980, pp. 229–253.

[2]O'Rourke, P. J., and Bracco, F. V., "Modelling of Drop Interactions in Thick Sprays and a Comparison with Experiments," Institute of Mechanical Engineers, Pub. 1980-9, London, England, 1980, pp. 101–116.

[3]Reitz, R. D., and Diwakar, R., "Effect of Drop Breakup on Fuel Sprays," Society of Automotive Engineers, Warrendale, PA, SAE Paper 860469, 1986.

[4]O'Rourke, P. J., and Amsden, A. A., "The Tab Method for Numerical Calculation of Spray Droplet Breakup," Society of Automotive Engineers, Warrendale, PA, SAE Paper 872089, 1987.

[5]Reitz, R. D., "Modeling Atomization Processes in High-Pressure Vaporizing Sprays," *Atomisation and Spray Technology*, Vol. 3, 1988, pp. 309–337.

[6]O'Rourke, P. J., "Collective Drop Effects on Vaporizing Liquid Sprays," Ph.D Thesis 1532, Princeton Univ., Princeton, NJ, 1981.

[7]Gosman, A. D., and Ioannides, E., "Aspects of Computer Simulation of Liquid-Fueled Combustors," AIAA Paper 81-0323, 1981.

[8]Chatwani, A. U., and Bracco, F. V., "Computation of Dense Spray Jets," *Proceedings of the International Conference on Liquid Atomization and Spray Systems (ICLASS 85)*, Paper 1B/1/1, Institute of Energy, London, England, 1985.

[9]Hiroyasu, H., and Kadota, T., "Fuel Droplet Size Distribution in Diesel Combustion Chamber," Society of Automotive Engineers, Warrendale, PA, SAE Paper 740715, 1974.

[10]Williams, F. A., *Combustion Theory*, Benjamin/Cummings, Menlo Park, CA, 1985.

[11]Harlow, F. H., and Amsden, A. A., "A Numerical Fluid Dynamics Calculation Method for All Flow Speeds," *Journal of Computational Physics*, Vol. 8, 1971, pp. 197–213.

[12]Wu, K.-J., Coghe, A., Santavicca, D. A., and Bracco, F. V., "LDV Measurements of Drop Velocity in Diesel-Type Sprays," *AIAA Journal*, Vol. 22, Sept. 1984, pp. 1263–1270.

[13]Chehroudi, B., Chen, S.-H., Onuma, Y., and Bracco, F. V., "On the Intact Core of Full-Cone Sprays," Society of Automotive Engineers, Warrendale, PA, SAE Paper 850126, 1985.

[14]Martinelli, L., Reitz, R. D., and Bracco, F. V., "Comparisons of Computed and Measured Dense Spray Jets," *Dynamics of Flames and Reactive Systems*, Vol. 95, edited by J. R. Bowen, N. Manson, A. K. Oppenheim, and R. I. Soloukhin, Progress in Astronautics and Aeronautics, AIAA, New York, 1985, pp. 484–512.

[15]Andrews, M. J., and Bracco, F. V., "On the Structure of Turbulent Dense Spray Jets," *Encyclopedia of Fluid Mechanics*, Vol. 8, Gulf, Houston, TX, 1989.

[16]Andrews, M. J., private communication, 1989.

[17]Bracco, F. V., "Structure of High-Speed Full-Cone Sprays," *Recent Advances in the Aerospace Sciences*, edited by C. Casci, Plenum, New York, 1985.